INFORMATION TO USERS

This manuscript has been reproduced from the microfilm master. UMI films the text directly from the original or copy submitted. Thus, some thesis and dissertation copies are in typewriter face, while others may be from any type of computer printer.

The quality of this reproduction is dependent upon the quality of the copy submitted. Broken or indistinct print, colored or poor quality illustrations and photographs, print bleedthrough, substandard margins, and improper alignment can adversely affect reproduction.

In the unlikely event that the author did not send UMI a complete manuscript and there are missing pages, these will be noted. Also, if unauthorized copyright material had to be removed, a note will indicate the deletion.

Oversize materials (e.g., maps, drawings, charts) are reproduced by sectioning the original, beginning at the upper left-hand corner and continuing from left to right in equal sections with small overlaps. Each original is also photographed in one exposure and is included in reduced form at the back of the book.

Photographs included in the original manuscript have been reproduced xerographically in this copy. Higher quality 6" x 9" black and white photographic prints are available for any photographs or illustrations appearing in this copy for an additional charge. Contact UMI directly to order.

UMI

A Bell & Howell Information Company
300 North Zeeb Road, Ann Arbor MI 48106-1346 USA
313/761-4700 800/521-0600

CHARACTERIZATION OF DOWNFLOWING HIGH VELOCITY FLUIDIZED BEDS

by

CHUNSHE CAO

A dissertation submitted to the Graduate Faculty in Engineering in partial fulfillment of the requirements for the degree of Doctor of Philosophy, The City University of New York

1998

This manuscript has been read and accepted for the Graduate Faculty in Engineering in satisfaction of the dissertation requirement for the degree of Doctor of Philosophy.

9/10/98
Date

Professor Herbert Weinstein
Chairman of Examining Committee

9/10/98
Date

Dean Mumtaz Kassir
Executive Officer

Dr. David C. Skouby
Exxon Research & Engineering Co.

Prof. R. A. Graff
Dept. of Chemical Engineering, CCNY

Prof. G. Tardos
Dept. of Chemical Engineering, CCNY

Prof. A. Couzis
Dept. of Chemical Engineering, CCNY

Supervisory Committee

THE CITY UNIVERSITY OF NEW YORK

Abstract

CHARACTERIZATION OF DOWNFLOWING HIGH VELOCITY FLUIDIZED BEDS

by

Chunshe Cao

Advisor: Professor Herbert Weinstein

It has been proposed that gas-solid cocurrent downflowing high velocity fluidzed beds would have advantages for very short residence time reactions over the conventional upflow riser by minimizing backmixing. However, present databases do not supply sufficient information for a process development. In this work, a downer-riser circulating high velocity fluidization apparatus has been developed to study experimentally the fundamentals of gas-solid particle mixture downflow. The downer consists of a Plexiglas tube with 12.7cm ID and a length of 4.6m. A single gas-solid entrance design is employed, which is the simplest configuration that can be applied commercially. A pressure balance is maintained between the downer and the return riser during the operation. Fast response pressure transducers hardwired to a computerized data acquisition system are used to record the instantaneous pressure distribution around the loop. An x-ray chordal absorptometry technique is used to provide flow visualization and to measure instantaneous solid fractions and its radial and axial distributions. The local solids flux profiles are obtained by an aspirating

probe device. Gas lateral and back mixing properties are studied by using helium tracer detected by an on-line analyzer.

Experimental data show that the acceleration and deceleration of solids in the downer due to the influences of the entrance and exit sections result in a relatively uniform axial solids distribution. Radial solid density profiles detected with an X-ray imaging system show the existence of a core-annulus flow with a dilute core surrounded by a denser wall region. The local solids flux profiles and the solid velocity profile obtained from these two measured quantities confirm that the majority of solids aggregates in the wall region but flows faster than in the core region.

Measurements show that gas backmixing is very limited in the downflow high velocity fluidized bed, and the lateral mixing is comparable with that in the riser. A mathematic model is applied to characterize the behavior of the gas dispersion in the two-phase downflow.

The downer reactor furnishes significant advantages over the conventional riser reactor particularly for short residence time reactions due to its specific flow pattern, reduced backmixing, shorter flow developing region and capability of handling very high solids/gas loading ratios.

ACKNOWLEDGMENTS

I am sincerely grateful to my mentor, Professor Herbert Weinstein. In the course of completing my doctoral studies and this investigation, I have received so much encouragement, guidance, and support from him. I hereby also want to express my deep appreciation for his personal interest in me.

I would like to acknowledge the members of my thesis committee, Dr. David C. Skouby of Exxon Research & Engineering Co., Professor Robert A. Graff, Professor Gabriel Tardos, Professor Alexander Couzis in the Department of Chemical Engineering at CCNY for their interest in this project and helpful suggestions.

I also wish to thank the entire faculty and technical staff of Chemical Engineering Department at City College of New York for their assistance, especially Mr. Andrew Eng and Mr. Zhenrong Xu who helped me to build the first generation Dower-Riser Fast Fluidization System.

Financial support for this work was given by a National Science Foundation grant, number CTS-9312099. Exxon Research and Engineering Company was the cooperating industrial organization. W.R. Grace Co. graciously provided the cracking catalyst powder.

To My Wife

Mom, Dad and Sisters

TABLE OF CONTENTS

LIST OF TABLES

LIST OF FIGURES

NOMENCLATURE

a_0, a_1, ...	constants of polynomial
b_0,b_1,...	constants of polynomial
c	measured tracer concentration, volume %
c_0	tracer injection concentration, mean mixed volume %
D	bed diameter, m or sometimes distance of centerline bed to x-ray source as indicated in the text, m or sometimes gas dispersion coefficient, m^2/s as indicated in the text
d_p	particle diameter, μm
f	frequency, Hz
G_s	solid flux, kg/m^2s
g	gravitational acceleration, m/s^2
I	detected intensity of x-ray beam
I_0	detected intensity of the reference x-ray beam
I_{w+s}	x-ray intensity after the beam passes through the fluidized bed
I_w	x-ray intensity after the beam passes through the empty bed
J_0, J_1	Bessel functions
k	x-ray absorption coefficient of absorbing beam, cm^2/kg
L	distance from the solid entrance of the downer, m
P	pressure in gauge, psig
Pe	Peclet Number

r	radial coordinate, m
R	column radius, m
U_g	gas superficial velocity, m/s
U_p	particle velocity, m/s
x	distance between the injector and detector planes, cm
x_s	x-ray travel distance in the fluidized bed, cm
x_w	travel distance in the bed wall detected intensity of the x-ray beam, cm

GREEK SYMBOLS

ε	bed voidage
ε_{app}	apparent bed voidage evaluated from pressure readings
θ	chord angle
λ_n	roots of Bessel function equations
μ	x-ray attenuation coefficient of medium
ξ, η	nondimensionlized coordinates
ρ_p	particle density, kg/m^3
$\rho(r)$	local density in radial direction, kg/m^3

I. INTRODUCTION

The application of gas-solid cocurrent downflowing high velocity fluidized beds has become, very recently, more and more attractive in newly proposed industrial processes with very short residence times, such as thermal cracking, advanced catalytic cracking of hydrocarbons and various other proprietary processes. When combined with a solid-gas separator and an entrained bed combustion system, a complete process for endothermic reactions such as olefins production, LPG dehydrogenation or heavy oil upgrading can be developed. It is expected that the downflow reactor would not only keep the advantages of the conventional upflow riser, but also overcome its shortcomings by minimizing backmixing.

Performance criteria such as yield and selectivity are typically adversely affected by backmixing in short contact or residence time processes. These processes are typically catalytic or thermal cracking processes in which both overcracking and undercracking which result from backmixing provide some very low value products. As unit residence times become shorter, the backmixing inherent in the conventional upflow riser system becomes more critical in limiting process yields and selectivity. The significant gas and solids backmixing is a result of the radially and axially non-uniform gas and solids flow as well as of entrance mixing and exit separation sections. The core-annulus radial structure and the axially non-uniform density of the

suspension in the upflow riser which results in backmixing and reduced contacting between the two phases is due in part to the flow opposing the direction of the gravitational field.

It has been proposed that a reactor-reaction scheme utilizing a gas-solid mixture downflow concept would minimize backmixing and achieve a closer approach to the plug flow condition in the reactor. When both the gas and solids flow directions are downwards, in the same direction as gravity, backmixng is expected to be limited to the inlet gas-solid mixing section and the exit gas-solid separation section. The proposed advantages of the downer reactor come from the fact that particles are co-currently flowing downwards with the gas phase in the direction of the gravitational force, rather than against it as in conventional riser reactors. The expected key advantages include:

(1). Both axial and radial gas-solids flow structures would be much more uniform. Reactions, thus, could be carried out under near plug flow conditions. The gas-solid contact efficiency would be significantly improved. The possibility of local hot spots in the reactor would be reduced allowing higher operating temperature without the risk of over-heating locally.

(2). Because the limit of a minimum gas velocity to transport solids upward

does not exist in a downer as it does in a riser circulating fluidized bed, the solids/gas loading ratio could be much higher.

(3). The developing flow region in which the particles accelerate should be shorter in a downer than in a riser. This better fits the kinetic requirements of relative short contact time reactions.

The heterogeneous structure of an upflow riser has been well explored in the last two decades. It has not been demonstrated clearly whether heterogeneities will also occur in downflow or whether there are different regimes of flow which can be distinguished by their differing properties. To develop the potential industrial applications of downer reactors, the behavior of this type of two-phase flow must be understood before downflow reactor schemes will ever be considered for commercial processes. At present, only a limited number of studies have been reported on the fundamentals of downers. A sufficient data base for high velocity downflow of gas-solid powder mixtures upon which a process development can be based and the backmixing level evaluated does not exist. In this investigation, a downflow reactor system which incorporates a downer and a parallel riser has been developed to study the fundamentals of gas-solid particle mixture downflow. The aims of this project are to provide a picture of the flow structure and the general nature of the high velocity two-phase downflow, and increase the size and value of the data base. The data base

obtained is to be sufficient for the evaluation and calibration of computational fluid dynamic models of this type of two phase flow.

The experimental measurements obtained in this work describe the axial pressure profile, the radial solid fraction profile, and the local solid flux. Fast response pressure transducers and an X-ray system are used to record real time flow quantities and provide flow visualization. Solid flux measuring equipment is developed to obtain the local solid flux and estimate the local gas-solid velocities. A helium tracing technique and two-dimensional pseudo homogenous model are applied to describe the behavior of the gas dispersion and backmixing in the downer. Finally, flow patterns in the downer are compared with those in the riser.

II. LITERATURE REVIEW

2.1 The Concept of the Downer

The concept of a cocurrent downflow high velocity fluidized bed reactor was proposed to improve the performance of traditional upflow or riser reactors with very short residence time reactions. In the early 1970's, Stone and Webster Corporation began to develop a downer type of reactor referred to as the "Quick Contact" (QC) reactor. (Figure 2.1; Gartside and Ellis, 1983, 1989). Basically, this reaction system consists of four patented components which are a solids-gas feeder, a downflow reactor, a gas -solids separator and a quench section. Solids are rapidly mixed with the reactants which are typically gases or gases containing entrained liquids, and flow down into the tubular reactor. Once the two phases are mixed, reaction takes place, and the solids are rapidly separated from the mixture at the end of the reaction zone. The effluent gas is quenched if necessary to freeze thermal reactions. The QC reactor system is reported to be able to offer short residence times, as low as 200 ms, near plug flow, and a high temperature reaction environment.

Similar to the idea of the QC, an ultra rapid fluidized reactor (Figure 2.2) was developed for a biomass pyrolysis process. (Berg, et al., 1986, 1989; Graham, et al., 1991; Rodden, et al., 1993). In this design, eight jets of hot thermofor particles

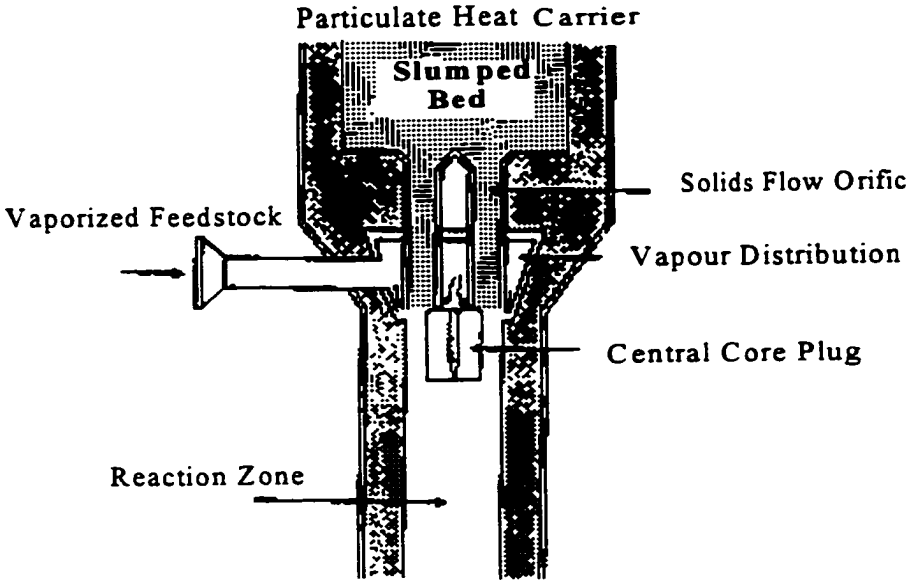

Figure 2.1 QC Reactor Solid Feed Mixer (Gartside R. J., 1989)

impinging upon a central jet of biomass was constructed to be a "mixer". Both turbulent shear forces and particle momentum were utilized to achieve rapid mixing. The solids flow rate to each of the biomass and thermofor jets was regulated by separate gravity flow feeders. The flow of solids from each feeder was mixed with the transport gas and transported directly into the downflow reactor through dilute phase pneumatic transport lines. To accelerate the particles before injection into the downer, acceleration lengths were provided.

Murphy (1992) proposed a future FCC/ heavy oil cracker unit which

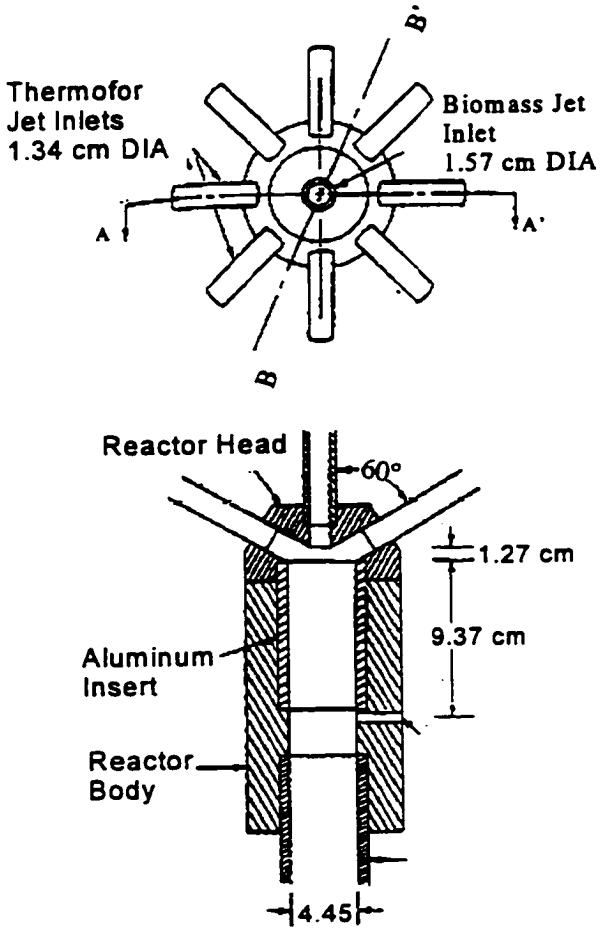

Figure 2.2 Pyrolysis Reactor System (Berg, et al.,1989)

incorporated a downflow reactor and a riser regenerator, as shown in Figure 2.3. Catalyst flows from a hopper into a number of parallel downflow reactors of length necessary to give the desired reaction time. Solids flow is controlled by plug valves free of gas bubbles. The regenerated catalyst is fed back into the hopper and the fine powder is collected by high efficient cyclones.

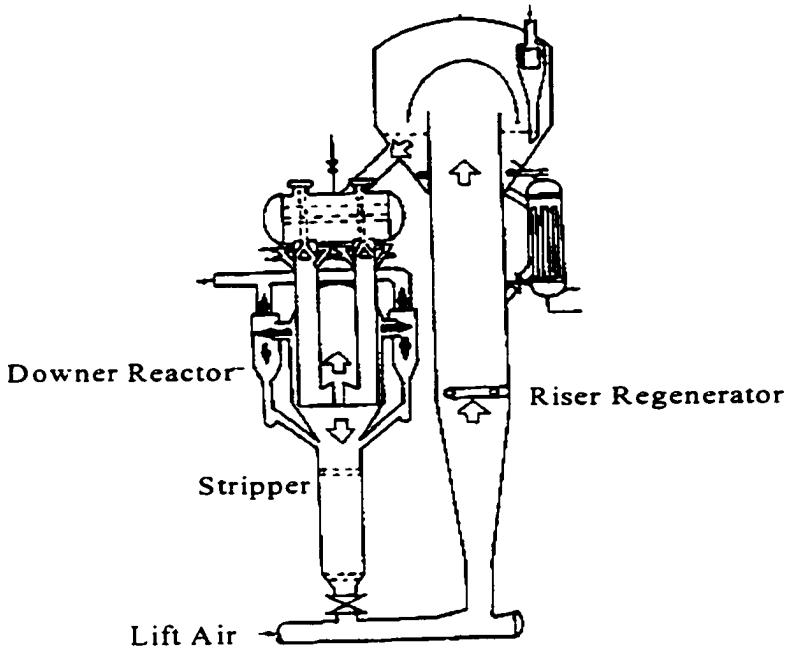

Figure 2.3 A Proposed Future FCC Design with Downer Reactors(Murphy, 1992)

Mobil and Texaco have patented downer reactors for the FCC process(Gross and Ramage, 1983; Gross, 1983; Niccum and Bunn, 1985).They claim improved yield of light products and reduced coking.

Tests have also been done for coal liquefaction by flash hydropyrolysis in a downer (Oberge and Falk, 1980). A high solids mass flux and short residence time reactor is necessary since higher liquid yields are favored when coal is allowed to react with hydrogen for only a brief period followed by rapid quenching. Two advantages of downer reactors, short contact time and high solids loading, are utilized.

2.2 Hydrodynamic Research on the Downer

Most of the research for potential industrial applications has been concentrated on the mixing section of the reaction system. Studies on the hydrodynamics of the downer reactor itself are limited. The research was pioneered by Shimizu et al.(1978) and Kim et al. (1983). They studied pressure drop and heat transfer for cocurrent downflow of gas-solids suspensions at high gas velocities (above 8 m/s) with low solids loading ratios (less than 20 kg solid / kg gas) in small tubes (diameter below 2.5 cm). The results showed that the particle acceleration length in the downer was larger than that in the riser under the same operating conditions. The frictional pressure drop for downflow was found to be weaker function of the solids loading ratio than in the upflow case. The suspension Nusselt number, defined in terms of the wall-to-gas mixed-mean temperature difference, decreased with increasing solids loading ratio at high Reynolds numbers. The sketch of the equipment used by Kim et al. is shown in Figure 2.4. It has a test section of 13 mm inside diameter and 6.7 m long. Apparently, the usefulness of the data is strongly compromised by the small diameter of the downer column and the low solids loading ratio. Columns of this size can exhibit strong wall effects which result in flow patterns somewhat different than those found in columns only twice as wide.

Starting in the late 1980s, researchers at Tsinghua University carried out a

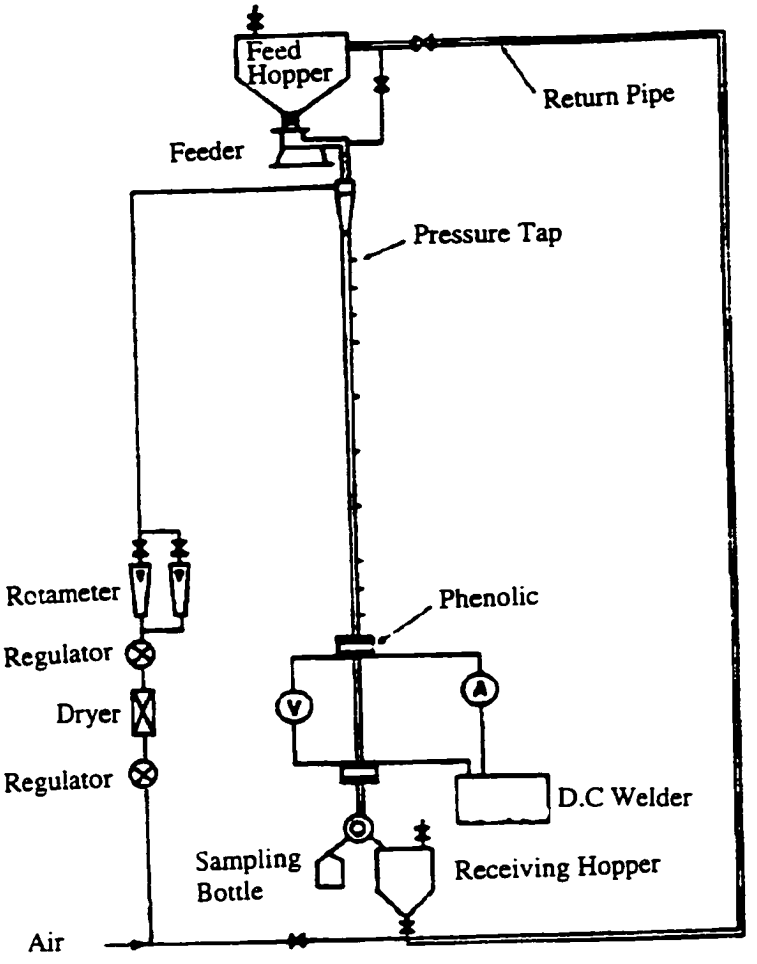

Figure 2.4 Downer Reactor Loop (Kim et al., 1983)

series of downer studies in their pilot plant scale (14 cm ID, 5 m height) circulating system. (Figure 2.5). (Jin's Group: Bai, et al.,1991; Yang, et al., 1991; Wang, et al., 1992; Cao, et al.. 1994).

The axial pressure profiles, radial solids concentration distribution and gas-solids velocity profiles are reported, as shown in Figure 2.6, Figure 2.7, Figure 2.8

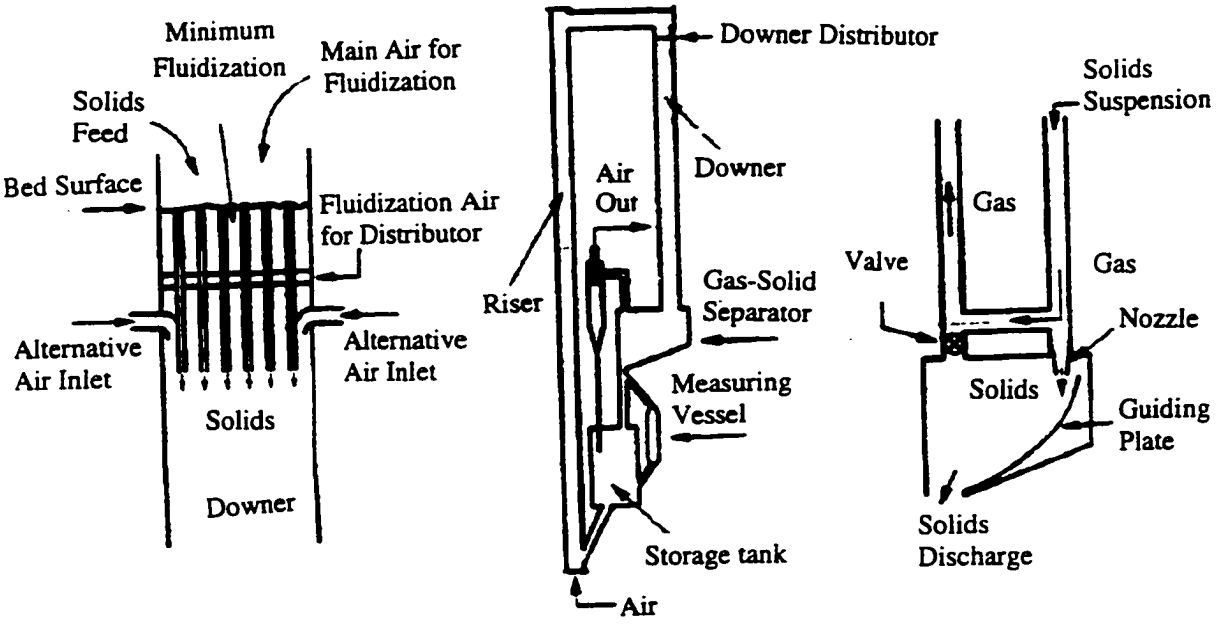

Figure 2.5 Tsinghua's Downer Reactor (Zhu et al., 1995)

and Figure 2.9. They discovered that three different regions appear to exist across the cross section of the downer: a dilute core region from the axis to r/R of about 0.85, where the local solids concentration and particle velocity are rather uniform; a relatively dense annular region for $0.85 \le r/R \le 0.96$, where both variables have their maxima; and a wall region for $r/R \ge 0.96$, where both variables decrease towards the wall to fit the non-slip gas boundary condition. This radial flow structure is quite different from the core-annulus structure observed in risers. It is worth noting that all the radial solid density and velocity profiles reported were measured in an apparatus

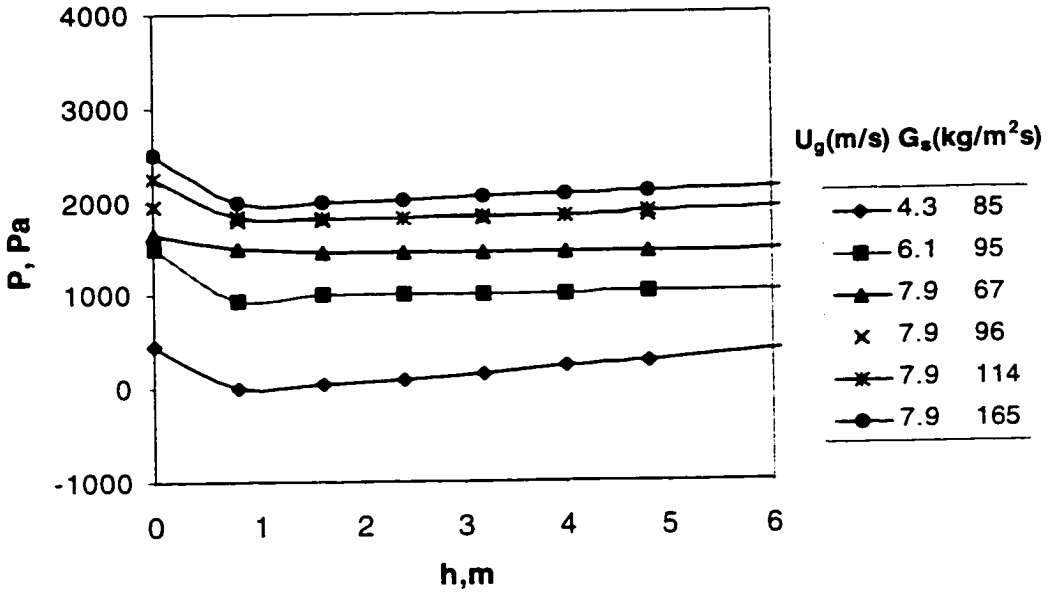

Figure 2.6 Axial Pressure Distribution (Zhu et al., 1995)

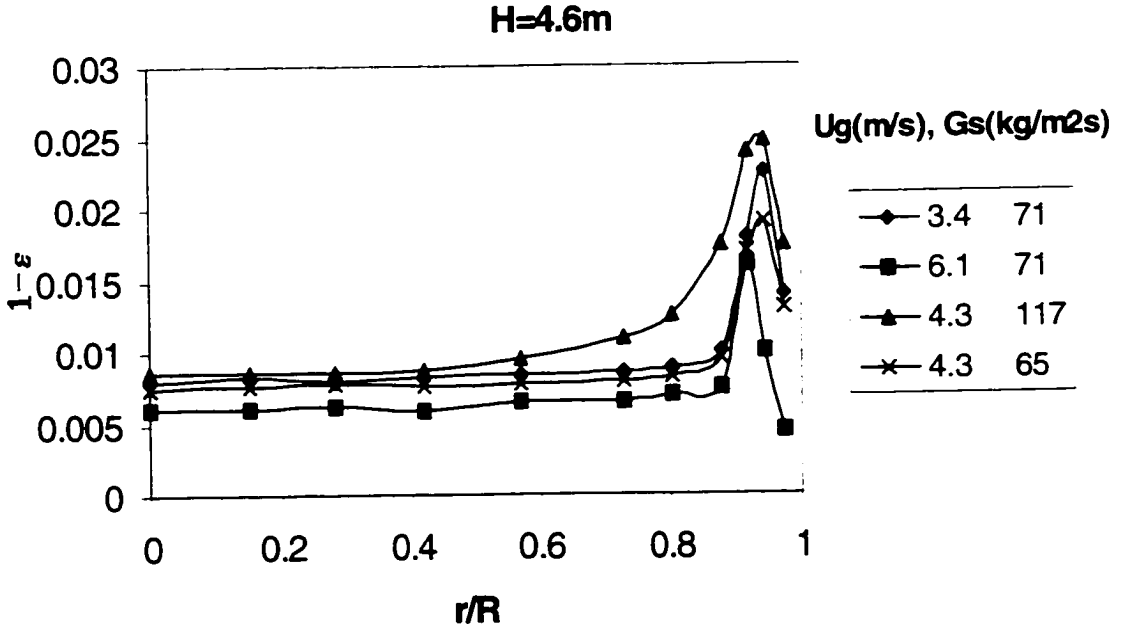

Figure 2.7 Solid Fraction Profiles (Bai et al.,1991)

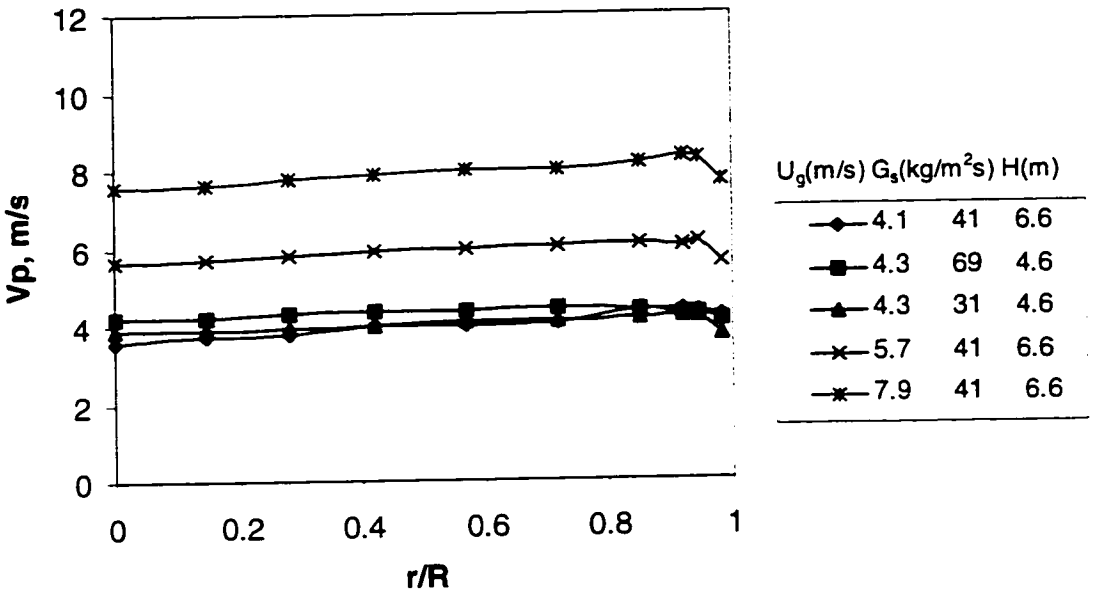

Figure 2.8 Particle Velocity Profiles (Yang, et al., 1991)

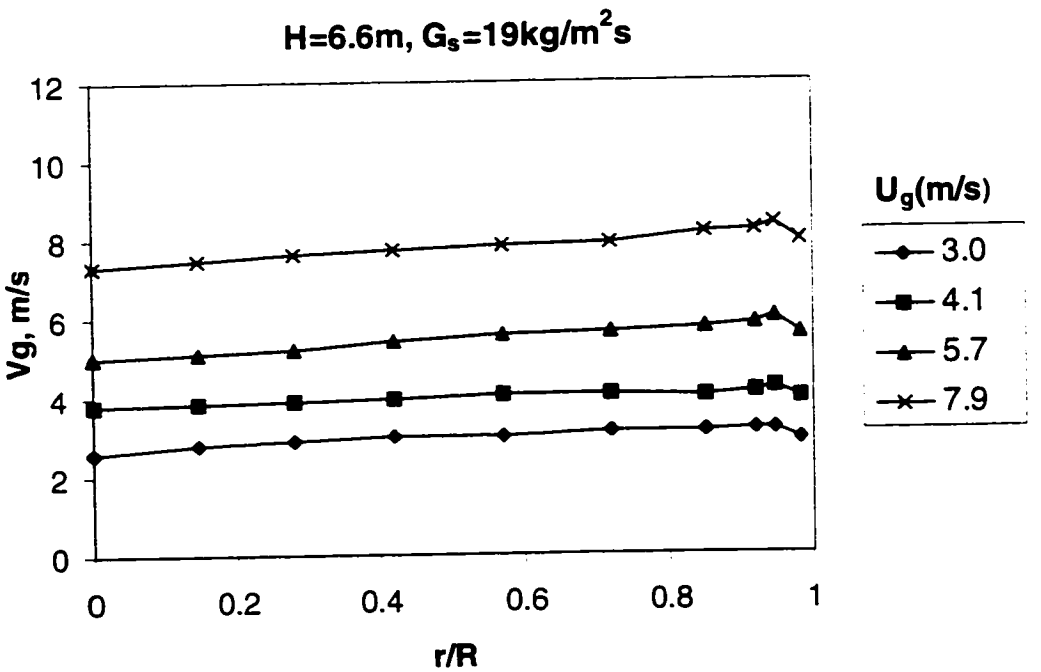

Figure 2.9 Gas Velocity Profiles (Cao, et al., 1994)

with one type of solid distributor which has a significant influence on the radial profiles. In their investigation, the gas and solids flow rates were controlled by conditions in the riser instead of an independent control for the downer. Furthermore, most of their tests were carried out in very dilute bed conditions which would compromise the feasibility of practical design for a downer application. Obviously, further study in different units is required.

In the study by Aubert et al. (1994), a circulating fluidized bed loop with a 5m high and 50mm ID downer was used to measure the pressure drop and slip velocity along the downflow column.(Figure 2.10). The slip velocity is defined as:

$$u_{slip} = \frac{G_g}{\rho_g \epsilon} - \frac{G_s}{\rho_p (1-\epsilon)}$$

A capacitance probe was used to measure the solid hold up. It was reported that the hydrodynamics strongly depended on gas superficial velocity. At low gas velocities, the particles flow faster than the gas and gravity seems to dominate the pressure gradient. At higher gas velocities, the gas flows faster than the particles indicating that the entire column was an acceleration zone, and the frictional effects dominate the pressure gradient. (See Figure 2.11). However, the invasive probe measurement has the disadvantage of disturbing the gas-solid flow stream to a great extent in such

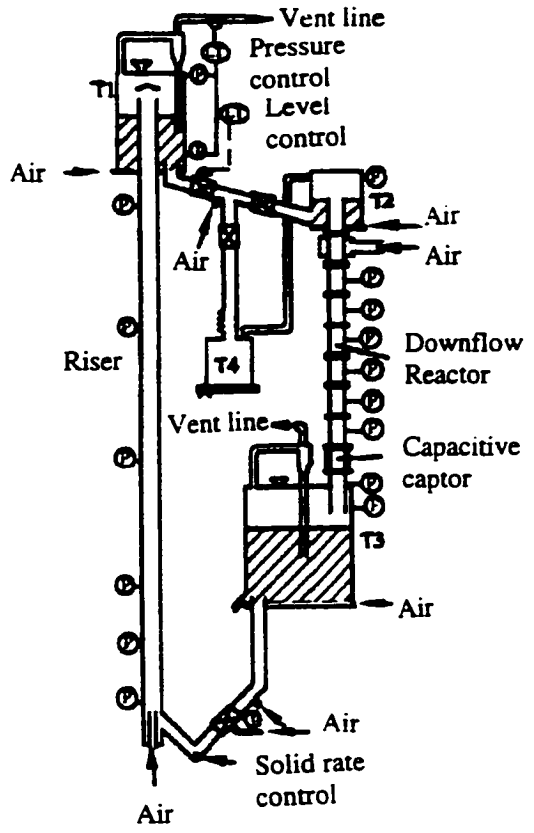

Figure 2.10 The Circulating Fluidized Bed (Aubert et al., 1994)

a small flow channel. In addition, the radial heterogeneities in the two-phase flow have not been shown in their investigation.

A single-fiber reflective fiber optic probe was applied in Aubert's equipment (1994) by Herbert et al. (1994) to measure the local particle velocity and concentration in dilute gas-solid flow. A radially symmetric profile of solid velocity and a solid concentration distribution were achieved as shown in Figure 2.12 and 2.13. However, as the author mentioned, it must be kept in mind that the particle

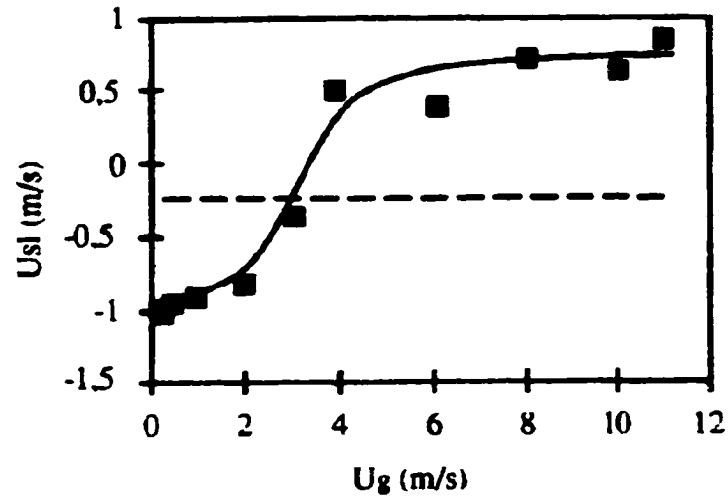

Figure 2.11 Slip Velocity as a Function of Gas Superficial Velocity for a Given Solid Mass Flux of 79kg/m²s (Aubert et al., 1994)

concentration measurements were very sensitive to outside disturbances and therefore they should be verified by an independent method. Higher solids loading would also exhibit different flow patterns in a wider downer.

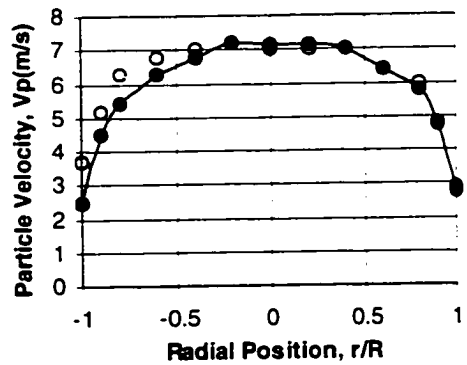

Figure 2.12 Radial Velocity Profile in Downer [U_g=6.1m/s, G_s=71kg/m²s]; (●) 0-180 °C, (O) 90-270 °C (Herbert et al. ,1994)

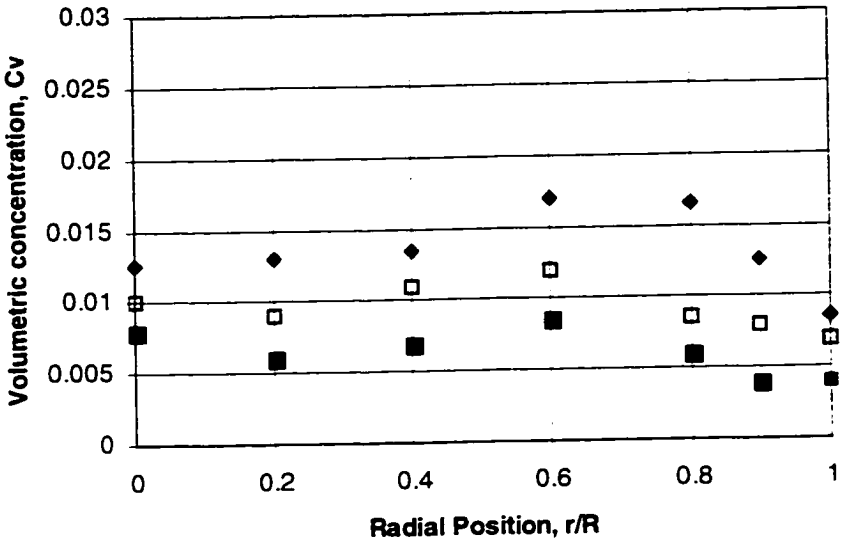

Figure 2.13 Radial Profile of Solid Concentration at Constant Gas Velocity, U_g=6.1m/s, (■) G_s=56kg/m^{2}s, (□) G_s=73kg/m^{2}s, (♦)G_s=96kg/m^{2}s (Herbert et al. ,1994)

Roques et al. (1994) duplicated the pilot unit of the ultrapyrolysis process to mock up the cold flow or hydrodynamic behavior. The Plexiglas equipment (Figure 2.14) had a 1m long, 2 cm diameter reactor tube. An attempt was made to measure the residence time distribution of solids in a short residence time system without any mechanical interference with the flow. Phosphorescent particles were used as tracer. It was found that the solids axial dispersion increases with the gas residence time. (Figure 2.15). A simple axial dispersion model was employed to describe the slip phenomenon in the co-current gas-solid downflow. It was shown that an inversion of

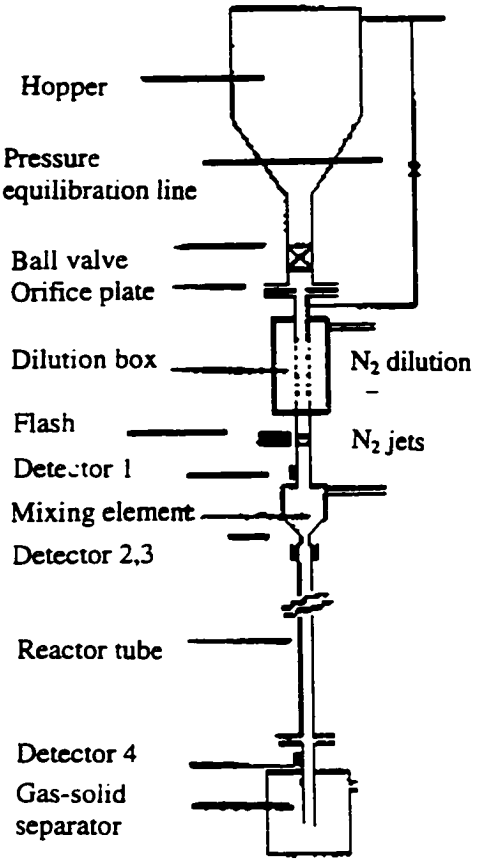

Figure 2.14 The Downer Reactor Setup (Roques et al.,1994)

the sign of the slip velocity occurs near a mean gas residence time of 800 ms. (Figure 2.16). It could be seen that the gas flows faster than the particles at shorter gas residence time, while the slip velocity was close to the particle terminal velocity at larger gas residence time. This is in agreement to Aubert et al. (1994)'s results. But the narrow tube presents strong wall friction effects which may prevent the development of the radial heterogeneities in the two-phase flow.

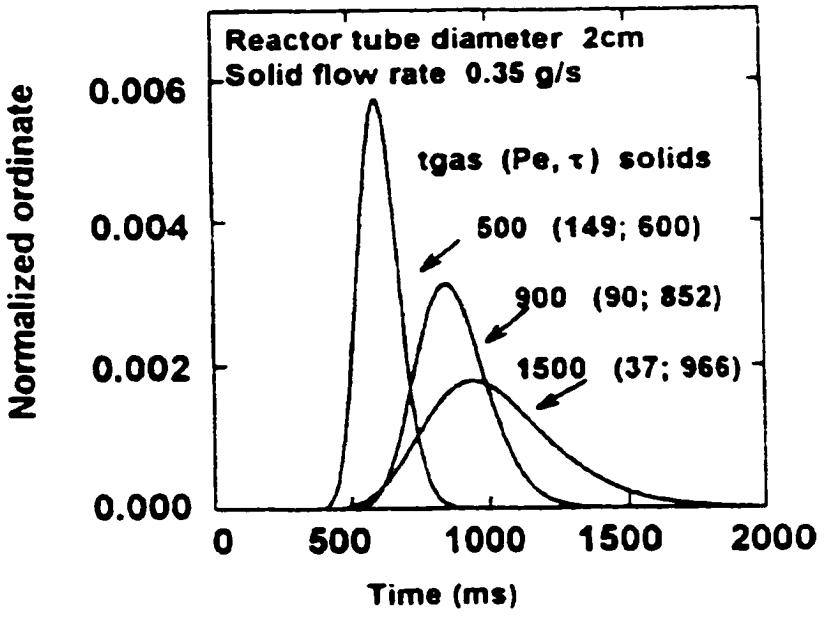

Figure 2.15 Influence of the Average Gas Residence Time on the Residence Time Distribution of Solids. (Roques et al., 1994)

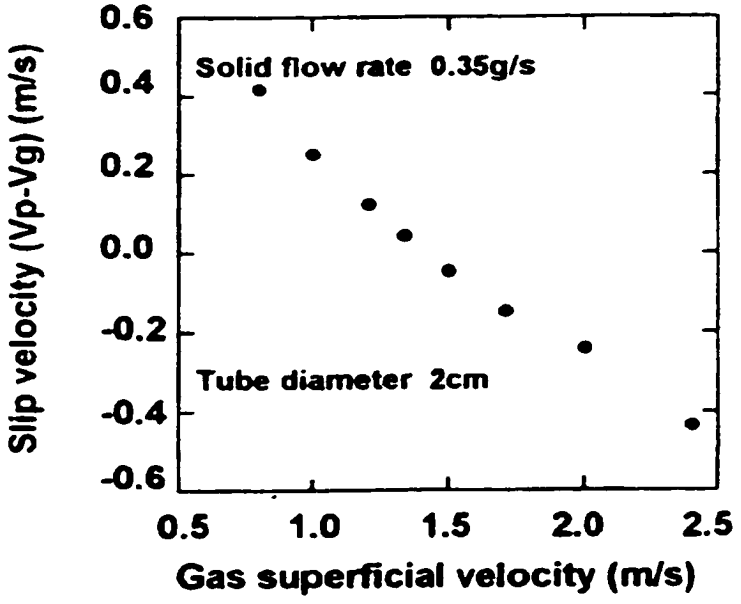

Figure 2.16 Slip Velocity vs. Gas Superficial Velocity (Roques et al., 1994)

As pointed out by Wei et al. (1997), the gas/solid entrance design has a large influence on the flow pattern of the downflowing fluidized bed. A strong downward jet will enlarge the length of the entrance region and cause uneven solid radial distribution. Therefore, a proper feeding system is important in the application of the downer.

More recently, researchers in Switzwerland (Zenklusen et al., 1997) developed a new solid feeding system (see Figure 2.17) to provide homogeneous downflowing gas/solid suspensions at high velocities. Two solid dispersion devices used in their investigation are basically classified as mechanical inserts and fluid dynamic nozzles. A Γ-ray absorptometry technique was used to detect radial solid fraction profiles. As shown in Figure 2.18, 3-D surface plots of cross-sectional solid fraction confirm that either a "U-shape" or a nearly uniform radial solids concentration profile had been achieved, depending on the dispersion device used, for solids loading ratios up to 5. However, a stream with a large solid loading was not investigated.

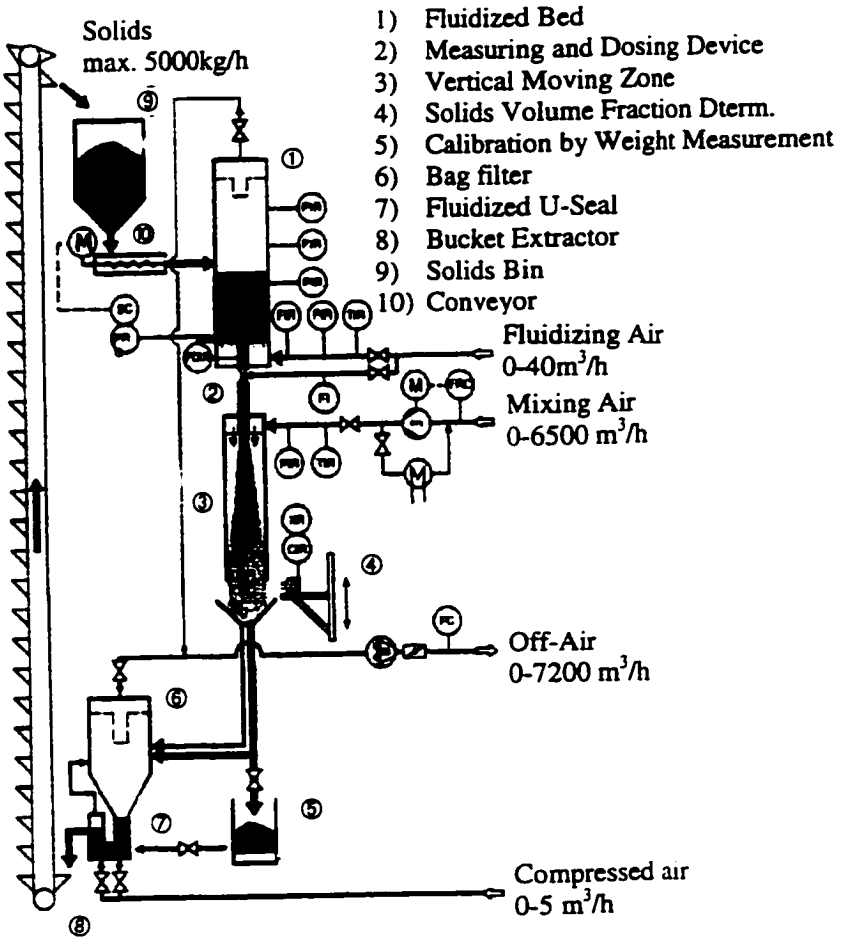

Figure 2.17 Test Unit for the Preparation of Homogeneous Gas/solid Suspensions (Zenklusen et al., 1997)

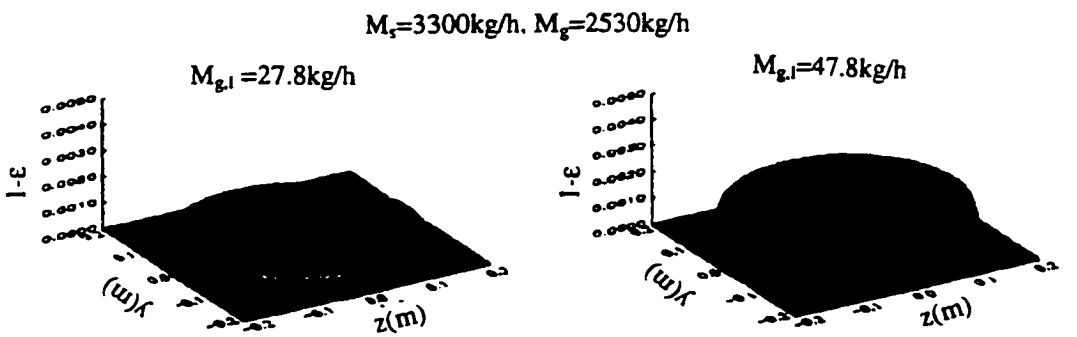

Figure 2.18 Cross-sectional Profiles of Solid Volume Fraction for Two Different Aeration Mass Flow Rates. (Zenklusen et al., 1997)

2.3 Proposed Research Program on Downer

While a considerable amount of fundamental study has been carried out on downer hydrodynamics in the above units, studies are rarely reported from other industrial sources. In addition, most of the experimentation was done in small diameter downer reactors. The measured data are thus compromised for use in industrial design. Therefore, further experiments are needed to compare with and possibly confirm the existing results. The direct mockup of an industrial scale unit would reveal more clearly the hydrodynamic behavior in co-current two-phase flow but because of the expense involved, no industrial organization will undertake such a study without a well-developed interest in a process utilizing such a reactor concept. Conversely, no industrial organization will develop such a process without a much larger data base than is currently available.

In this study, a pilot plant downflow reactor system which incorporates a downer and a parallel riser has been designed and constructed. The object of this project is to develop, over a range of operating conditions in the new equipment, a picture of the flow structure of the high velocity two-phase downflow and additional basic information which would be useful in process design. The experimental program includes the application of fast response pressure transducers, an X-ray system and solid flux measuring equipment. They are used to record real time flow

quantities and flow visualization. Solid fraction and velocity profiles are obtained. Fluctuations in pressure gradient are analyzed in order to give an indication of turbulent flow activity and describe any flow regimes observed. Measurements are also presented of gas mixing in the downer using helium tracer detected by an on-line analyzer. A mathematic model is applied to characterize the gas dispersion and backmixing in the two-phase downflow. Finally, downflow patterns and mixing characteristics are compared with upflow in order to substantiate and/or modify the proposed advantages of the downer over the riser.

III. EXPERIMENTAL PROGRAM

3.1 The Downer-Riser Circulating Fluidized Bed System

The first generation of the City College Downer-Riser circulating fluidization unit has been designed and constructed for this investigation. A schematic of the system is shown in Figure 3.1. The key features of this unit include two linked parallel tubes serving as downer and riser, a storage tank, a solid feed device and a gas-solids separation system.

The downer consists of a Plexiglas tube with an inner diameter of 12.7cm and a length of 4.6m. A solid feeder is located on top of the downer with a gas distributor sitting on it. A tightly packed section of straws inside a 6"ID PVC pipe serves as a gas distributor and provides a uniform flow of air. The solids feeder is a PVC wye connecting the downer, the gas distributor and the solid storage tank. A hand operated valve placed between the storage tank and the solid feeder controls the solid rate. The solids are carried down by the main air supply to an U-bend section which connects the downer with the riser. The fluidizing medium is ambient air. It is provided by an INGERSOLL-RAND centrifugal compressor with output of 1.42 m^3/s at 1.4 atm gauge. Additional air regulated separately over four independent air supply lines with five nozzles enters the system in the U-bend section to help blow

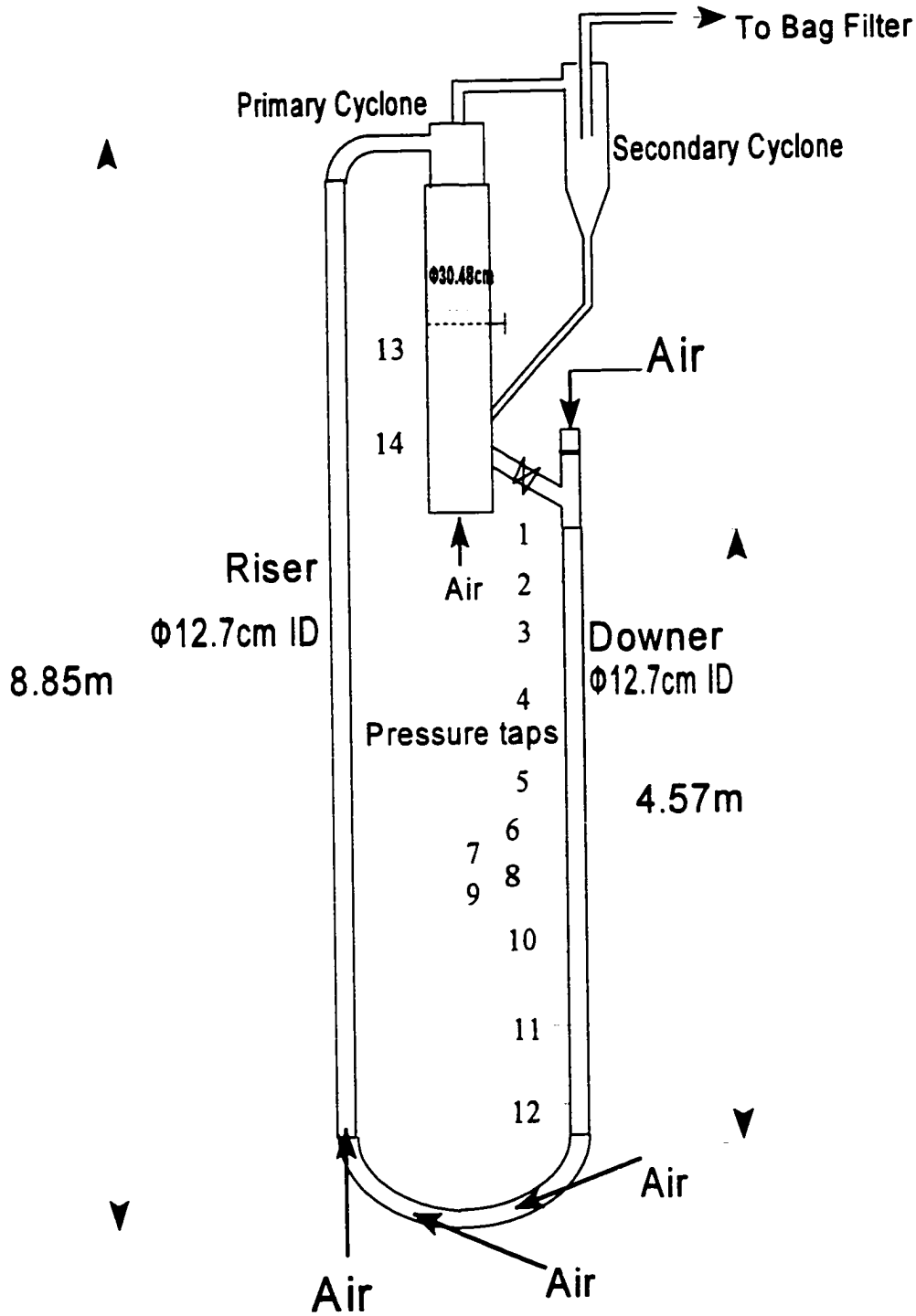

Figure 3.1 The City College Downer-Riser Circulating Fluidization Unit

the solids up through the riser. The riser is also made of Plexiglas with a height of 8.85 m and the same diameter as the downer's. The solid particles are carried up through the riser, which terminates in a flexible nylon tube, and are directed into the primary cyclone. The primary cyclone is located in the top of the storage tank. The Plexiglas vessel (0.3048m in ID, wall thickness 1.27cm) is used as a storage bed for the solid. The solids separated in the primary cyclone fall down along the wall of the storage bed which is kept at bubbling fluidization conditions. After passing through the secondary cyclone (Fisher-Klosterman Cyclone Collector), the air is exhausted through a bag filter which collects the fines. These fines are periodically returned to the reservoir. The solids from the secondary cyclone return to the storage tank by a standpipe. The butterfly valve in the middle of the storage bed is made out of a sintered plate. It is used to measure the solid flow rate.

In the unit shakedown period, several different combinations of gas velocities and solid circulating rates were tested in trial runs. Proper operating conditions for maintaining a pressure balance were found. Measurement tests are listed in Appendix A.

3.2 Fluidized Powder

The solid used in this investigation is Grace Davison fluid cracking catalyst. The catalyst is classified as a Geldart group A. The size distribution and statistical properties are monitored with a Malvern Series 2600c Laser Scattering based Particle Sizer. Figure 3.2 shows both the density distribution and the cumulative distribution. Table 3.1 gives the light scatting analysis sieve distribution and statistic calculation results. The Particle density is measured by using a Quanta Chrome Autoscan Porosimeter. The results show that the FCC particle density is 1480 kg/m^3.

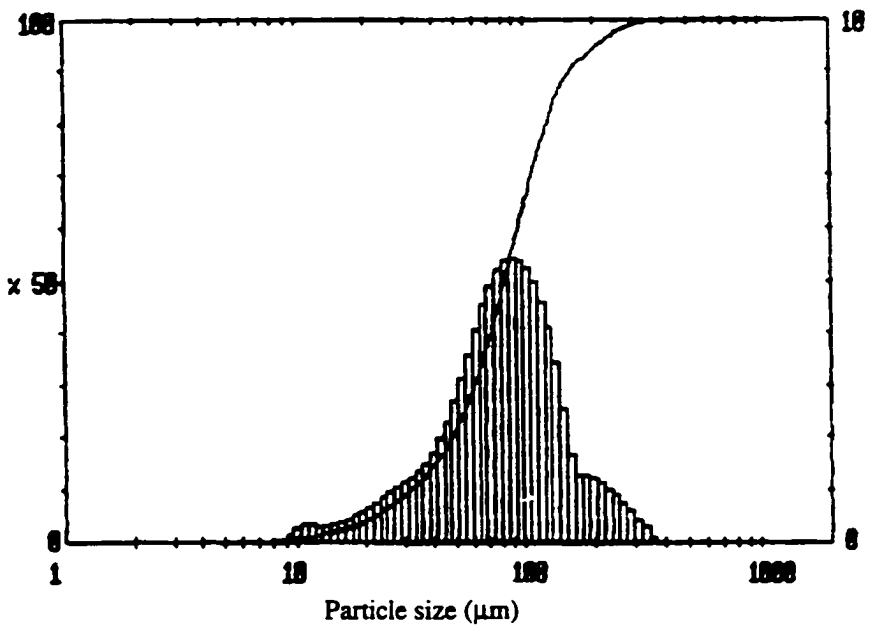

Figure 3.2 Particle Size Density Distribution and Cumulative Distribution

Upper in Lower Under	Upper in Lower Under	Upper in Lower Under	Span 1.54
564 0.0 487 100 487 0.0 420 100 420 0.0 362 100 362 0.5 313 99.5 313 1.1 270 98.4 270 1.7 233 96.7 233 2.3 201 94.4 201 2.5 173 91.9	173 3.3 150 88.6 150 6.6 129 82.0 129 9.4 111 72.6 111 10.4 96.0 62.2 96.0 11.3 82.5 50.8 82.5 10.3 71.5 40.5 71.5 9.4 61.5 31.1 61.5 7.4 53.0 23.7 53.0 5.4 45.8 18.4 45.8 4.0 39.5 14.4 39.5 3.1 34.1 11.3 34.1 2.5 29.5 8.8	29.5 2.1 25.4 6.7 25.4 1.7 21.9 5.0 21.9 1.3 18.9 3.6 18.9 1.0 16.3 2.6 16.3 0.8 14.1 1.9 14.1 0.6 12.1 1.2 12.1 0.7 10.4 0.5 10.4 0.4 9.05 0.1 9.05 0.0 7.80 0.0 7.80 0.0 6.70 0.0 6.70 0.0 5.80 0.0 5.80 0.0 1.50 0.0	D[4,3] 91.74μm D[3,2] 59.83μm D[v,0.9] 157.28μm D[v,0.1] 31.68μm
Source= data:FCC Record No. =1 Focal Length=300mm Presentation=pia	Beam length:10.0mm Log.Diff=4.701 Obscuration=0.0997 Volume distribution	Model indp Volume Conc. 0.0210% Sp.S.A. 0.1003m^2/cc	D[v,0.5] 81.59μm shape OFF

Table 3.1 Light Scattering Test Result

3.3 Pressure Measurements

Pairs of pressure taps, as shown in Figure 3.3, are connected across Honneywell Microswitch piezo-resistive pressure transducers and are hardwired to a Keithley Metrabyte DAS-20, 12bit A/D board mounted in the PC (Gateway 2000 486).

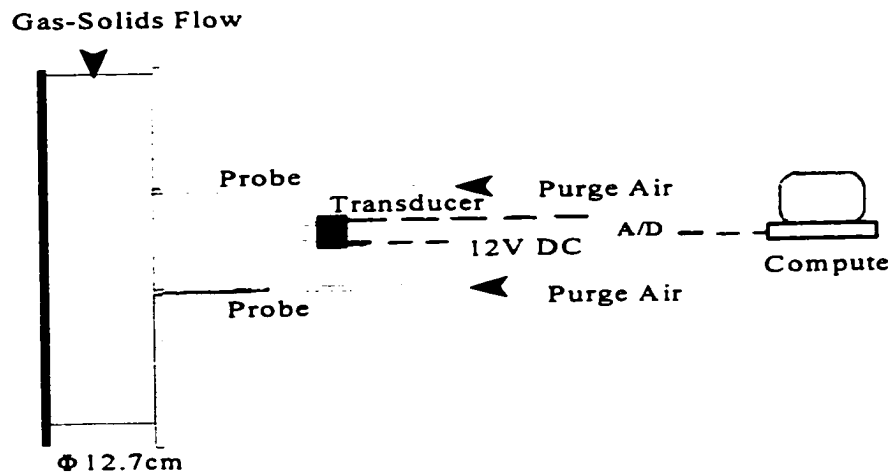

Figure 3.3 Axial pressure Difference Measurement Setup

The Pressure probes are straight copper tubes of 3.175mm ID which are inserted into the column terminating flush with the inside column wall. Purge gas is provided by a compressor with a pressure regulator with flowrate up to 16 CFM at 30 PSIG. The difference in the backpressures of the purge gas is measured by the pressure transducer. The proper purge gas velocity in the probes is determined by

experiment. It is found that the air velocity must be above 3.5m/s to prevent powder from entering the probe and to minimize distortion of the pressure fluctuation signal.

The output signal range of the transducers is 0--6volts. Their frequency response is between one and ten KHz.. To reduce the damping of the pressure signal, the tubing which connects the transducers and probes has to be as short as possible. A sensitive DWYER micromanometer is used to calibrate each individual transducer. Typical calibration curves are shown in Figure 3.4.

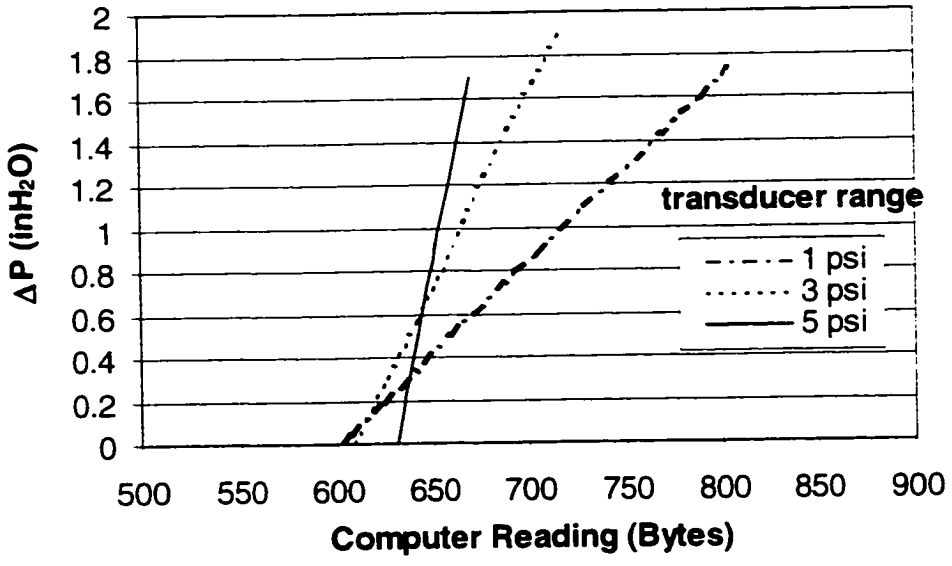

Figure 3.4 Calibration Curves of Pressure Transducers with Different Ranges

Data from the transducers are recorded at 100Hz., and record lengths of at least 8,000 points are provided from each transducer. The measuring time or record

length is an important parameter. Figure 3.5 shows the variation of the calculated mean pressure difference as a function of recording time. It can be seen that for record lengths of 60s or longer, the variation is typically less than 2%. The signal over a finite record length is converted into a mean pressure difference, which is also divided by the tap spacing to give a mean gradient, $\Delta P/\Delta L$, a normalized standard deviation, NSTD, of the fluctuations about the mean value, and a power spectrum of the fluctuations (done by Fast Fourier Transform) to determine the presence of characteristic fluctuation frequencies.

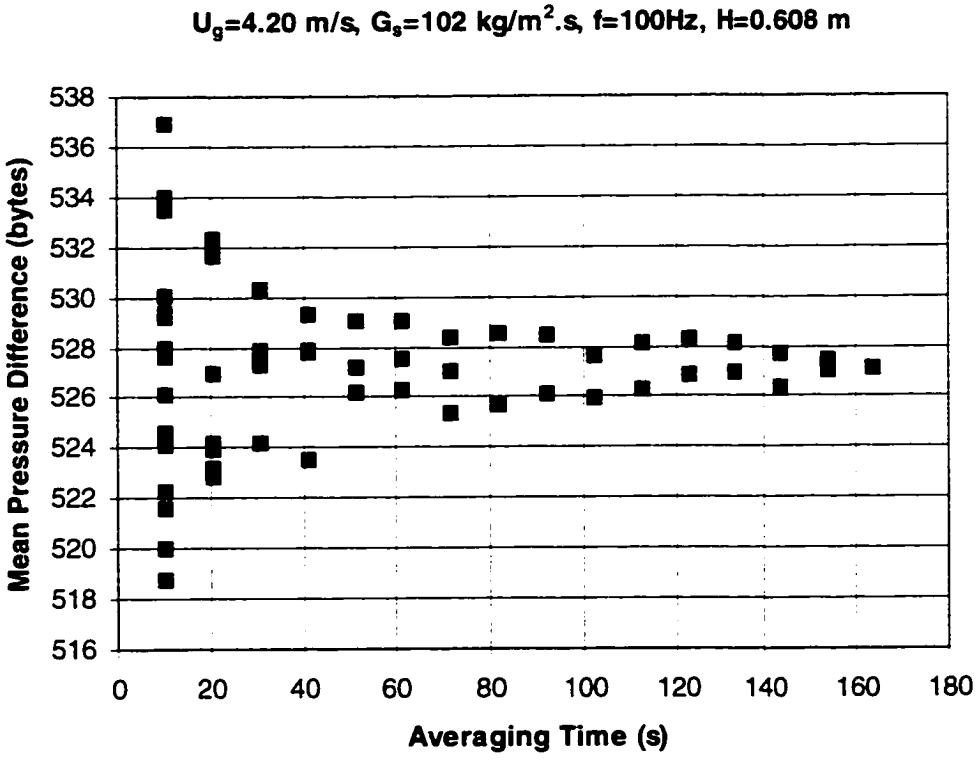

Figure 3.5 Variation of the Mean Pressure Difference with Recording Length

The radial pressure difference across the bed at a specific elevation of the downer is measured with a pair of typical static pressure probes. The setup is shown in Figure 3.6. One of the probes is traversable along the bed, the other is placed in an arbitrary location as a reference. The tips of the probes are smoothly rounded to have less influence on the flow field in the downer. The purge gas ports are located in the vertical section of the probes. To obtain steady pressure signals, the purge air for the two probes comes from the same air line split by a tee fitting. A verification measurement was carried out with only gas flow in the tube. The radial static pressure difference across the traversed chord was found to be very small and constant, less than 0.01 inches H_2O. (Figure 3.7). The dynamic head for this gas velocity is about 0.03 inches of H_2O which implies that these probes do not sense the dynamic head of the flow.

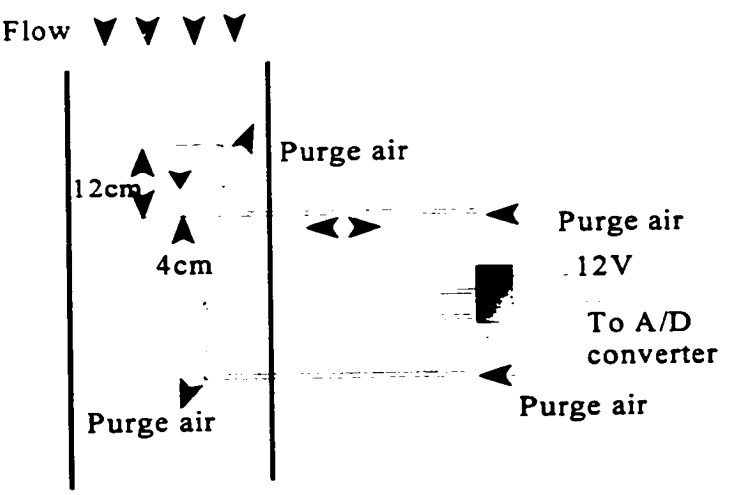

Figure 3.6 Radial Pressure Difference Measurement Setup

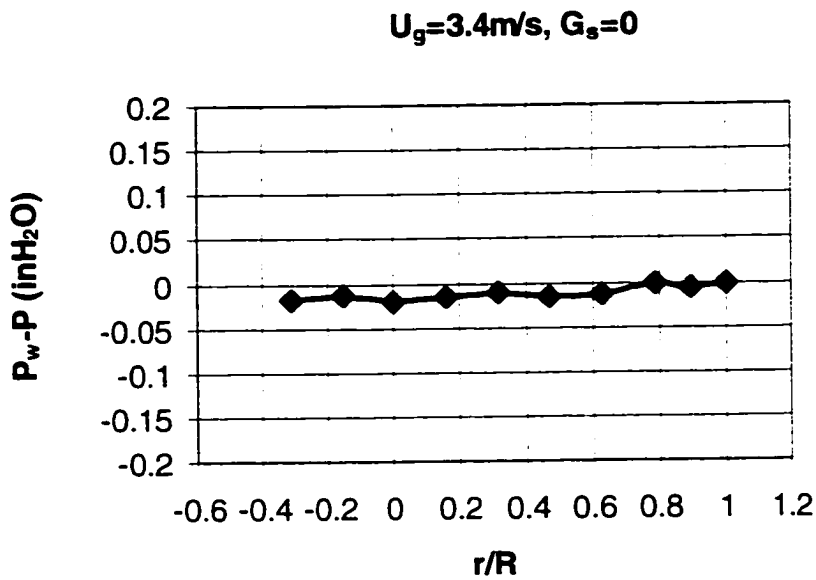

Figure 3.7 Static Pressure of the Air Flow in the Downer Tube

3.4 Solid Circulation Rate Measurement

As mentioned before, the butterfly valve in the middle of the storage bed is used to measure the solid flow rate when it is closed. It has a negligible influence on the pressure balance of the circulating system since it is made out of a sintered plate. The change in differential pressure between tap 13 and 14 in Figure 3.1 is recorded with the data acquisition system after closing the valve. When this valve is closed, the solids fluidize above the sintered plate and the bed below is carried away. The decay rate of the pressure drop due to the disappearing lower bed can be determined. Figure 3.8 shows a typical time series of the pressure signal change. In this particular run, the pressure difference decreased linearly after closing the valve during the recording time from about ten seconds to forty seconds. The valve was reopened afterwards and the pressure reading returned to normal running conditions. The slope of the signal decay from recording time of about 10 seconds to 35 seconds is calculated by applying linear regression. The storage bed is kept in a steady fluidized condition during the run. The rate of the pressure drop is assumed to be only a function of the mass flow rate of the fluidized solid between these two taps. The solid circulation rate can be evaluated by:

$$G_s = \frac{A_{storagetank}}{A_{downer}} \frac{1}{g} \frac{d(\Delta P)}{dt} \qquad (3.1)$$

Where : G_s is the solid circulation rate, kg/m ^{2}s

$A_{storage\ tank}$ is the cross-sectional area of the storage tank

A_{downer} is the cross-sectional area of the downer

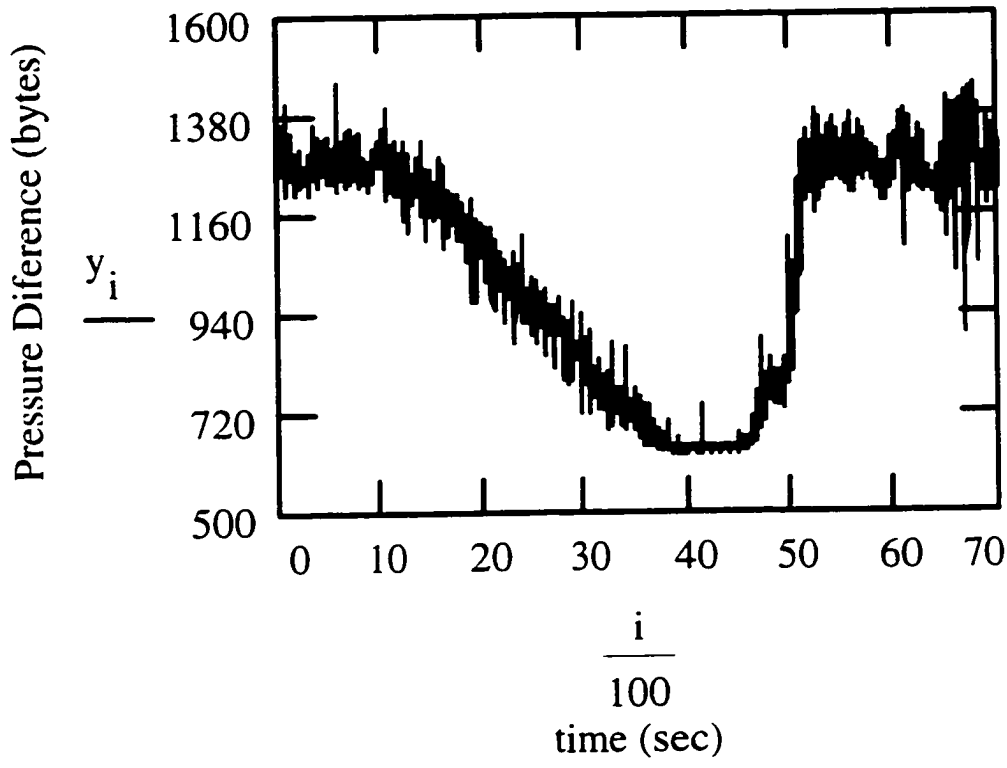

Figure 3.8 Time Series of the Pressure Signal for Solid Circulation Rate Measurement

The error range of the detected solid recirculation rate has been reported as less than 5%. (Schnitzlein and Weinstein, 1988).

3.5 X-Ray System

3.5.1 Hardware

An X-ray system which surrounds the downer is used to record real time flow visualization of bed operation and to measure the radial solid concentration in the downer. Schematic representation of the X-ray carriage assembly is illustrated in Figure 3.9.

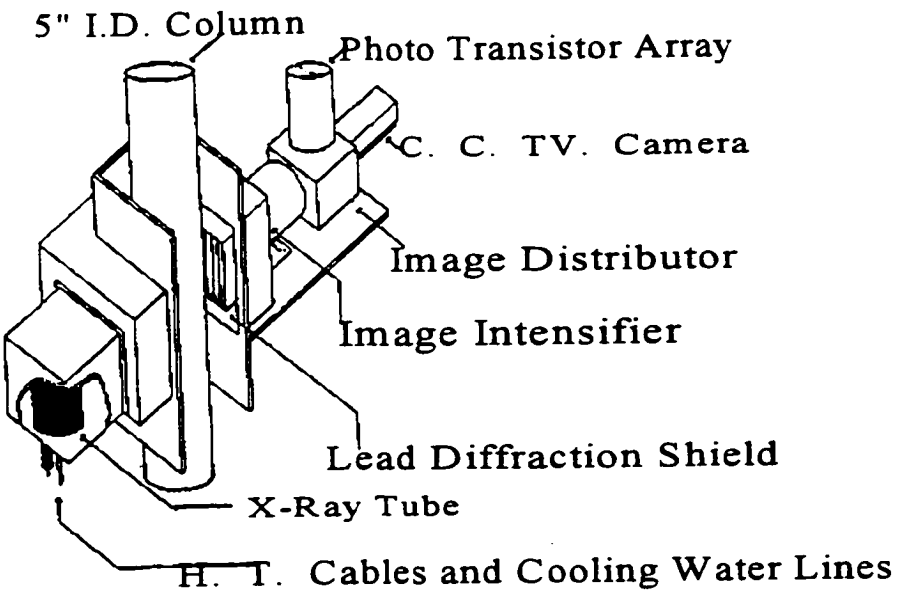

Figure 3.9 Schematic representation of the X-ray carriage assembly

Continuous output and high intensity x-rays come from a Norelco MG 150/300 generator. The voltage and current can be adjusted at the control panel. In this study, a 150 kV X-ray head is used with a maximum level of 30mA at 100KV and 20mA at 150kV. The X-ray tube is a fixed anode type with two focal points of 15 and 40 mm. The focal point of 40 mm is chosen because it provides a wider angle of X-rays. The X-ray image of the bed is projected onto a 9" Phillips image intensifier screen which converts the x-ray into visible light and projects it onto a 3" output screen. The visible light from the intensifier is distributed into two beams by a prism mirror box. Ten percent of the light passes through the mirror and is monitored by a closed circuit camera which is connected to a monitor and a video tape recorder. Nighty percent of the light is projected onto a curved 6" Plexiglas screen by a focal lens. The screen is equipped with photo transistors which convert the optical signal to an electrical one. The sensors are SKN 042 NPN silicon photo-transistors which have a frequency response of 1MHZ. Each of the transistors is connected to an operational amplifier to provide a low noise/signal ratio. (Figure 3.10). The output level can be adjusted by the 100kΩ trimpotentiometer. In this investigation, the output range is between 0 and 10 Volts. The electrical voltages are converted by a Metra-byte Das20 A/D board into digital bytes in a real time computer system (Gateway 2000 486).

The X-ray carriage assembly is mounted on a platform which is guided by

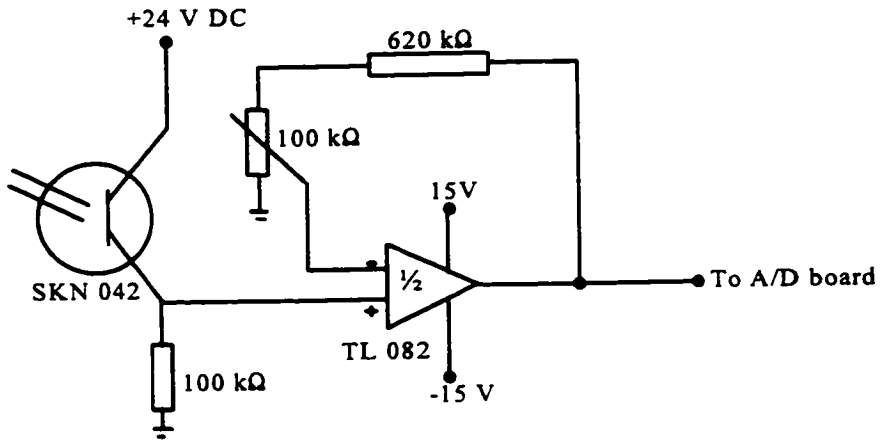

Figure 3.10 Sensor Element Amplifier Circuit

two vertical supports. A winch controlled from the control room is used to move the platform up and down. Every elevation of the downer beginning at 0.76 m(from the top gas-solid entrance) down to 3.5 m can be covered.

3.5.2 Radial Solid Fraction Profile Measurement Principle

The X-ray system beam is filtered to give a narrow frequency spectrum which is treated as monochromatic. The decrease in intensity of a monochromatic beam is proportional to the thickness of the absorbing material:

$$dI = -\mu I(dx) \qquad (3\text{-}2)$$

where:

I is the intensity of the beam

x is length of beam passing through absorbing medium

μ is attenuation coefficient

Boundary condition: $I=I_0$ at $x=0$

Integration of the above differential equation gives the Beer-Lambert Law:

$$I = I_0 . e^{(-\mu x)} \qquad (3\text{-}3)$$

For mono energetic beams, the amount of radiation absorbed by the material is proportional to the material density:

$$\mu = k\,\rho \qquad (3\text{-}4)$$

where k is the mass attenuation coefficient

Energy losses are due to absorption and scattering when the beam travels through the absorbing material. The effect of scattered radiation is reduced by means of a lead diffraction shield. The shield is made from 2.54cm wide lead strips which are mounted parallel to the X-ray path and is placed just in front of the image

intensifier screen.

The Beer-Lambert Law is applied when X-rays pass through the fluidized bed in the downer: (Figure 3.11).

$$Ln(\frac{I_{w-s}}{I_0}) = -(k\rho)_w x_w - (k\rho)_s x_s \qquad (3\text{-}5)$$

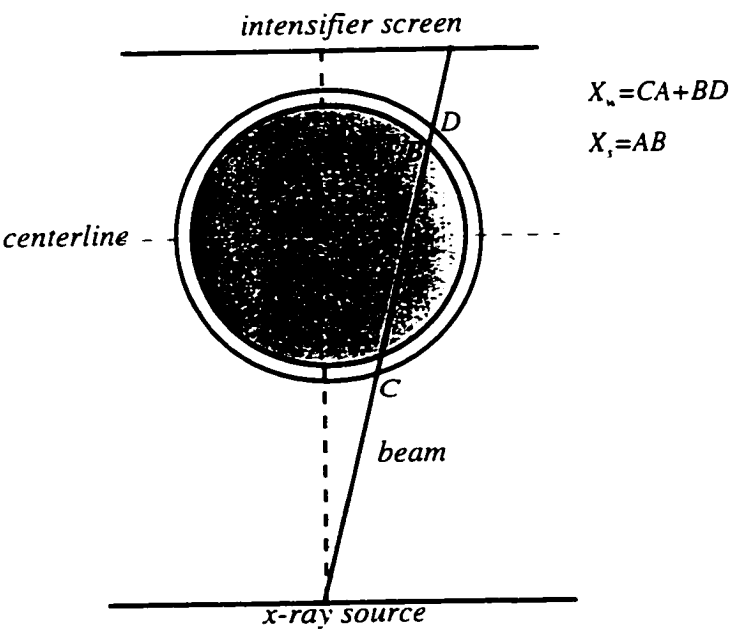

Figure 3.11 Schematic Setup for Chord Average Solid Fraction

The contribution by the downer wall can be obtained from the empty downer when the attenuation is only contributed to by the bed wall. Applying the Beer-Lambert Law gives:

$$Ln(\frac{I_w}{I_0}) = -(k\rho)_w x_w \qquad (3\text{-}6)$$

where: I_{w+s} is the intensity after the beam passes through the fluidized bed

I_w is the intensity after the beam passes through the empty bed

I_0 is the reference beam detecting the intensity of the X-ray source

x_s is the travel distance in the fluidized bed

x_w is the travel distance in the bed wall

Combining eq. (3-5) and (3-6) leads to the relation between the detected intensities and the bed bulk density:

$$Ln\frac{I_{w+s}}{I_0} - Ln\frac{I_w}{I_0} = -k\rho_p(1-\epsilon)x_s \qquad (3\text{-}7)$$

where ρ_p is the particle density.

The mass attenuation coefficient k for the solid is determined by calibration. Six Plexiglas boxes of varying widths (2.54-15.24 cm) were made having wall thickness of 0.64cm which is similar to that of the downer tube. The measurement is based on equation (3-7). The intensity is obtained with the box both full of solid (packed bed) and empty. Knowing the bed density and travel distance, the mass

attenuation coefficient k can be determined. Measurements were done for each of the fifteen photodiodes and an average k was found. (Figure 3.12). A linear fit to the data was obtained with deviation of less than 0.3%. The traveling distance across the downer bed by the x-ray beam to each detector is also determined by equation (3-7). The intensity of the beam passing through a packed bed in the downer is scanned with one row of the phototransistors. The axial beam travels the maximum distance through the aligned bed which has five-inch diameter. Equation (3-7) gives the bulk density of the packed bed with the absorption coefficient k obtained by the calibration procedure described above. The lengths of the traveling distance of the x-ray beams through the bed with known bulk density are obtained by equation (3-7) using the calibrated absorption coefficient.

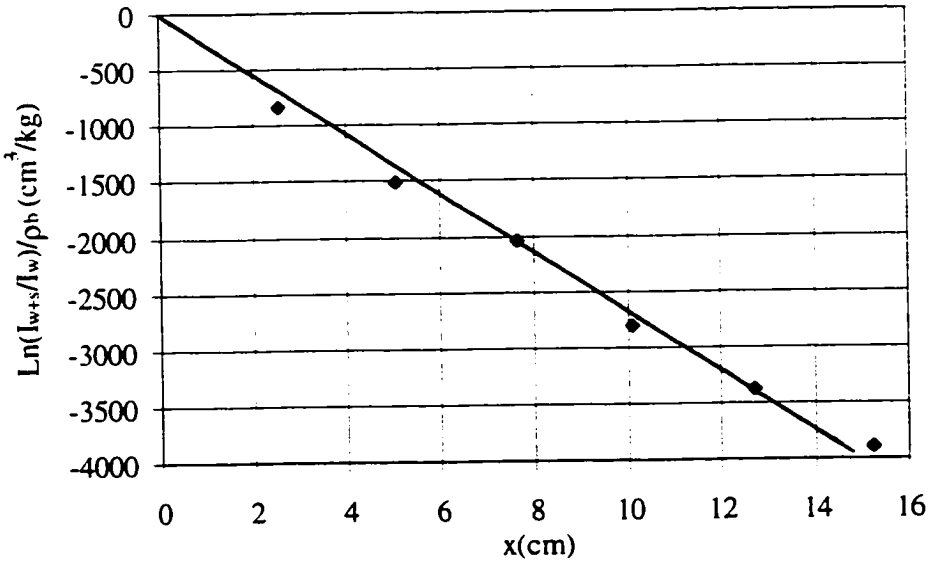

Figure 3.12 X-ray Calibration Curve for FCC

A radial solid density profile is obtained by using the method of image reconstruction. When the x-ray passes though the nonhomogeneous suspension the detected attenuation is the integral of the local attenuation along the beam path. As illustrated in Figure 3.13, the detected intensity is given by the following expression according to the Beer-Lambert law.

$$Ln\frac{I_{w+s}}{I_0} - Ln\frac{I_w}{I_0} = -\int_A^B k\rho(x,y)ds \tag{3-8}$$

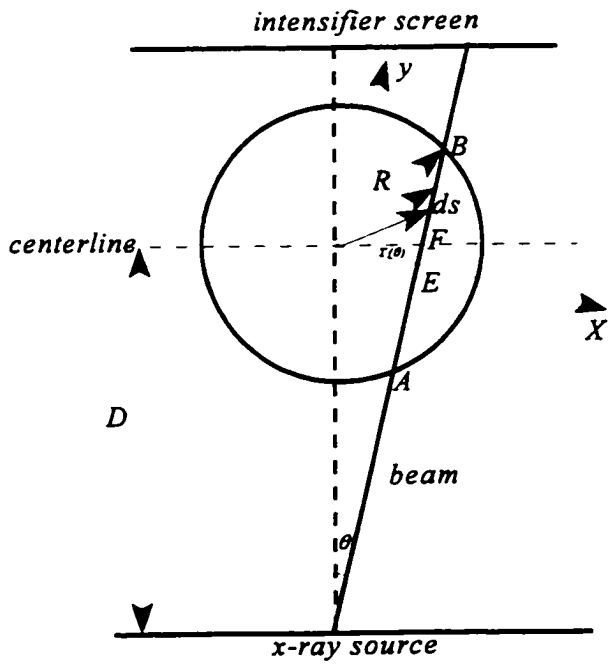

Figure 3.13 Geometry for Image Reconstruction

Assuming axial symmetry, the movable coordinates x and y are related to the radius r by

$$r=\sqrt{x^2+y^2} \tag{3-9}$$

The local solid fraction distribution $1-\epsilon(r)$ is then reconstructed as a function of the radius in a polynomial form:

$$1-\epsilon(r)=a_0+a_1r+a_2r^2+\ldots+a_nr^n \tag{3-10}$$

With the boundary condition at r=0

$$\left\{\frac{\partial \rho(r)}{\partial r}\right\}_{r=0}=0 \tag{3-11}$$

The coefficient a_1 in eq. (3-10) becomes zero. Equation (3-8) can be written as:

$$\left[Ln\frac{I_{w-s}}{I_0}-Ln\frac{I_w}{I_0}\right]\left(-\frac{1}{k\rho_s}\right)=\int_A^B(a_0+a_2r^2+\ldots+a_nr^n)ds \tag{3-12}$$

The integration along the beam path from A to B is equal to twice the integration from either A to E or E to B. Equation (3-12) becomes:

$$[Ln\frac{I_{w-s}}{I_0}-Ln\frac{I_w}{I_0}](-\frac{1}{k\rho_s})=2\int_0^{\frac{s}{2}}(a_0+a_2r^2+\ldots+a_nr^n)ds \tag{3-13}$$

Moreover:

$$\begin{gathered} x=T(\theta)=D\sin\theta \\ y=s, dy=ds \\ r=\sqrt{x^2+y^2}=\sqrt{D^2\sin^2\theta+y^2} \\ \frac{s}{2}=\frac{AB}{2}=y_2=\sqrt{R^2-D^2\sin^2\theta} \end{gathered} \tag{3-14}$$

so,

$$[Ln\frac{I_{w-s}}{I_0}-Ln\frac{I_w}{I_0}](-\frac{1}{k\rho_s})=\int_0^{y_2}(b_0+b_2r^2+\ldots+b_nr^n)dy=b_0P_0+b_2P_2+\ldots+b_nP_n \tag{3-15}$$

The coefficients a_0, a_2,...a_n are absorbed in b_0,b_2,...b_n.

$$\begin{gathered} b_0=2a_0 \\ b_2=2a_2 \\ \ldots \\ b_n=2a_n \end{gathered} \tag{3-16}$$

The Polynomial function P_0, P_2, ...,P_n are:

$$
\begin{aligned}
P_0 &= y_2 \\
P_2 &= \int_0^{y_2} (D^2 \sin^2\theta + y^2)\,dy = y_2 D^2 \sin^2\theta + \frac{1}{3} y_2^3 \\
&\cdots\cdots \\
P_n &= \int_0^{y_2} (D^2 \sin^2\theta + y^2)^{\frac{n}{2}}\,dy
\end{aligned}
\tag{3-17}
$$

In the calculation of reconstruction, the left-hand side of eq. (3-15) is known from the measured signals and the right-hand side is a polynomial. The set of equations with unknown coefficients can be solved by linear regression and optimization.

3.6 Local Solid Flux Measurement

A non-isokinetic sampling probe (Monceaux et al. ,1985; Rhodes et al., 1988) is used to estimate the local solid flux in the downer. The schematic of the sampling device is shown in Figure 3.14. It is a modified design developed by Kostazos (1997). A discussion of non-isokenetic probes for riser flow is given in this reference. This work is the first known use of these probes in downflow, and global

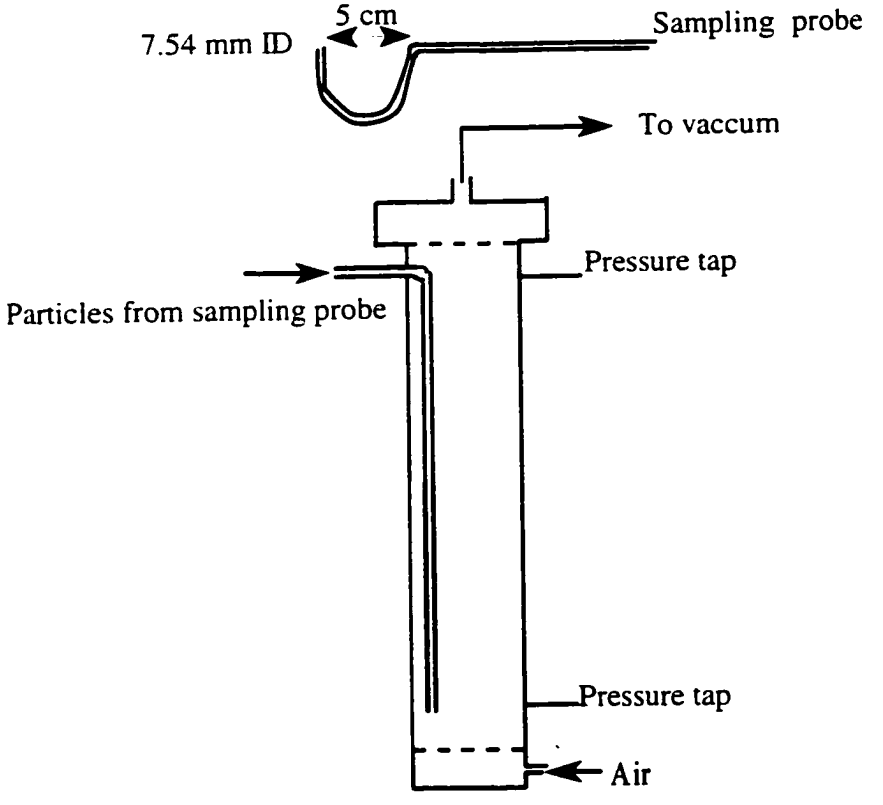

Figure 3.14 Local Solid Flux Measurement Device

solid flow continuity, as described below, is the only additional condition applied in this work to validate its use in downflow. The sampling probe is 7.54 mm ID and 9.54 mm OD. The solids in the downer are aspirated with the vacuum through the sampling probe into a 1.22m tall and 7.62 cm ID fluidized bed which maintains minimum fluidization. The top of the bed is a sintered plate to separate the solids and gas. Two pressure taps are installed along the bed to measure the increase of the pressure difference with time due to the filling of the solids from the downer. The increasing rate of the pressure difference gives the solid flux by:

$$[G_s(r/R)]_{UporDown} = \frac{A_{SamplingBed}}{A_{probe}} \frac{1}{g} \frac{d(\Delta P)}{dt} \qquad (3\text{-}18)$$

where $G_s(r/R)$ the local solid flux (kg/m^2s) is equal to $[G_s(r/R)_{Down}-G_s(r/R)_{Up}]$

$A_{sampling\ bed}$ is the cross sectional area of the sampling bed

A_{probe} is the cross sectional area of the sampling probe

The probe is traversable along the radial direction of the bed. The aspirating velocity was kept as small as possible to insure smooth suction flow from the downer. Rotating the probe 180 degrees to make the probe facing downwards did not change the elevation of the probe location in the bed due to the configuration of the probe. It was necessary to measure the solids flow rate with the probe tip facing both upwards and downwards and take the difference in order to eliminate the non-isokinetic sampling effect. A test to insure that the net rate of solids aspirated was

independent of the aspirating velocity over the range employed was conducted (Kostazos, 1997). Furthermore, the integral of the measured flux over the cross-section was always compared to the independently measured circulation rate. Agreement was always within ±11%.

3.7 Gas Dispersion and Backmixing Measurement

A gas tracing technique (Weinstein et al, 1989) is used to provide a picture of the gas mixing in the high velocity two phase downflow. In order to eliminate the effect of gas adsorption on catalyst, helium was chosen as a tracer.

The complete set up of the measurement is shown in Figure 3.15. A steady stream of tracer gas was injected by a probe at the center point of the bed at one

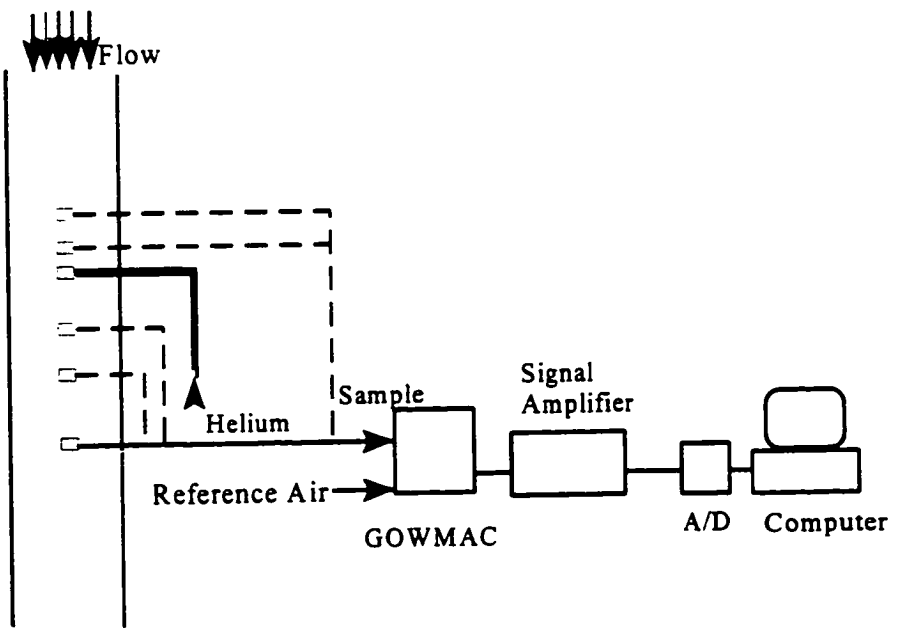

Figure 3.15 Experimental Setup of Helium Tracing Test

elevation. The injection could be considered as a point source since the inner diameter of the probe was only 3.175 mm. During the run, the helium injection velocity of the probe was kept smaller than the gas superficial velocity of the bed to minimize the disturbance of the flow. Samples were taken at three elevations (x=0.3m, 0.76m, 1.3m) downstream below the injector plane and at two elevations (x=-0.14m, -0.3m) upstream above the injector plane. The sampling probes were covered by a porous plug filter to prevent particles from entering the instrument. The sample gas and the reference air were drawn into an on-line GOWMAC thermal conductivity analyzer connected to a data acquisition system. The fluctuations in the signal from GOWMAC were smoothed by averaging 4096 readings at 100Hz. It was shown that such a recording length is long enough to give reproducible data.

IV. RESULTS AND DISCUSSION

4.1 Time Stability and Axial Symmetry

Typical time series of the pressure measurements are shown in Figure 4.1. The ordinate of the chart is the apparent solid fraction defined as:

$$\overline{(1-\epsilon)}_{apparent} = \frac{1}{\rho_p g}\left(\frac{\Delta P}{\Delta L}\right) \tag{4-1}$$

which is converted from the pressure difference reading.

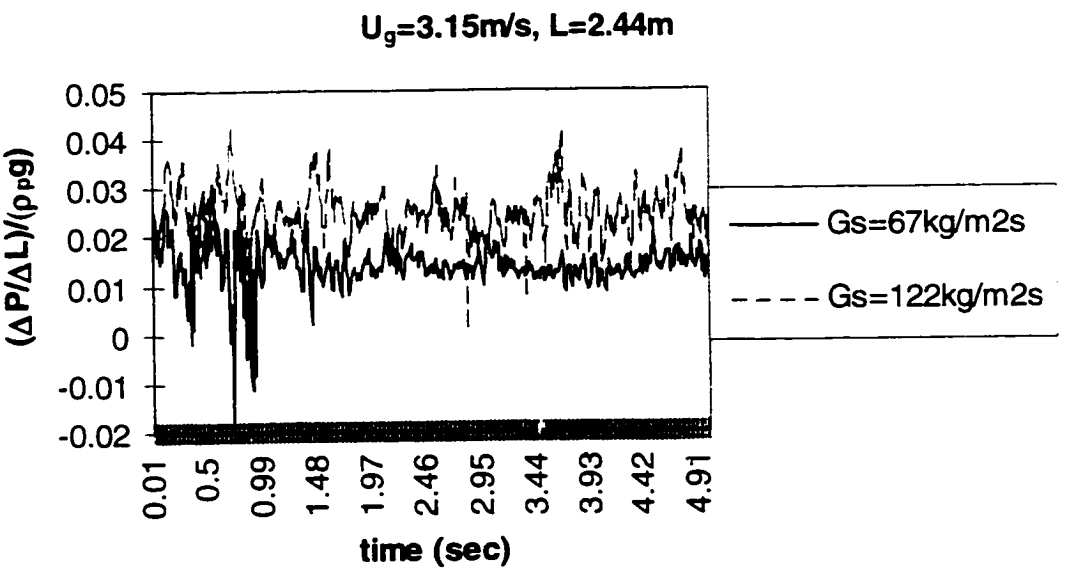

Figure 4.1 Time Series of Pressure Difference

To analyze fluctuation frequencies of the readings accurately, the sampling frequency should be ten times larger than the largest frequency to be analyzed (Paul, 1982). For this work, the sampling frequency of 100Hz was chosen, the detectable frequency can be as low as 10Hz with a negligible error. Typical power spectra of the pressure fluctuation are shown in Figure 4.2. The power, or ordinate of the graph represents the magnitude of the fluctuations while the abscissa is the frequency at which that power level is found. Characteristic frequencies of the turbulence flow would be denoted by spikes on these graphs. Note that the power is higher with larger solids/gas ratio than with lower ratio. Higher solid loading would increase the local density and/or turbulence of the flow and result in larger pressure fluctuations.

As described in the previous chapter, the record length must be considered to insure that the data are reproducible. It was found in Figure 3.5 that at least a one minute record length for pressure measurement is necessary. A similar test was carried out to find the required record time for the x-ray measurement. The solid fractions measured by x-ray are computed from time segments of ten seconds. It is seen in Figure 4.3 that with increasing averaging time the time dependence of the solid fraction decreases. To fall within ±1% error band, the x-ray readings must be averaged over a time period of at least 20 seconds. Although the standard deviation of the x-ray measurement is smaller than that of pressure difference measurement, a long record length is still chosen for both tests to obtain accurate values of the

normalized standard deviation of the readings. In this investigation, 102 seconds for pressure measurement and 82 seconds for x-ray measurement were chosen for the record lengths.

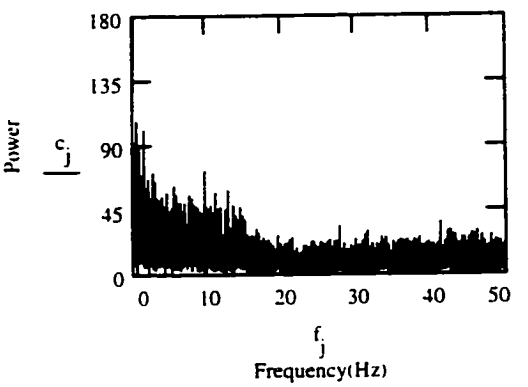

Figure 4.2(a) U_g=3.15m/s, G_s=67kg/m^{2}s

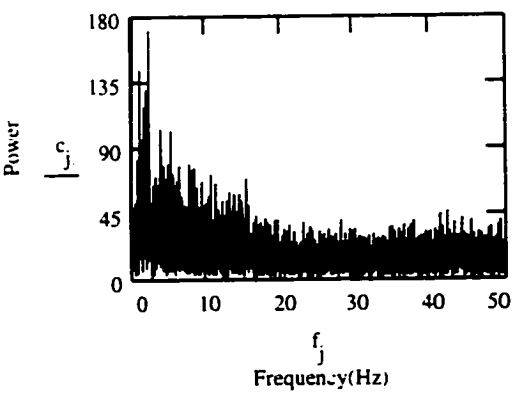

Figure 4.2(b) U_g=3.15m/s, G_s=122kg/m^{2}s

Figure 4.2 Power Spectrum of Pressure Fluctuations

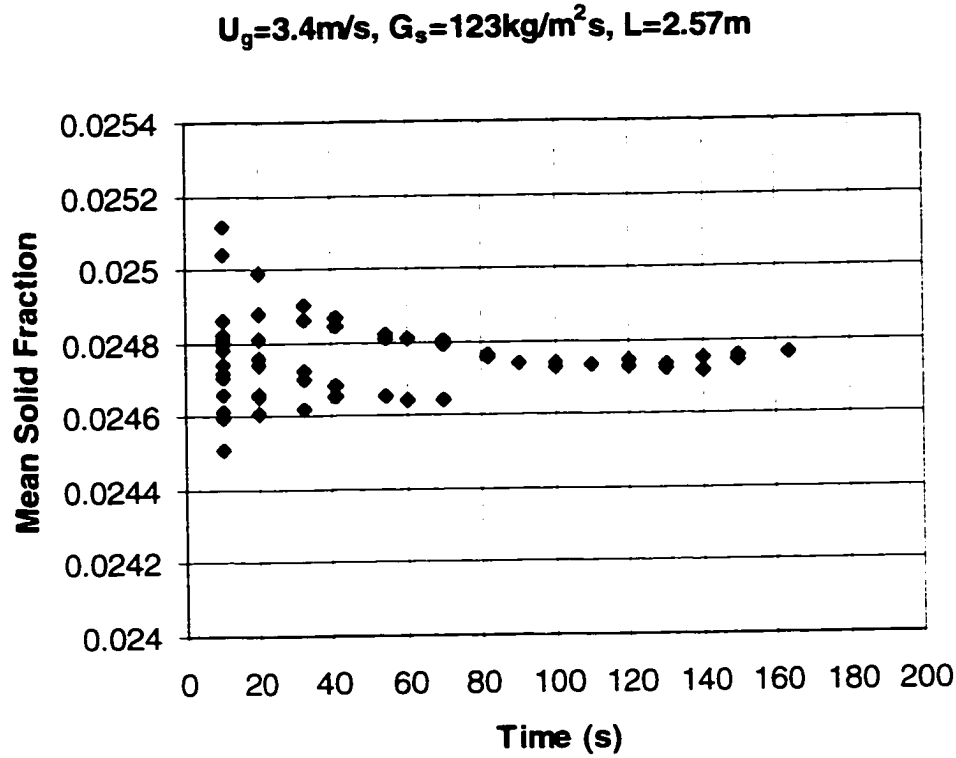

Figure 4.3 Variation of the Mean Solid Fraction with Recording Length

The projected x-ray image readings only give the chordal average solid fraction. The solid fraction profile is obtained with the chordal absorptometry technique which is based on an assumption of axial symmetry of the solids distribution in the downer tube. From the chordal average reading of each phototransistor without image reconstruction, the symmetry of the solids distribution in the x-direction in Figure 4.4 can be determined. Figure 4.5 shows that the solids distribution in the downer is asymmetric in the x-direction within the solids entrance region, and becomes symmetric about 1.4m below the solids inlet. To verify such

axial symmetry and prove the symmetry in the radial direction, a set of flux probes was designed to measure the solids downflow flux at four points in the cross-sectional area of the downer, as also shown in Figure 4.4. These four measured points are each located at the same elevation of the downer and with the same r/R radial position. As shown in Figure 4.6, the solids downflow flux can be considered to be axially symmetric after the solids entrance region.

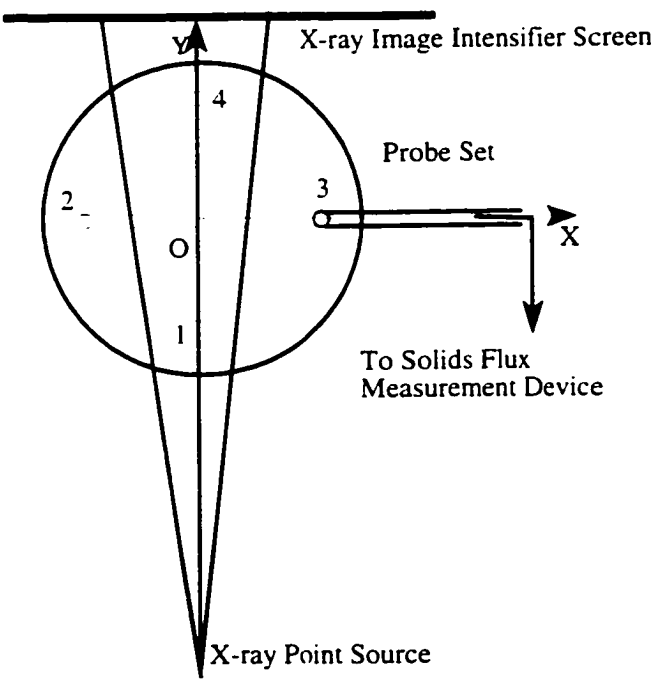

Figure 4.4 Cross-section of the Downer with Solids Downflow Flux Measurement Probe Set

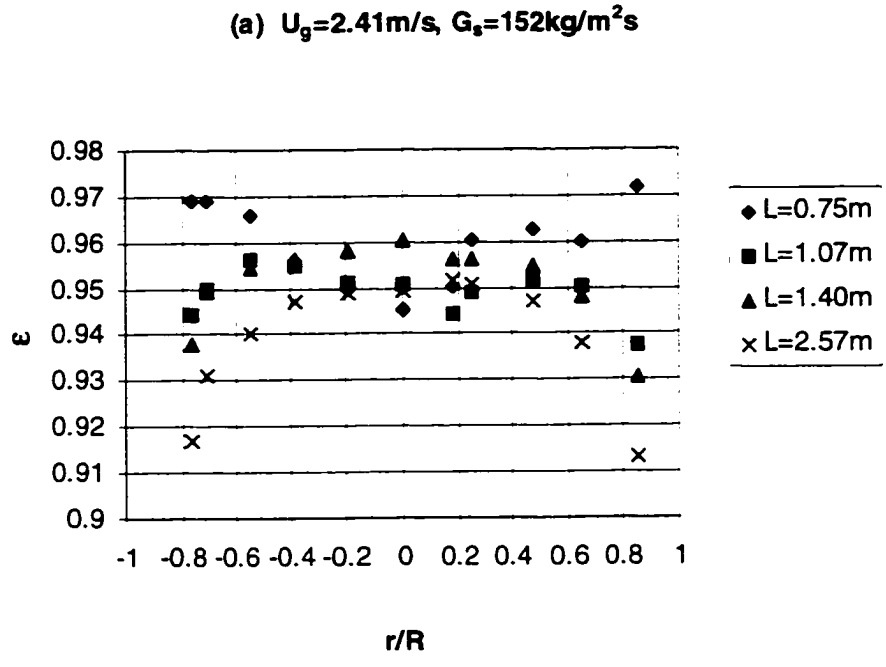

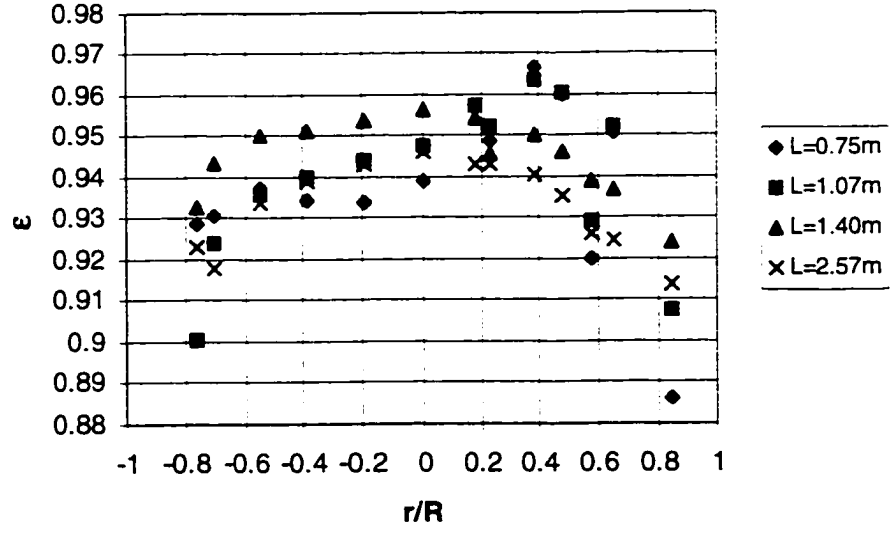

Figure 4.5 Chordal Average Bed Voidage Profiles

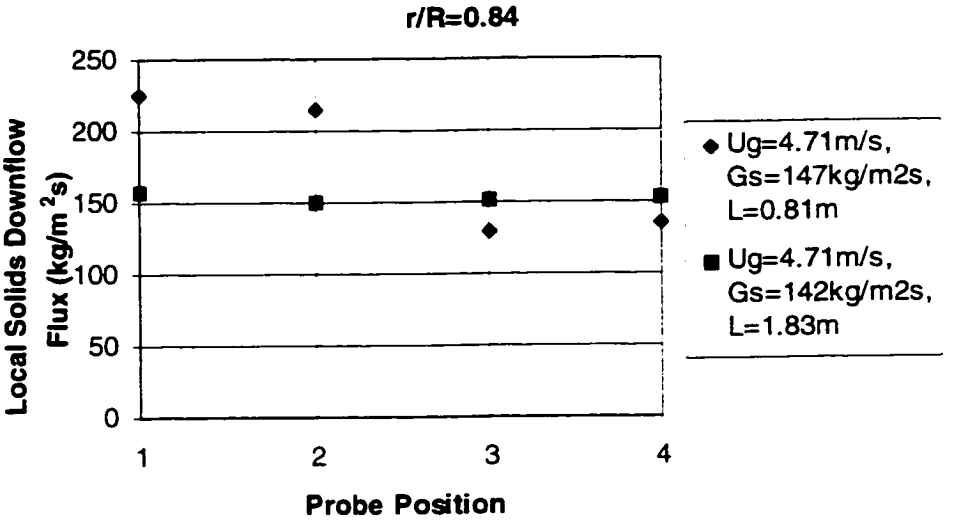

(a)

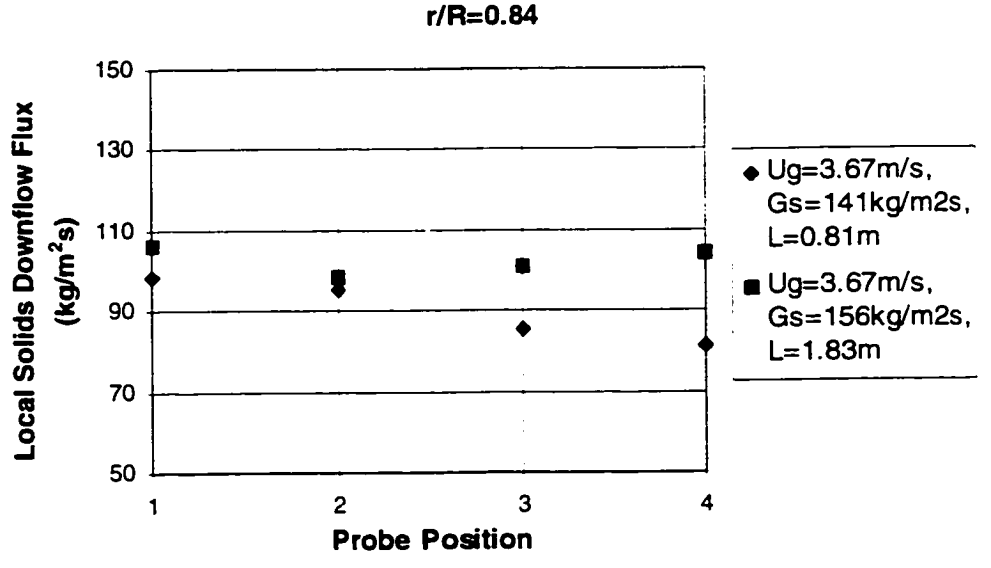

(b)

Figure 4.6 Local Solids Downflow Flux at Four Bed Locations

4.2 Pressure Profile

The axial pressure profile is presented in Figure 4.7. L is the distance measured downward from the solids entrance. Additional complete data sets can be found in Appendix B. The measurements indicate a "bow" shape distribution of the pressure in the downflow fluidized bed. The pressure first decreases from the flow inlet downwards along the axial direction, then increases gradually to the highest point at the bottom of the downer. The pressure gradient changes sign from negative to positive along the flow path. The location of the minimum pressure depends on the operating conditions.

In Cartesian coordinates, the one-dimensional momentum equation for the gas-solid flow in the downer can be expressed as:

$$-\frac{dp}{dx}+\rho_p g(1-\epsilon)=G_s\frac{du_p}{dx}+\frac{dP_f}{dx} \qquad (4\text{-}2)$$

where x is the direction of the flow, i.e. the direction of gravity, and dP_f/dx is the frictional pressure drop. It is usually considered to be of two parts: a gas phase resistance dP_{fg} and a solid phase resistance dP_{fs}.

$$dP_f=dP_{fg}+dP_{fs} \qquad (4\text{-}3)$$

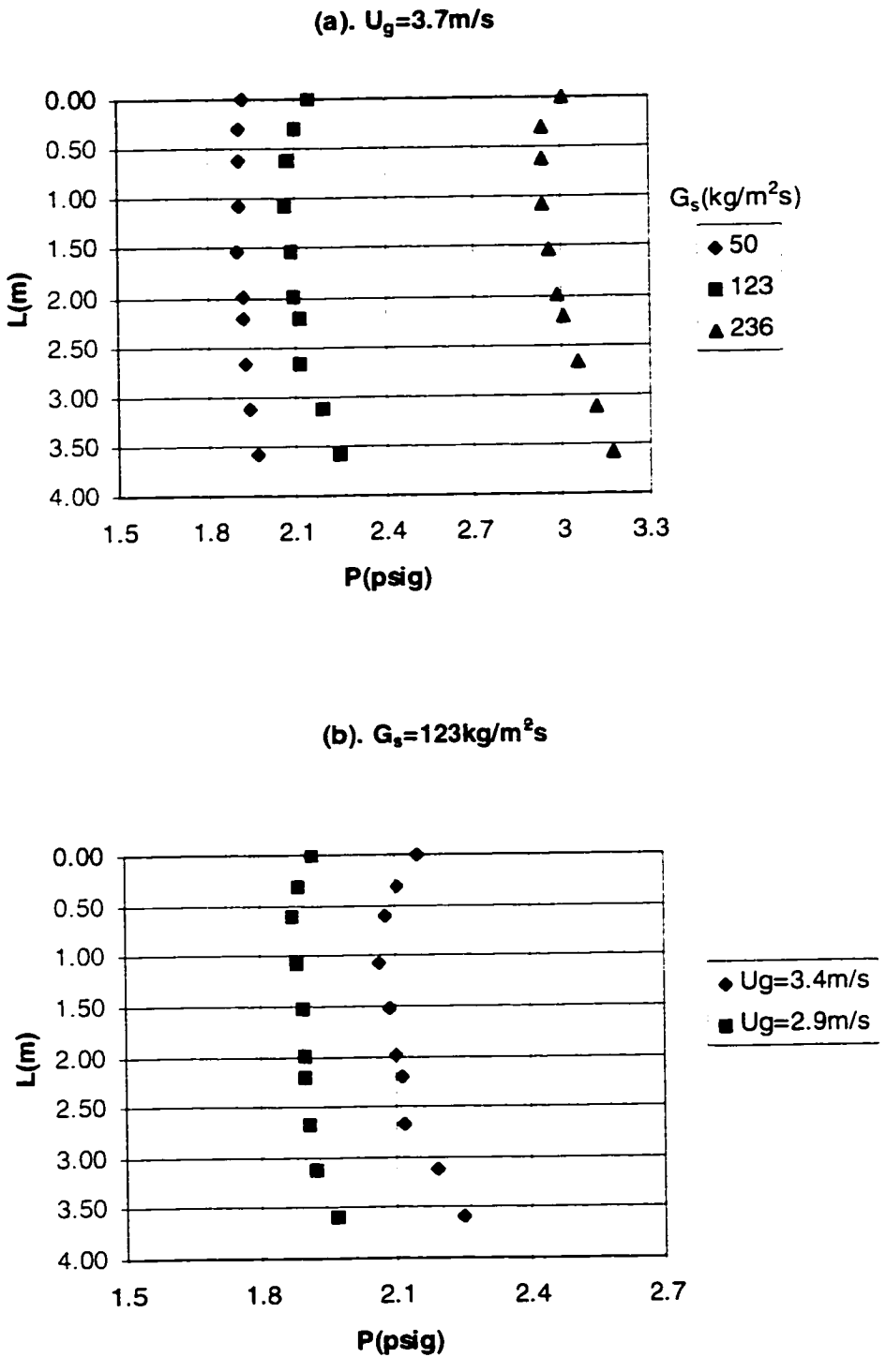

Figure 4.7 Axial Pressure Profile in the Downer

Fanning's equation gives:

$$\frac{dP_{fg}}{dx} = 2f_g \frac{\rho_g u_g^2}{D} \tag{4-4}$$

where f_g is the frictional coefficient.

dP_{fs} can be calculated from the empirical relation:

$$\frac{dP_{fs}}{dx} = \frac{\pi}{2} f_p \frac{\rho_g u_g^2}{2} \left(\frac{\rho_p}{\rho_g}\right)^{\frac{1}{2}} \frac{G_s}{u_g \rho_g \epsilon} \frac{1}{D} \tag{4-5}$$

where f_p is the solid phase frictional coefficient.

Calculation of dP_f/dx based on (4-4) and (4-5) indicates that this term is usually small and negligible compared to the others. Equation (4-2) can be rewritten as:

$$\frac{dp}{dx} = \rho_p g(1-\epsilon) - G_s \frac{du_p}{dx} - \frac{dP_f}{dx} \tag{4-6}$$

The terms of the right-hand side of equation (4-6) represent the gravitational effects, the solid acceleration and the frictional effects on the pressure gradient respectively. The competition between these terms in the above expression can be seen in the experimental results. When particles enter the downer reactor, they accelerate to a

high velocity driven by the gravity and gas drag forces. The second term $G_s(du_p)/(dx)$ is thus positive and large. The negative pressure gradients indicate the predominance of solid acceleration and friction over gravity head. In the process of acceleration, the slip velocity decreases rapidly, going through zero and eventually becoming negative, and the acceleration effects decline compared with those due to gravity. When $G_s(du_p)/(dx)$ decreases to the extent that the gravity becomes predominant, the pressure head begins to increase. Because of the restriction of the U-bend structure and the pressure balance requirement of the circulating system, the particle velocity will decrease before reaching the U-bend section. This deceleration of the particles results in a large increase in the solid fraction and hence, of the pressure. In general, the minimum pressure point (dP/dx=0) is typically located between 0.5 and 1.5m from the entrance for this downer-riser loop configuration.

As shown in Figure 4.7(a), in the higher solid flux case, the pressure at the bottom of the downer is relatively high due to the accumulation of particles just above the U-bend section. The absolute value of the pressure is higher for the higher solids flux cases since more dynamic power is needed to transport denser suspensions back up the riser. It also can be seen from Figure 4.7(b) that the absolute value of the pressure is higher at higher superficial gas velocity with the same solid circulation rate. The larger pressure head required to overcome the resistance of the entire flow system in the higher gas velocity operating condition gives a higher value

of pressure everywhere in the system than that in the lower gas flow rate case.

It has been found that the radial static pressure difference in the downer is very small and hardly detectable. Compared with the riser, the downer gives a much more uniform pressure distribution radially. (See Figure 4.8).

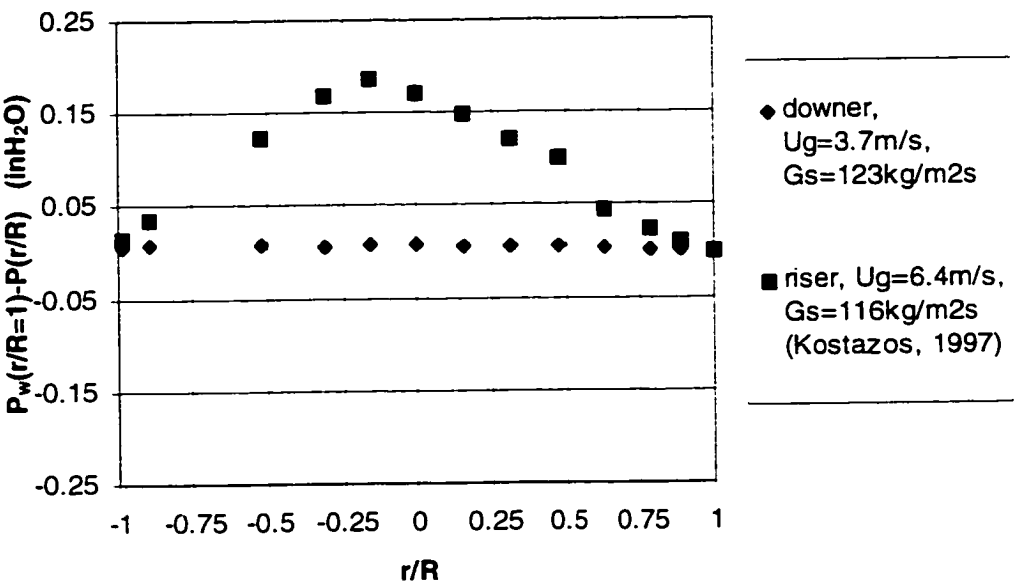

Figure 4.8 Radial Pressure Profiles in the Downer and the Riser

4.3 Radial Solid Fraction Profile

The radial catalyst density distribution in a downer reactor is an important characteristic and it plays a significant role in the yield and selectivity of the reaction. It also has great influence on the mixing of reactants and catalyst.

In this investigation, the bed x-ray image from the image intensifier is read with a phototransistor array to A/D board and the chordal absorptometer technique described in section 3.5.2 is used to obtain radial profiles of solid loading. Measurements were taken at four different elevations of the downer, from 6 L/D to 26 L/D below the solids material entrance.

Figure 4.9(a) and 4.9(b) show the radial solid density profiles at four different locations in the downer bed. It can be seen that the curve representing the radial solid fraction distribution in the entrance region (L=0.89m) shows different behavior from the other curves below the inlet region. This is because of the lack of axial symmetry of the solids distribution within the entrance region. The axial symmetry assumption on which the image reconstruction method is based is not valid. Therefore, the curve for L=0.89m is not the true solid fraction radial distribution. Below the inlet region, flow is essentially symmetric and the radial solid concentration profiles indicate a segregation of the two phase flow (as also occurs in

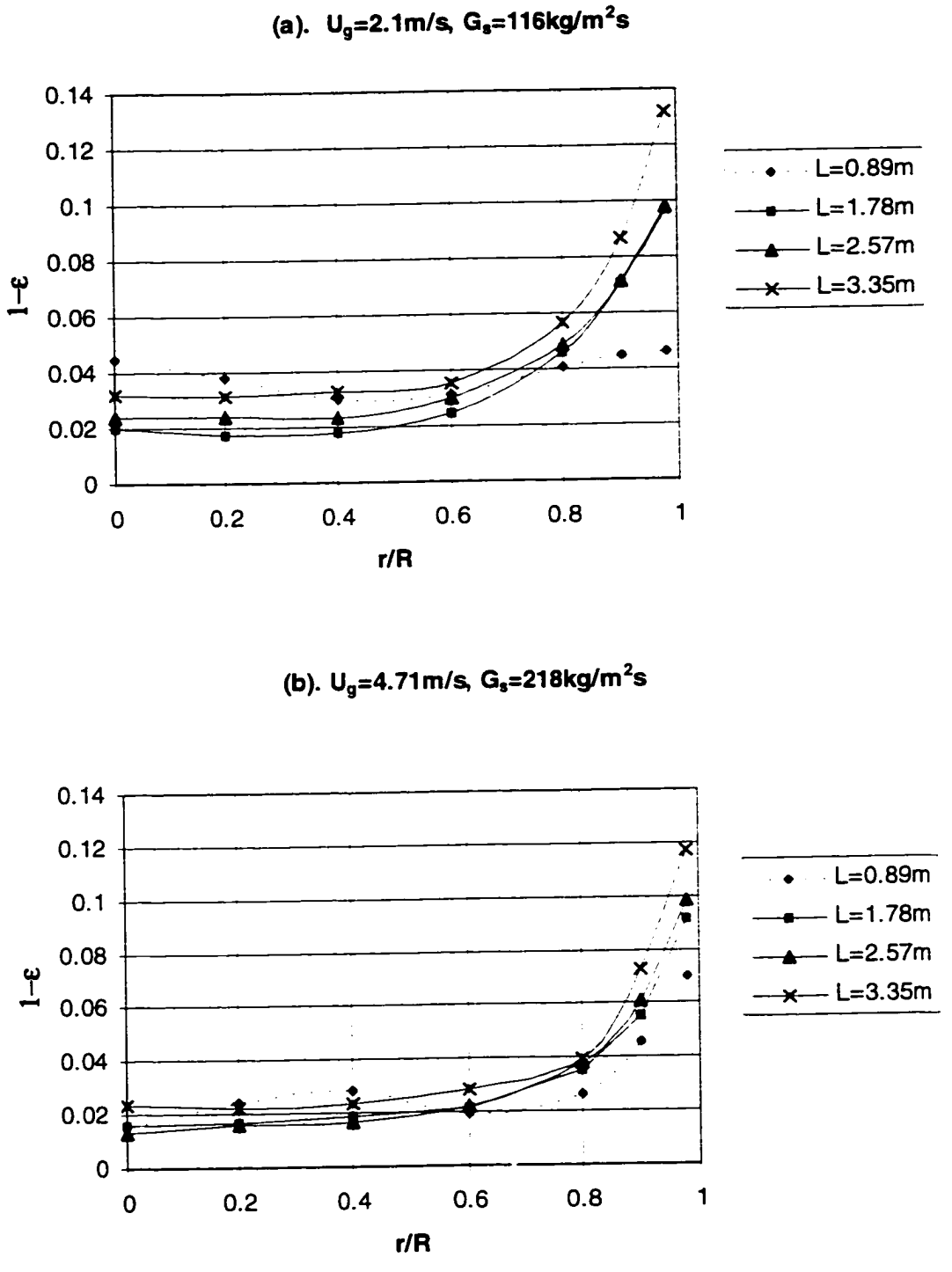

Figure 4.9 Radial Solid Density Profiles at Different Elevations in the Downer Bed

a riser) with a dilute core region surrounded by a dense annular wall region. The shape of the solid fraction profile is near-parabolic in the dense region and is flatter in the dilute region. This core-annulus structure occurs throughout the downer. Such a solid distribution is typical and independent of the operating conditions for the L/D=35 downer used in this investigation. It is also observed that the solid fraction at the bottom of the downer is slightly higher than that at the other locations along the whole downer radius which is proof of the particle deceleration.

Figure 4.10(a) and 4.10(b) display the solid concentration profiles at two locations with a variation of solid circulation rate at the same superficial gas velocity respectively. It is obvious that the larger the solid/gas ratio, the denser is the bed based on a cross-sectional area average. Figure 4.11 shows the solid fraction profiles for different superficial gas velocities with the same solids circulation rate.(The solid flowrate could not be held absolutely constant and varied from 112 to 123 kg/m^2s). The results are consistent with that in Figure 4.10. That is, raising the gas velocity while keeping the same total solid flux leads to the lower solid/gas flow rate ratio and further decrease the whole bed density.

The non-uniform radial solid distribution in downers was reported by other workers using γ-ray absorptometry or fiber optic probes. (Zenklusen, 1997; Herbert et al, 1994; Bai et al., 1991). Comparison of the results between this work and the

others is shown in Figure 4.12. It can be observed that the solid fraction exhibits a larger value near the column wall than the central region of the downers in all the works. Note that Zenklusen's experiment was carried out with a very dilute gas-solid suspension even if in a big column. He claimed that "homogenous" flow had been achieved although the microview (Figure 4.13) of the solid distribution in the downer shows a similar profile to this work. Results obtained by Herbert et al. and Bai et al. show similar solid fraction profiles which have dense annular regions but which get dilute very close to the walls. However, the small diameter downer used by Herbert et al. usually results in strong wall region effects, Bai's experiment measured the solid fraction very close to the wall which could have had a strong reflection effect on the optical fiber probe. Nevertheless, the solid fractions measured away from the wall show similar profiles to this work. In this investigation, relatively large solid/gas ratios which form a dense bed in a pilot plant scale downer have been investigated. The core-annulus flow pattern is very clear in this unit. Additional measurement results of solid fraction can be found in Appendix C.

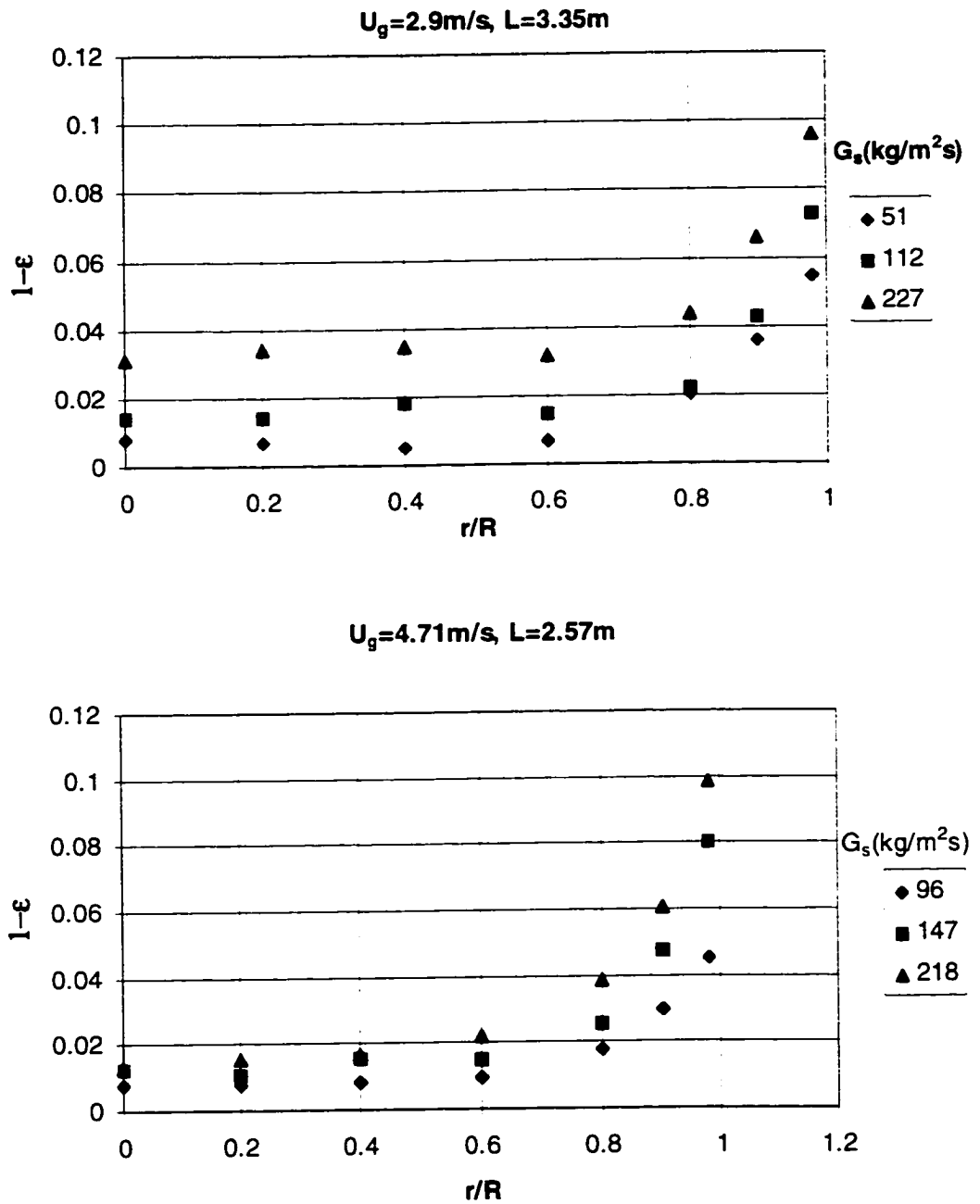

Figure 4.10 Solid Flowrate Influence on the Radial Solid Density Profile

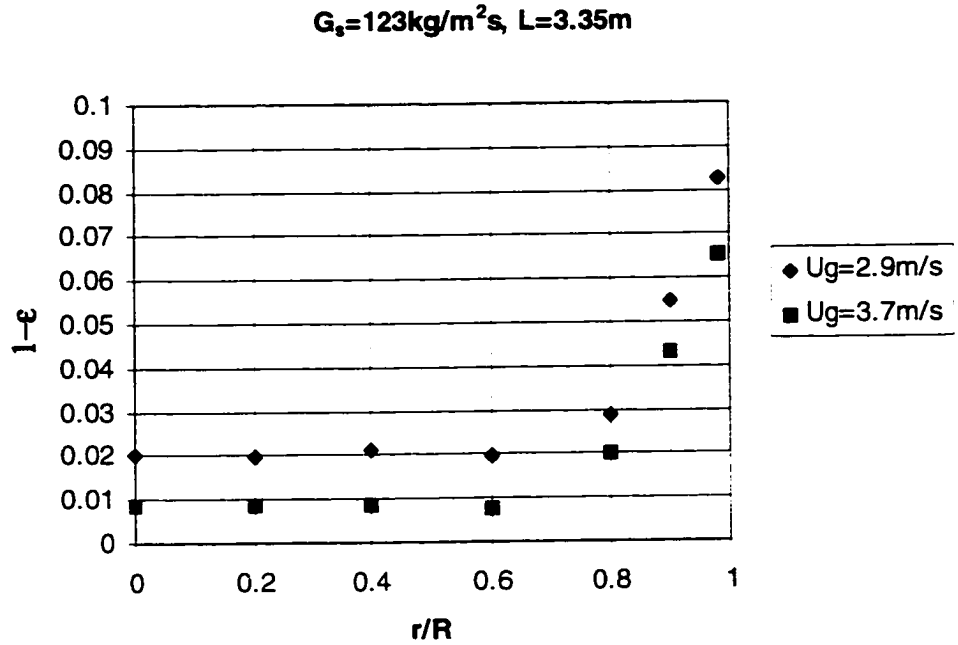

Figure 4.11 Superficial Gas Velocity Influence on the Radial Solid Density Profile

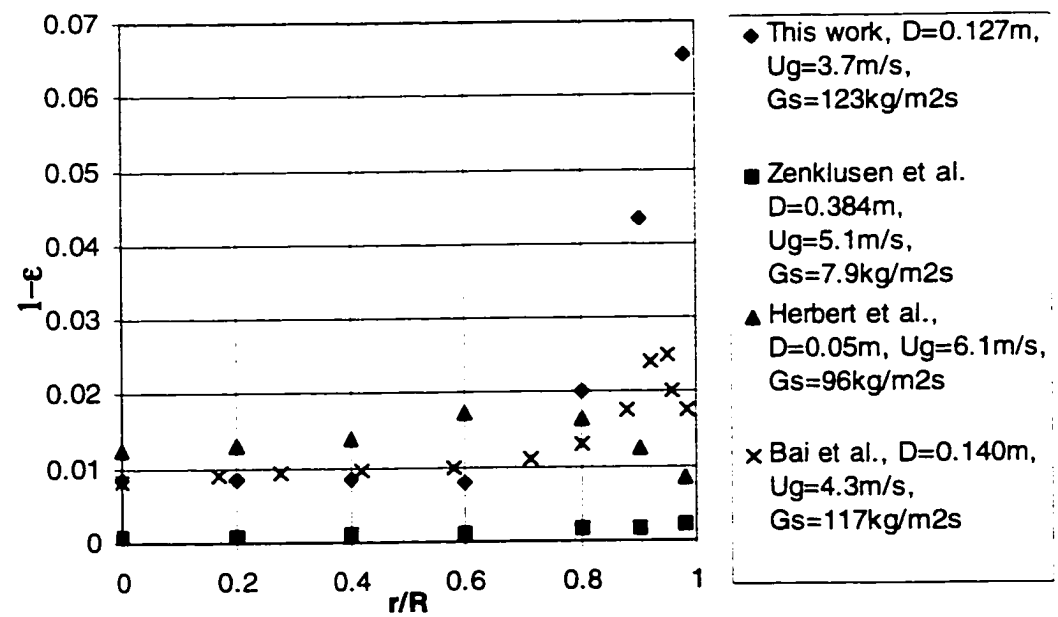

Figure 4.12 Comparison of Solid Fraction Profiles Obtained in Different Units

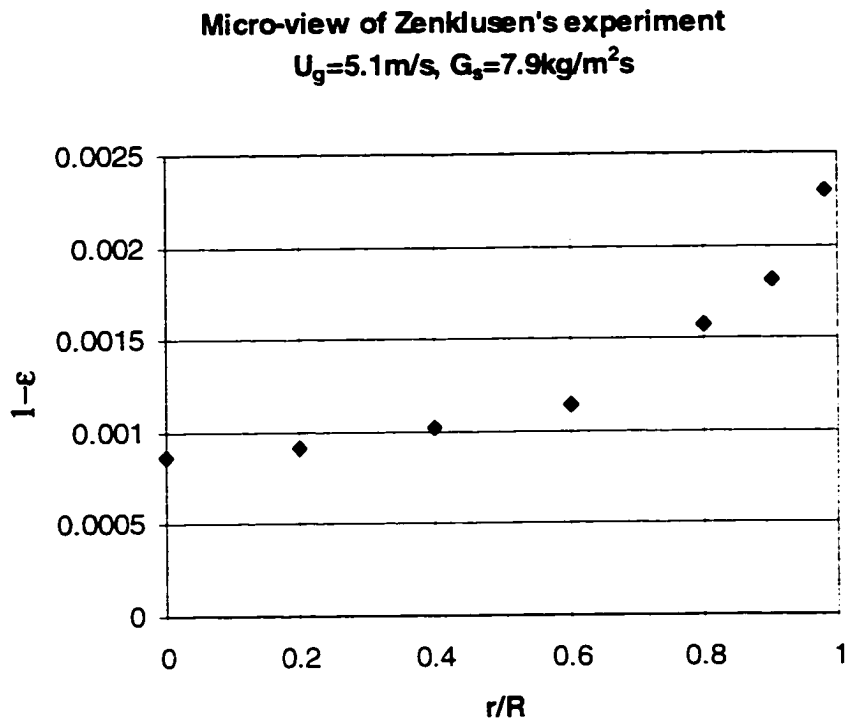

Figure 4.13 Micro-view of Zenklusen's Experimental Results in a Very Dilute Case

4.4. Axial Solid Fraction Profile

The axial catalyst distribution in a downer reactor is another important factor in determining reactor efficiency. A uniform catalyst density profile should benefit reaction yield and selectivity for most cracking processes. The mean solids distribution along the downer axial direction can be obtained by integrating the local solid fraction data measured with the x-ray image method across the radius at different measuring locations. The apparent solid density can be evaluated with the pressure difference measurements.

The axial solids concentration profiles are shown in Figure 4.14. More test results can be found in Appendix D. It can be seen that the integrated solid fraction obtained from the x-ray measurements does not vary much from the top to the bottom of the downer generally, although the value of solid fraction at the bottom of the downer is higher which indicates particle deceleration. However, the apparent solid fractions evaluated from the pressure gradient, $(1/\rho_p g)(dP/dx)$, show negative values in the solid entrance region [Figure 4.15(a) and Figure 4.15(b)]. The difference is caused by acceleration of solid in the entrance region. Below the entrance region the agreement between time average x-ray measurements and time mean pressure gradient measurements is much better. Because of the restrictions imposed by the two ends of the downer, the particle acceleration in the entrance

region and the deceleration in the exit region result in a relatively uniform axial solid distribution. However, the two phase flow cannot be considered to be fully developed.

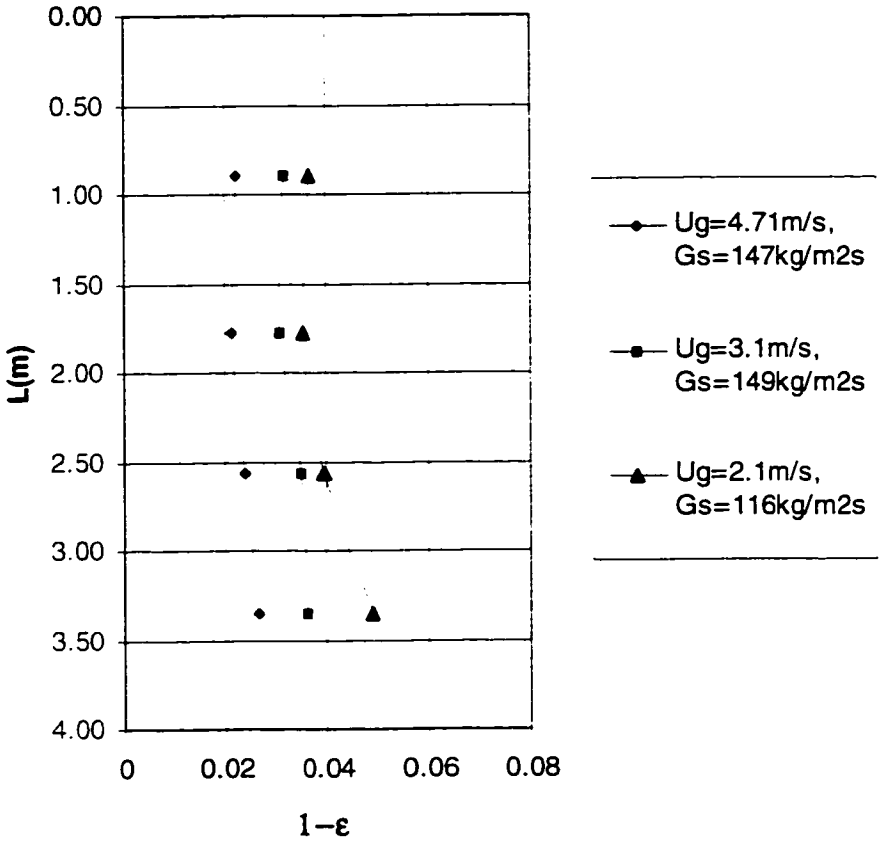

Figure 4.14 Axial Solid Concentration Profiles

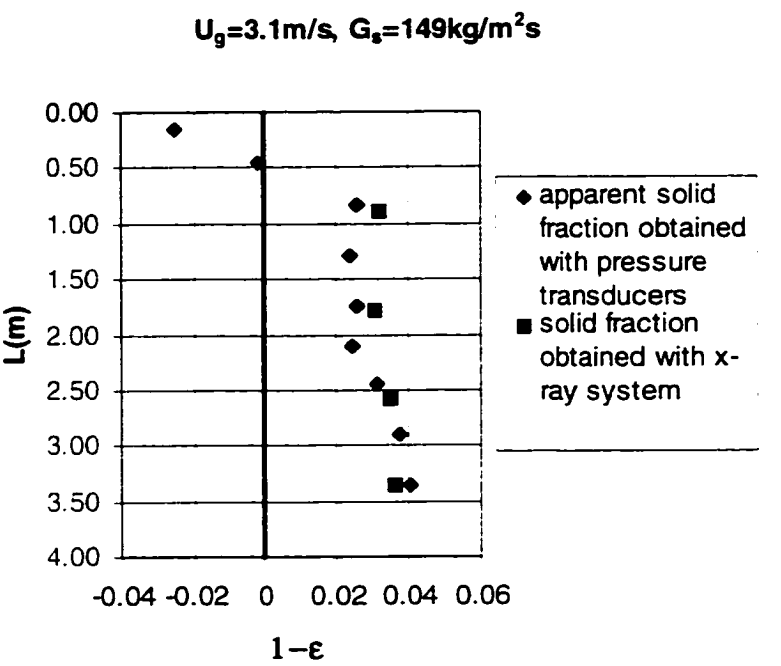

Figure 4.15(a) Axial Solid Concentration Profiles of Pressure Readings and X-ray Measurements

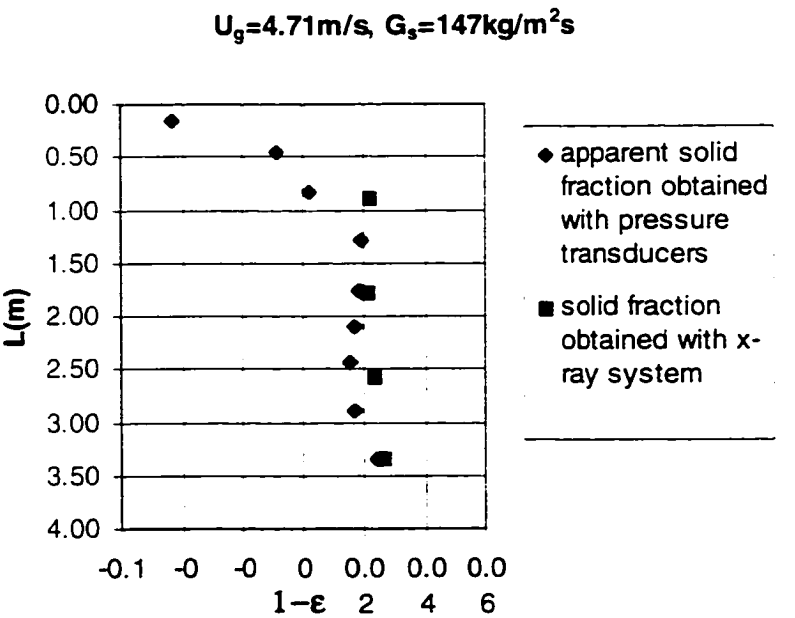

Figure 4.15(b). Axial Solid Concentration Profiles of Pressure Readings and X-ray Measurements

4.5 Radial Profiles of the Axial Solid Flux

The downflow solids flux and its distribution along the column radius provide important information about the flow structure of the downer. A modified non-isokintec probe and solid collection unit were installed in the City College Downer-Riser unit to measure this flow parameter. Typical signals of pressure difference due to the filling of the aspirated particles are shown in Figure 4.16. The linearity of the curve is good when the particle collecting fluidized bed is kept just above minimum fluidization conditions.

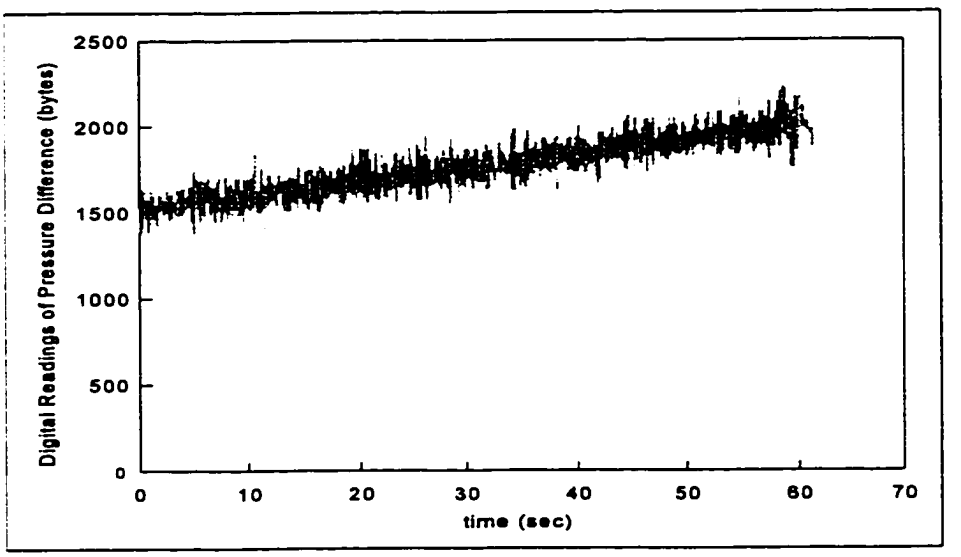

Figure 4.16 Pressure Signals of Solid Flux Measurement at U_g=3.7m/s, G_s=123kg/m^{2}s and r/R=0.85

Data collected with the local solid downflow flux measurement device at two locations of the downer, both downstream of the entrance region, are plotted in Figure 4.17. The solid flux distribution does not change much between these two measurement locations. They show that the solid flux is small in the central core and relatively constant. The solid flux in the wall region, however, rises sharply to a large value near the wall. This is an important difference between downer and riser flow where the high density wall region is characterized by low flux values.

As shown in Figure 4.18, the local solids flux increases with increase in the overall solids flow rate for a constant superficial gas velocity, especially in the annular region. For a given solids circulation rate, however, increasing superficial gas velocity increases the local solids flux slightly in the central core region while dramatically reducing the local solids flux in the wall region, as shown in Figure 4.19. Therefore, the solids flux of the dense annulus is more sensitive to the overall solids-gas loading ratio in the bed. Additional measurement results of local solid flux in the downer are shown in Appendix E.

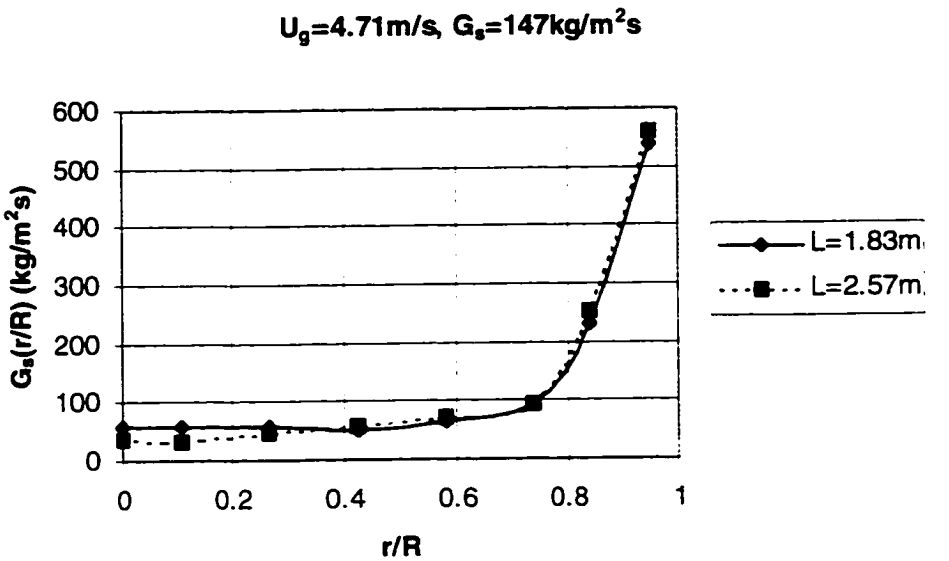

Figure 4.17 Local Solids Flux Profile in the Downer

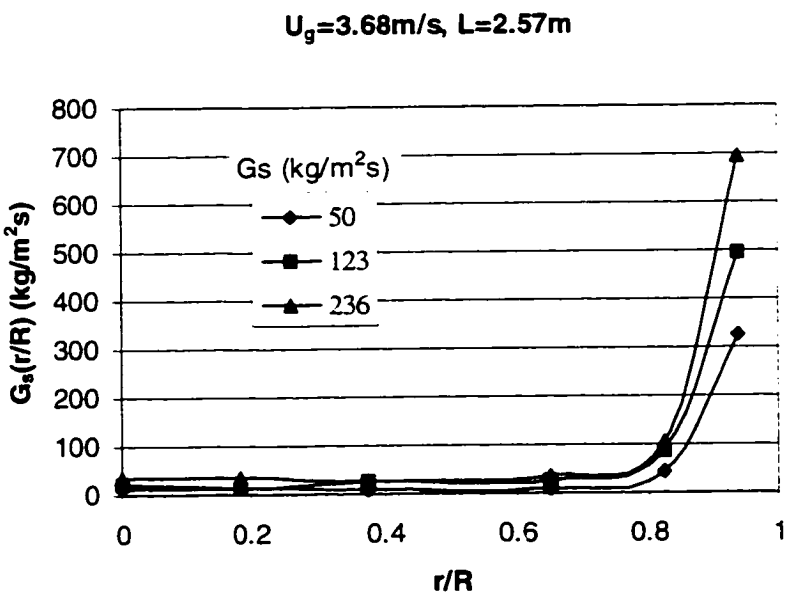

Figure 4.18 Local Solids Flux Profiles with Different Solid Flow Rates at the Same Superficial Gas Velocity

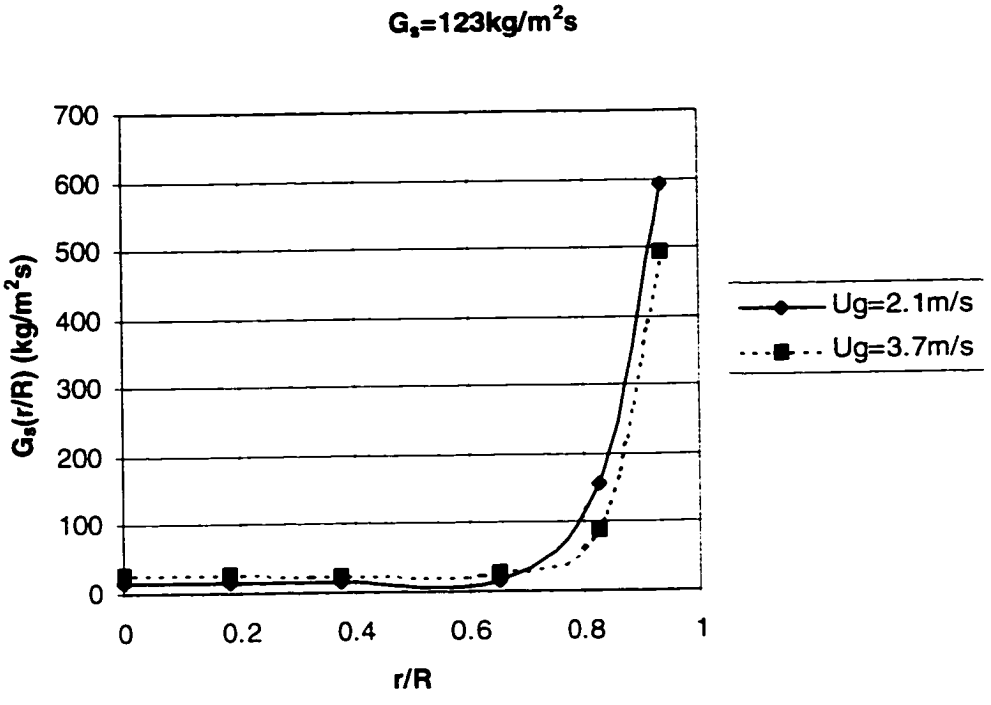

Figure 4.19 Local Solids Flux Profiles with Different Superficial Gas Velocities at the Same Solid Flow Rate

4.6 Estimation of Solid and Gas Velocity

The local fluid dynamic state in the downer is characterized not only by the radial variation of the solid fraction but also by that of the gas and solid velocities. It has been recognized that even for a minimal understanding of the two-phase flow, a description of both the local particle concentration and the particle and gas velocities are required. The estimation of gas and solid velocity provides the fundamental database for the development of a hydrodynamic flow model.

Based on the local values obtained of downflow solid flux and of solid fraction, the particle velocity can be estimated by:

$$U_p(r/R) = \frac{G_s(r/R)}{\rho_p[1-\epsilon(r/R)]} \qquad (4\text{-}7)$$

Figure 4.20 shows the particle velocity profiles given by the above expression. The dense wall region has a much higher particle velocity than the dilute core in two-phase downflow. Thus, the particle aggregation and gravitational force field provide a dense, fast-moving annulus and a slow, dilute core in direct contrast to riser flow. Plug flow-like behavior could only occur in downflow with a very dilute flow since the particles move to the wall as in upflow, but speed up near the wall dragging gas along rather than slowing down.

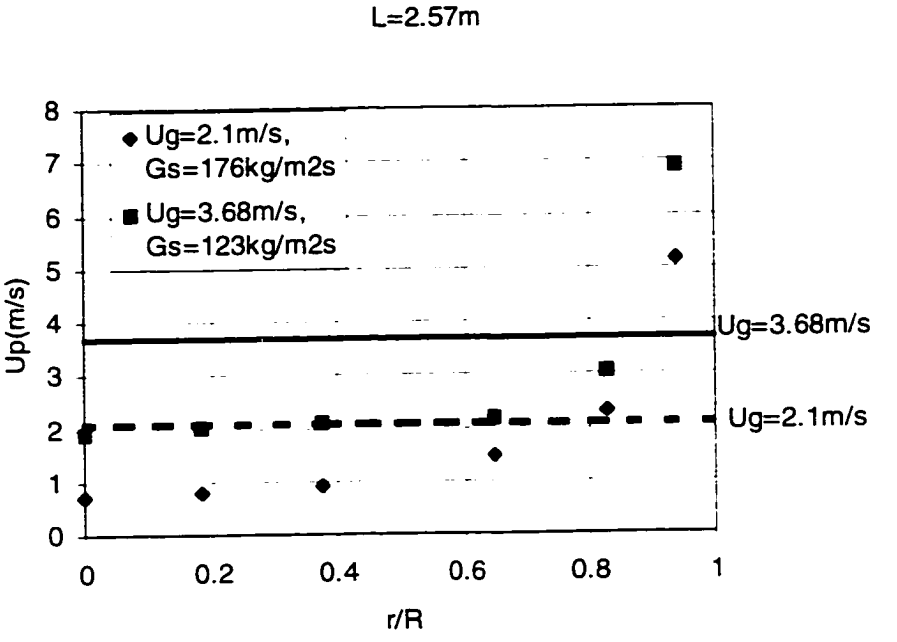

Figure 4.20 Local Solid Velocity Profile

This significant difference in radial structure between the downer and the riser is determined by the characteristics of the gas-solids suspension in the downer. In the downer, particles are not supported by the gas flow, but fall due to the gravity. After the acceleration zone in the upstream of the flow, particle flow is actually resisted by the gas drag force. More concentrated particle clusters produce less drag per particle than on an individual particle, leading to higher particle downflow velocity. Therefore, high solid aggregation must be accompanied by high downflowing particle velocity, while high solid concentration corresponds to low particle velocity in the riser.

The solids flux experimental data combined with a correlation for the slip velocity give an estimate of the radial profiles of gas velocity. A modified Matsen equation (Matsen, 1988) is used to correlate the local gas velocity with the local particle velocity. A radial profile of local gas velocity can be estimated with the slip velocity definition:

$$U_g(r/R) = U_p(r/R) + \alpha[1 - \epsilon(r/R)]^{0.3} \tag{4.8}$$

where α is a constant which is determined by applying (4.8) with the gas continuity equation:

$$U_g = 2\int_0^1 U_g(r/R)\epsilon(r/R)(\frac{r}{R})d(\frac{r}{R}) \tag{4.9}$$

Note that the estimation is crude because the slip velocity correlation was obtained for a cross-sectional average in riser flow and the slip behavior in the downer bed is unknown at present. Nevertheless, the magnitude and shape of the gas velocity profile can be estimated by this method.

Figure 4.21 shows the estimates for the radial distribution of local gas and solid velocity for a typical unit running condition. Similar to the particle velocity profile, gas flows faster near the wall than in the core region as well, which is in

direct contrast to the behavior of a riser. It confirms solids flow faster than gas as the calculated slip parameter α is negative for all the measurement cases at bed location of L=2.57. (See Figure 4.22 also). It suggests that the gas redistributes after entering the downer, speeds up in the wall region and slows down in the central core. The gas is dragged by the fast moving dense annulus in the wall region and by the slower dilute solid core in the central region. However, in the entrance region, the gas drags the solids at the beginning of the particle acceleration zone. The solids velocity exceeds the gas velocity after a certain acceleration length in the downer.

It is observed from Figure 4.21 and 4.22 that the slip velocity (U_p-U_g) profile is non-uniform radially. Calculating the slip velocity profile (Figure 4.23), it can be seen that the slip velocity in the dilute core region is relatively equal to or slightly larger than the terminal velocity of a single particle of mean particle diameter. However, as expected, the slip velocity is higher, about twice the terminal velocity, in the dense annulus. This distribution of the slip velocity along the radial direction indicates that particle aggregation is significant in the dense wall region and not in the core region of the downer.

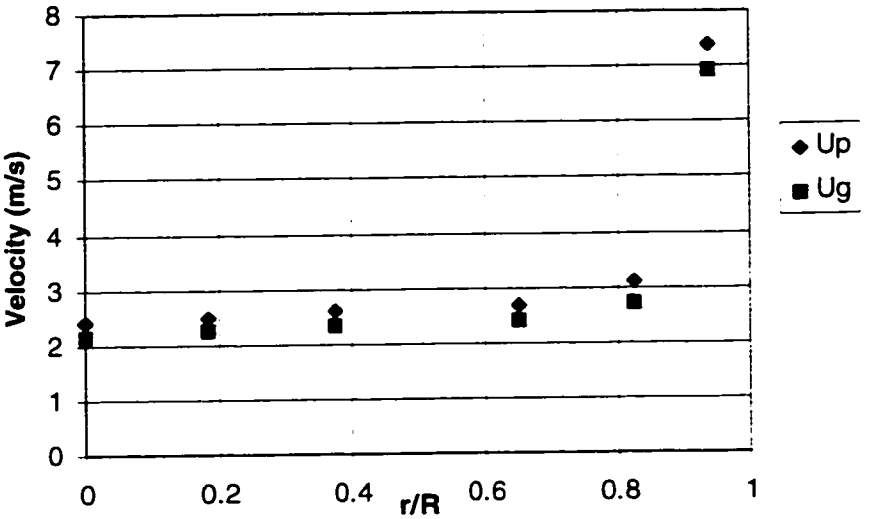

Figure 4.21 Local Gas and Solid Velocity Profile at Superficial Gas Velocity U_g= 3.7m/s, Solids Circulation Rate G_s=123kg/m^{2}s

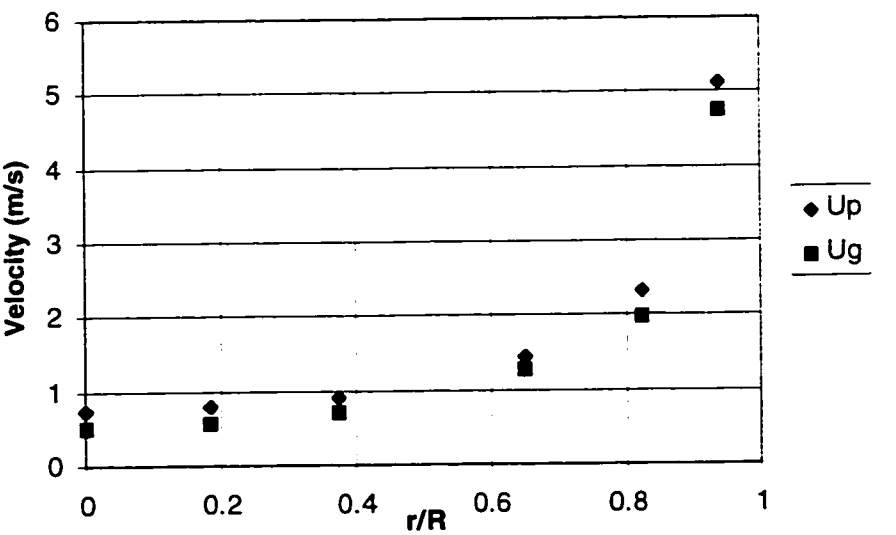

Figure 4.22 Local Gas and Solid Velocity Profile Superficial Gas Velocity U_g= 2.1m/s, Solids Circulation Rate G_s=176kg/m2s

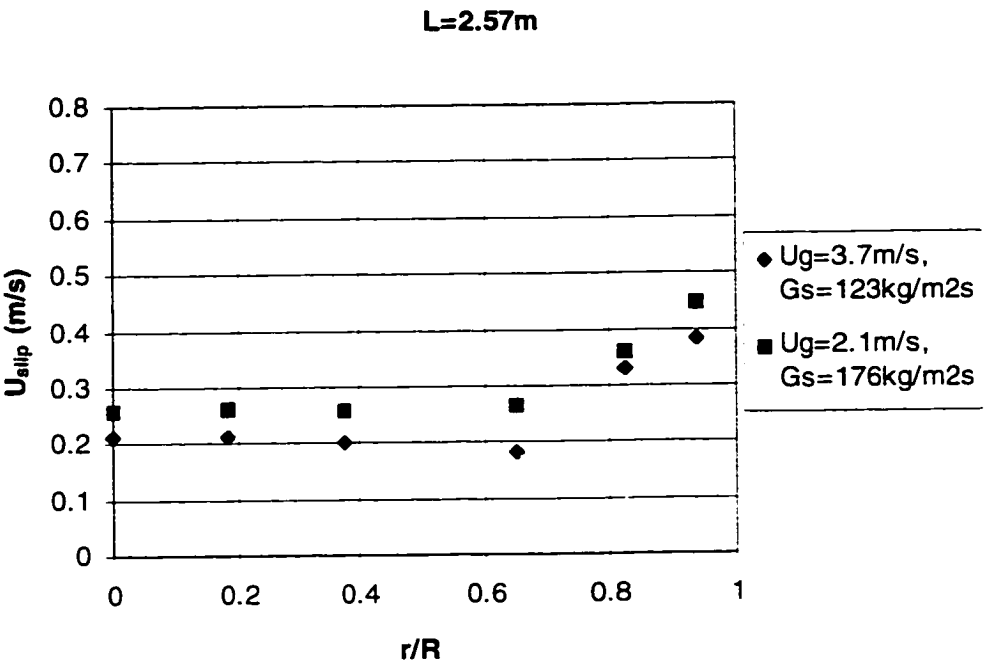

Figure 4.23 Local Slip Velocity Profile

Gas-solid velocities of dilute suspensions in a small diameter downer were studied by Herbert et al (1994) with optical fiber reflection probes. Shown in Figure 4.24, the parabolic shape of the particle velocity profile is typical in a very narrow flow channel with very high velocity regardless of the direction of the flow. A 14cm diameter downer was used to study gas-solid velocities in very dilute beds by Yang et al (1991) and Cao et al (1994) with a laser Doppler velocimeter technique. In those cases, the velocity distribution is quite uniform in the downer. However, with the large solid/gas loading ratios used in this investigation, the velocity profiles display very different patterns from those in the very dilute cases of Yang et al and Cao et al,

but show higher velocities near the wall. See Figure 4.24.

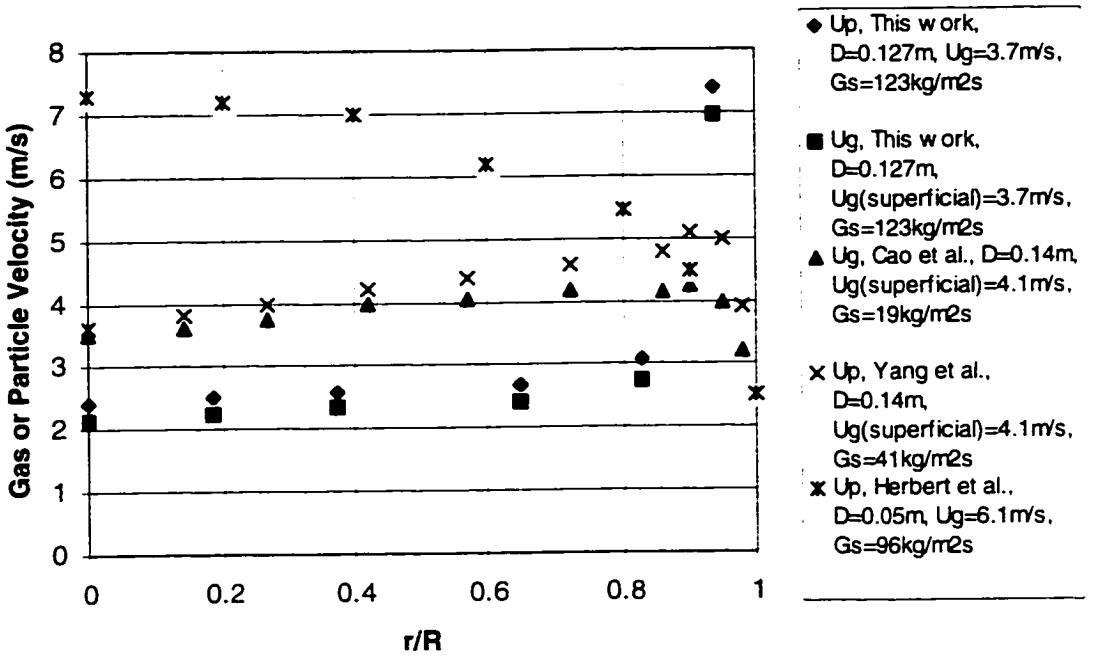

Figure 4.24 Comparison of Gas-solid Velocities in Different Units

4.7 Gas Dispersion and Backmixing

The efficiency of a downer reactor depends on its ability to mix adequately the incoming flows of reactants with the solids, and performance criteria such as yield and selectivity are typically adversely affected by backmixing in short contact or residence time processes. A low gas backmixing level has been expected in proposals for the development of the downer reactor. Thus, a clear understanding of gas lateral dispersion and backmixing in the downer is important. Flow patterns in the downer show solids aggregation, non-uniform radial gas and solids velocity distribution and relatively uniform axial solids concentration profiles which are different from those in the riser. This indicates that there is a significant difference in gas mixng behavior between the downer and the riser and independent downer measurements are required.

4.7.1 Experimental Results

The gas dispersion in a single gas phase was investigated first to provide the basis for a comparison with that in two phase flow. The profiles of the dimensionless helium concentration detected at several sampling locations are shown in Figure 4.25. The distribution of helium tends to be uniform when the sampling position is far from the injection source.

When solids are added, creating a two phase flow, the helium concentration distribution becomes significantly flatter over the column cross-sectional area than in one phase flow, as shown in Figure 4.26. The gas flow has been modified by the presence of the solids which enhance the turbulent mixing and result in a higher degree of lateral mixing.

Figure 4.27 shows the helium concentration profiles detected at three sampling positions between the tracer injector and the sampling probe in the downer. It is obvious that closer sampling gives more non-uniform tracer distribution. A flat profile is achieved at a location of about 6 tube diameters downstream of the injection.

The effect of solid circulation rate on the gas dispersion is illustrated in Figure 4.28. It is shown that increasing the solid rate at a fixed superficial gas velocity leads to more rapid gas lateral mixing. On the other hand, higher superficial gas velocity at constant solids circulation rate gives a larger radial variation of the tracer concentration, as shown in Figure 4.29. Both illustrations show that increasing the solids fraction in the downer gives better lateral mixing of the gas.

Figure 4.30(a) and 4.30(b) confirm the expected low backmixing in the downer. Due to the fact the gas and particles are flowing downwards in the direction

of gravity, convection predominates over axial dispersion, therefore, true backmixing detected upstream of the source is very limited. Only at a very close sampling distance between the injector and sampling probe elevations and at high helium injection rates can any direct helium backmixing be detected. Figure 4.30 shows direct backmixing levels with the helium detector upstream (above) the injector. In Figure 4.30(a) the backmixing level in the slow moving central core is surprisingly high and increases with increasing solid flux. In the gas only case, Figure 4.30(b), the backmixing level is lower, confirming that the presence of solids enhances backmixing or axial dispersion. Also, the helium is readily detected both with and without solids present 14cm above the injector but is essentially undetectable 30cm above. These data also confirm that the presence of solids enhance the turbulent mixing and indicate that the largest turbulent eddies with and without solids present are on the order of one to two tube diameters.

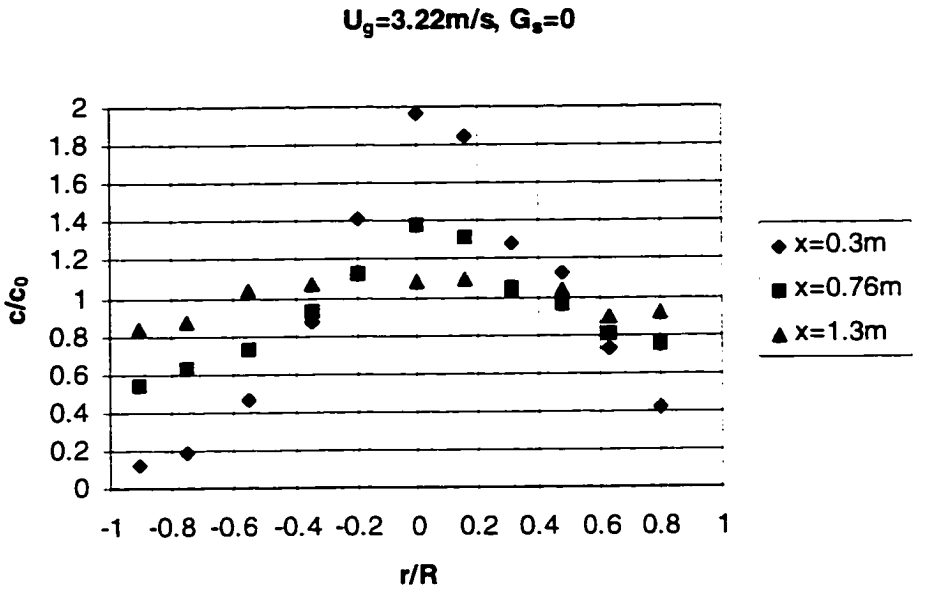

Figure 4.25 Gas Dispersion in One (gas only) Phase flow

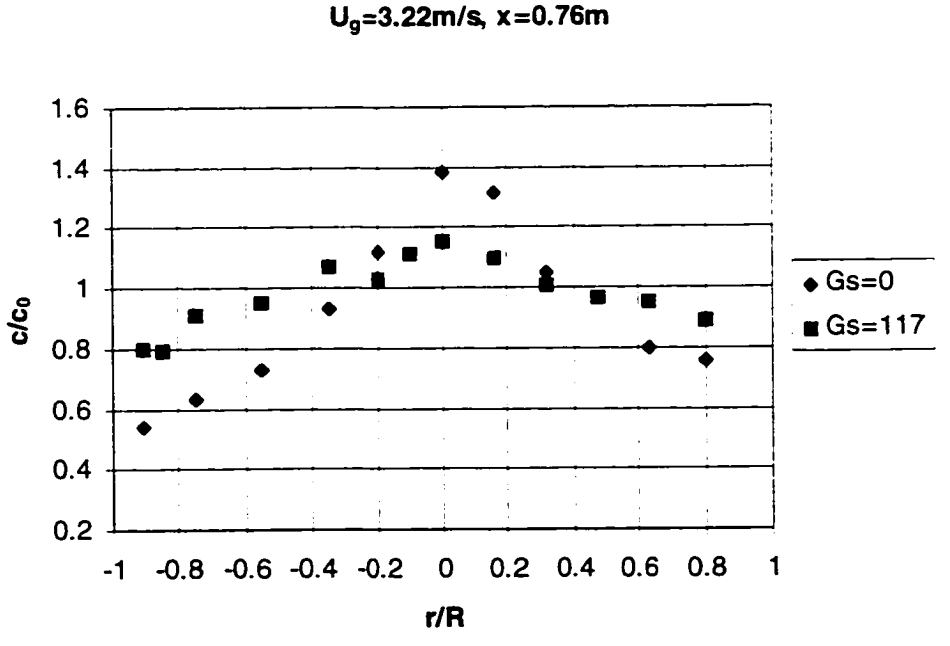

Figure 4.26. Effect of Particles on the Tracer Profile

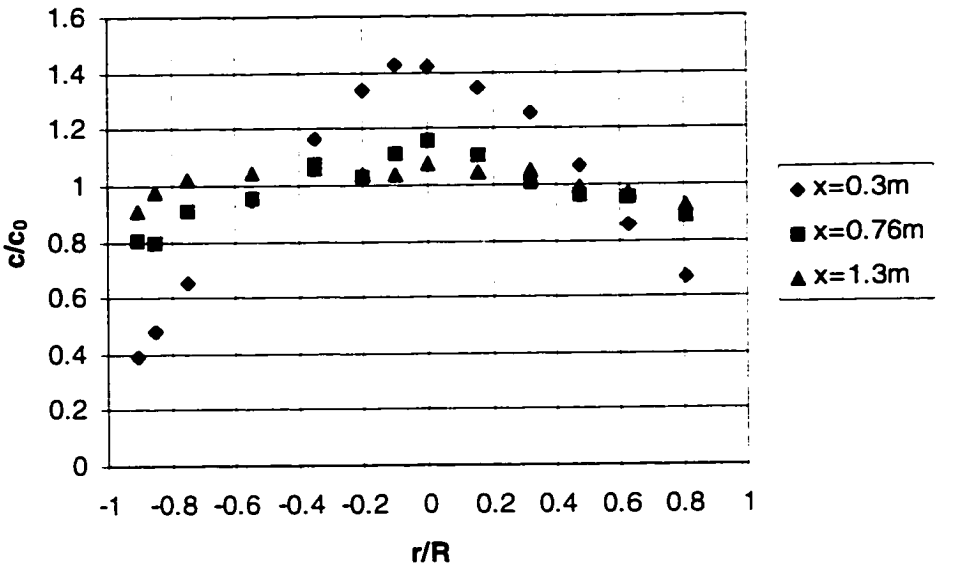

Figure 4.27 (a) The Profiles of Dimensionless Tracer Concentration at U_g=3.22m/s, G_s=128kg/m^{2}s

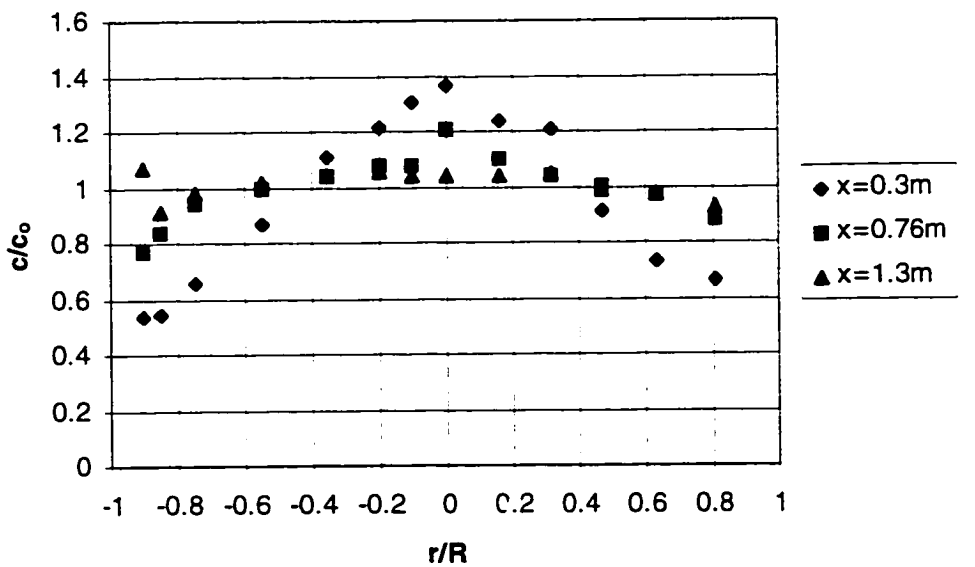

Figure 4.27 (b) The Profiles of Dimensionless Tracer Concentration at U_g=2.52m/s, G_s=142kg/m^{2}s

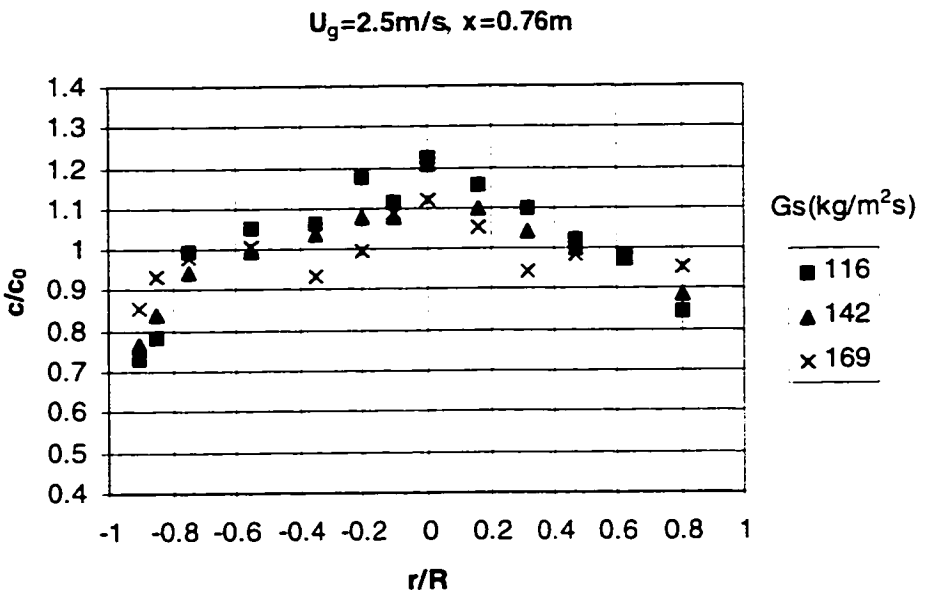

Figure 4.28 Effects of Solids Circulation Rate on the Gas Dispersion

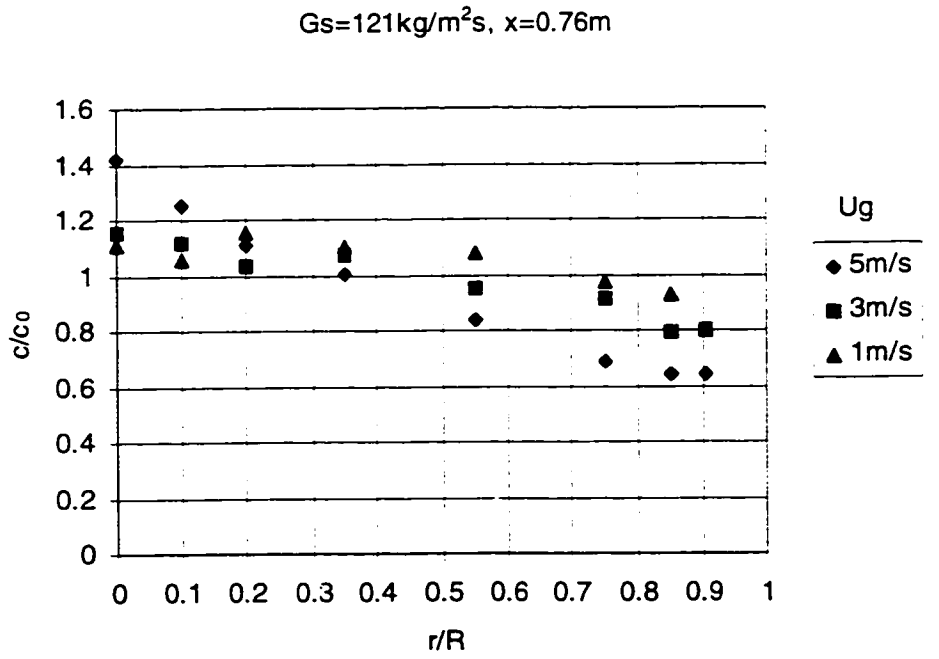

Figure 4.29 Effects of Gas Superficial Velocity on the Gas Dispersion

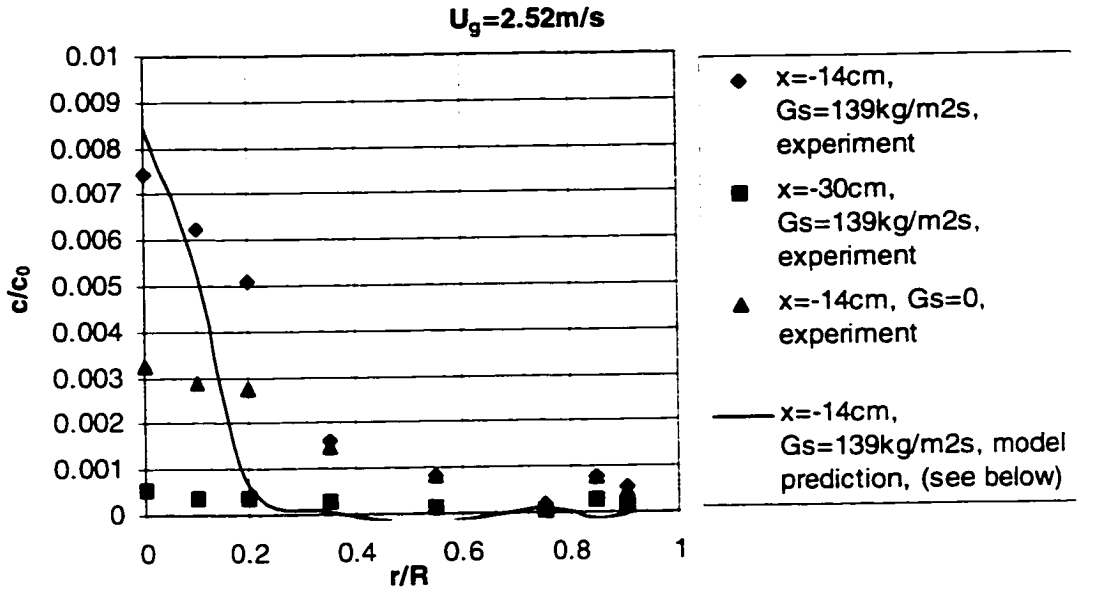

Figure 4.30(a) Gas Back mixing in the Downer at U_g=2.52m, G_s=0 and 139kg/m^{2}s

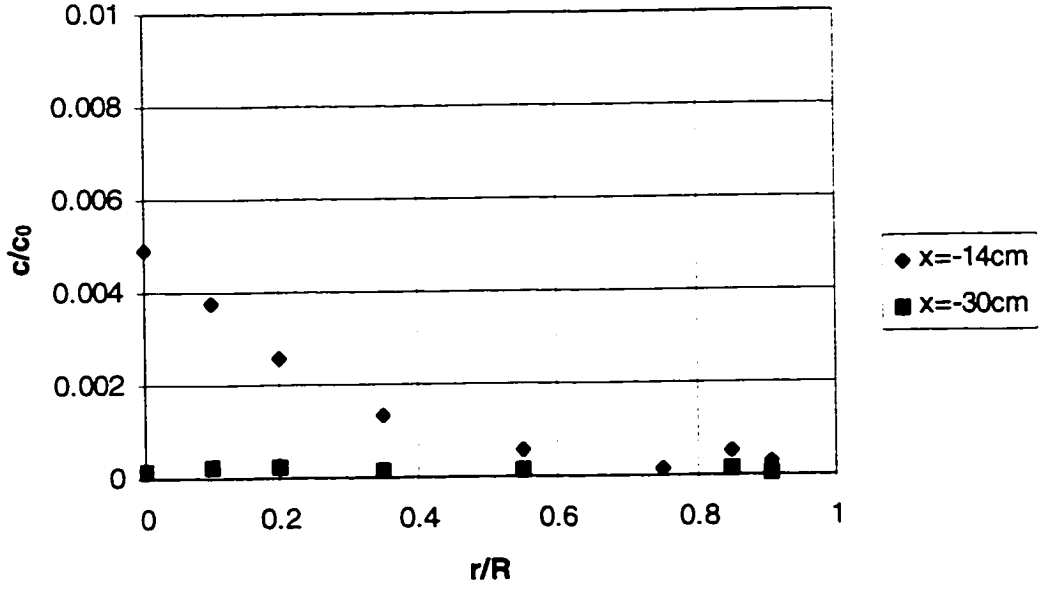

Figure 4.30(b) Gas Back mixing in the Downer at U_g=3.22m, G_s=0 and 128kg/m^{2}s

4.7.2 Dispersion Model

A two-dimensional, pseudo-homogenous model is used to describe the behavior of the gas dispersion in the downer. The assumptions follow:

(I) Isotropic dispersion takes place in the column, the dispersion coefficient is independent of the local position in the column;

(ii) Gas velocity is uniform in the column;

(iii) Convection occurs only in the axial direction of the column.

In cylindrical coordinates, model is formulated as follow:

$$U\frac{\partial c}{\partial x}=D[\frac{1}{r}\frac{\partial}{\partial r}(r\frac{\partial c}{\partial r})+\frac{\partial^2 c}{\partial x^2}] \tag{4-10}$$

with boundary conditions:

$$\begin{gathered}\frac{\partial c}{\partial r}|_{r=0}=0\\ \frac{\partial c}{\partial r}|_{r=R}=0\\ c(0,0)=c_0\delta(r,x)\\ c(r,-\infty)=0\end{gathered} \tag{4-11}$$

The solution of the above equation is:

$$\bar{c}=\frac{c}{c_0}=Pe\sum_{n=0}^{\infty}\frac{J_0(\eta\lambda_n)e^{-\frac{\xi}{4}[-Pe-\sqrt{Pe^2+16\lambda_n^2}]}}{J_0^2(\lambda_n)\sqrt{Pe^2+16\lambda_n^2}} \qquad \text{when } \xi\geq 0 \qquad (4\text{-}12)$$

$$\bar{c}=\frac{c}{c_0}=Pe\sum_{n=0}^{\infty}\frac{J_0(\eta\lambda_n)e^{\frac{\xi}{4}[Pe-\sqrt{Pe^2+16\lambda_n^2}]}}{J_0^2(\lambda_n)\sqrt{Pe^2+16\lambda_n^2}} \qquad \text{when } \xi\leq 0 \qquad (4\text{-}13)$$

where, η and ξ are nondimensionlized coordinates:

$$\eta=\frac{r}{R}$$
$$\xi=\frac{x}{R} \qquad (4\text{-}14)$$

Pe is Peclet group:

$$Pe=\frac{U(2R)}{D} \qquad (4\text{-}15)$$

λ_n is the root of Bessel Function equation and can be obtained by

$$J_1(\lambda_n)=0 \qquad (4\text{-}16)$$

Setting up the objective:

$$\sum_{Minimum}=\sum_{i=0}^{m}(\bar{c}-\bar{c}_{experiment})^2 \qquad (4\text{-}17)$$

The model parameter Pe in the equation can be obtained with an optimization technique. The results shown in Figure 4.31 indicate that the model prediction fits the experimental data well. Backmixing predictions also agree with the experimental data.[See Figure 4.30(a)]. The average relative error is 5.4%. Bigger deviations occur in the wall region. The reason is that the model assumption neglects the non-uniform distribution of gas velocity. The Peclet number of the two phase flow in the downer is estimated from the above description. The variation of calculated Peclet number with the apparent bed density defined as $(1-\epsilon)=(1/\rho_p g)(\Delta P/\Delta L)$ is plotted in Figure 4.32. It can be seen that the Peclet number decreases with increasing bed density. This suggests that the particles enhance the turbulent intensity of the flow.

The measured magnitudes of the gas dispersion coefficients are on the order of 10-100 cm^2/s, which agrees with the results obtained in the core region of the riser (Adams C. K, 1988). The calculated Peclet number is on the order of 100, which agrees with the results obtained in a 6-inch downer-riser combination system (Zhu J. et al, 1995). The true gas backmixing (upstream of injection) is much less than that in the riser. Thus there is an advantage to the downer reactor in that it can reduce the gas backmixing level that exists in the riser, but still maintain good lateral mixing.

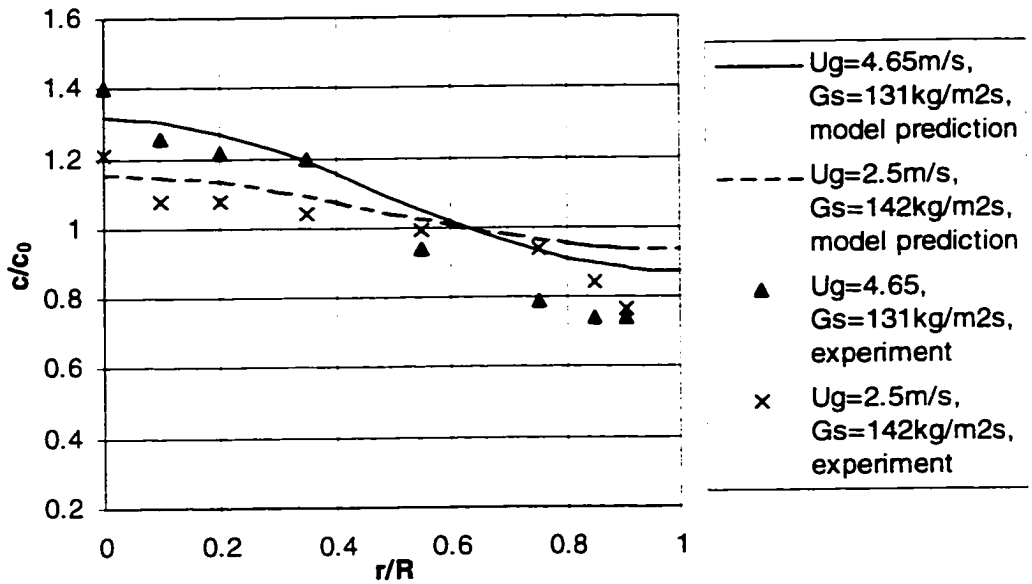

Figure 4.31 Comparison of the Experimental Results with the Model Predictions

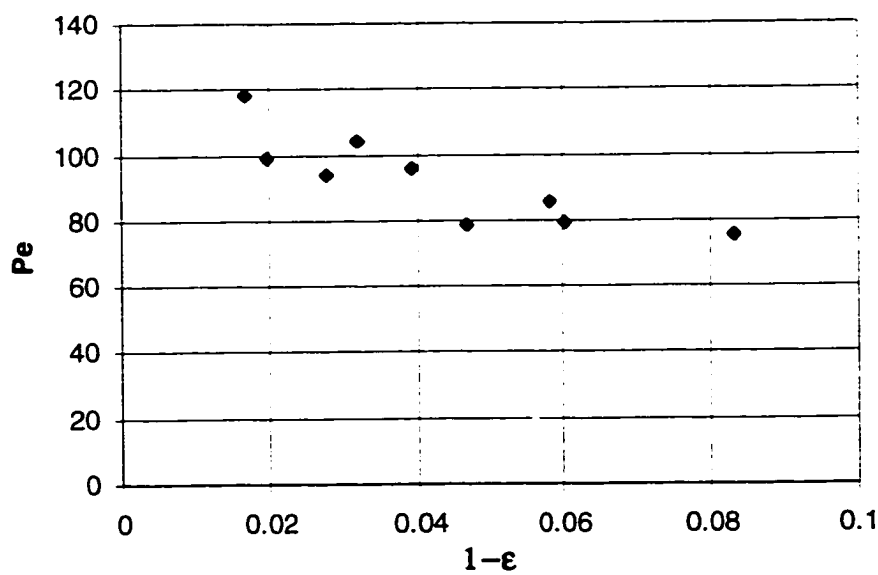

Figure 4.32 Estimation of the Peclet Number

4.8 Overall Flow Structure and Gas Mixing Behavior

From above discussion, the overall flow structure of the downer can be summarized as follows:

There exists an axial "bow" shape pressure profile and a relatively uniform axial solid distribution in the downer. Particles accelerate in the entrance region and decelerate in the exit regions. Radially, the non-uniform solid concentration distribution forms a core-annulus flow with a high speed annulus and a slow moving core. The gas velocity profile is distorted by the fast moving aggregated solids in the annulus. Both solids and gas flow faster in the dense wall region than in the dilute core. Furthermore, the downer reactor provides very good lateral mixing and rapid intermixing of gas with solids. The gas backmixing level is reduced compared to that in a riser.

4.9 Comparison between a Downer and a Riser

The newly proposed downer reactor system has become a candidate for short residence time reactions, high solids/gas feed ratio processes and catalytic reactions with rapid catalyst deactivation. To evaluate the performance of such a reactor, comparison between the downer and the riser is essential.

Hydrodynamic studies in the downer carried out in this investigation have shown very significant differences in the gas-solid flow patterns between the downer and the riser. Gas tracer experiments have also demonstrated differences between the downer and the riser in mixing properties. Comparisons between the downer and a riser are made for the following aspects:

(1). Axial solid distribution

(2). Radial solid fraction distribution

(3). Solid flux distribution

(4). Gas and solid velocity distributions

(5). Gas lateral dispersion and axial backmixing

The experimental data for a riser used in this comparison was obtained in a riser with a 15.2 cm inner diameter. (Kostazos, 1997). Because of relatively small geometry and dimensional differences between the two vertical systems and the

differences in operating conditions, it is difficult to find identical operating conditions in the two databases on which the comparison can be conducted. However, comparisons between cases which are relatively close and in general treads are adequate to show the dramatic differences in flow patterns between the downer and the riser.

In both upflow and downflow, the high velocity fluidization regime can be described with "at higher voidages and slip velocities, the continuous phase of turbulent fluidization disappears and the solids are only present as discrete particles or as ephemeral assemblages or clusters of a statistical-hydrodynamic nature" (Matsen,1988). Typical voidage profiles for an upflow fast fluidized bed(riser) are shown in Figure 4.33. The general criterion for the upflow fast fluidized bed(riser) is that the bed contains both a dense phase and a dilute entrained phase above it, described as an "S-shaped" density profile.(Kwauk and Li, 1980).

Axial apparent solid fraction profiles measured with differential pressure transducers in both the downer and the riser are shown in Figure 4.34 at the superficial gas velocity of 3.1m/s and solid circulation rate of 149kg/m^{2}s. The positive value of the ordinate in Figure 4.34 represents the bed height of the riser, and the absolute value of the negative numbers represent the distances from the entrance of the downer. It can be observed that the overall axial solid fraction profile

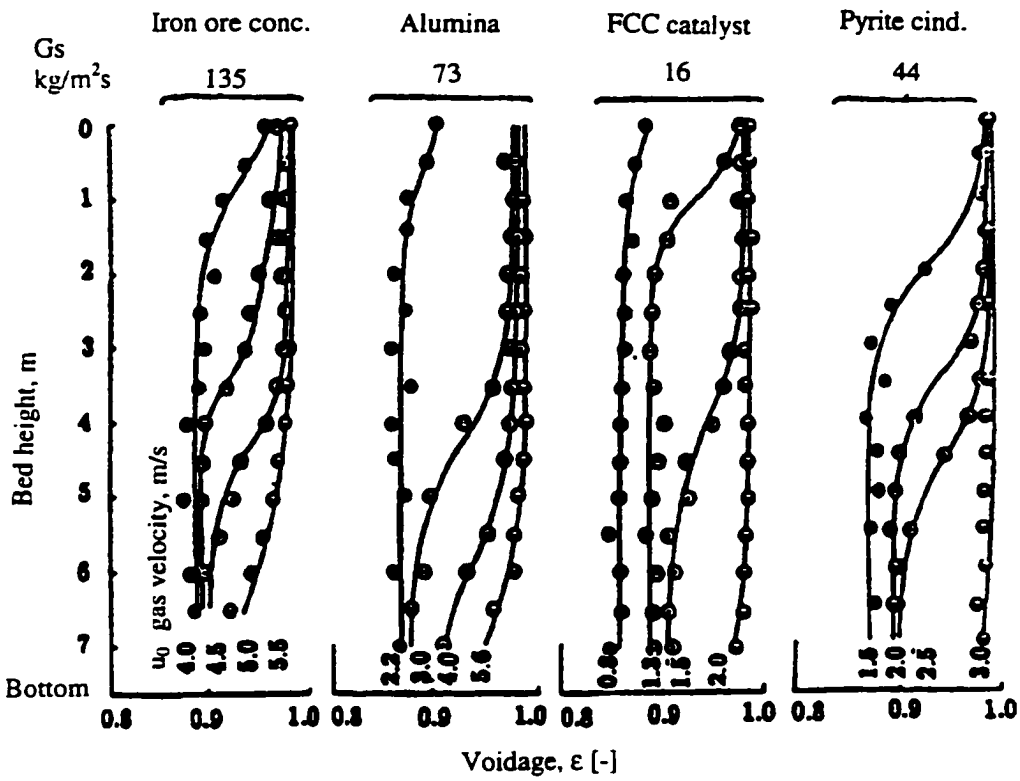

Figure 4.33 Axial Voidage Profile for Fast Fluidized Bed (Li and Kwauk, 1980)

along the downer vertical column shows a much more uniform distribution than that in the riser. The dense bed in the riser entrance region and the dilute entrained phase above make up the typical riser bed. The length of the riser from the inflection point down to the entrance in which particle velocity can be changing significantly is much longer than that in the downer. The shorter flow developing region in the downer would better meet the kinetic requirements of relative short contact reactions. Note that the measured negative apparent solid fraction in the entrance region of the downer is caused by the particle acceleration effect as pointed out in a previous chapter.

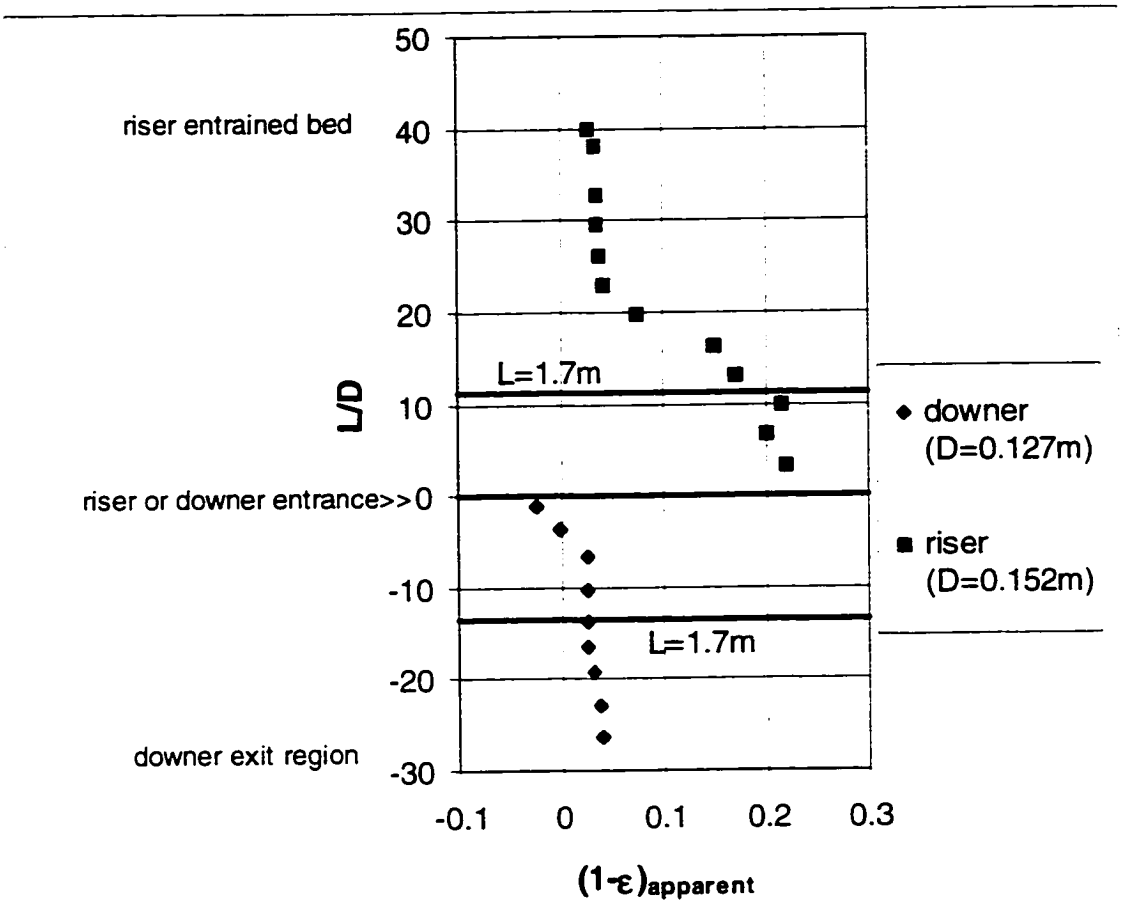

Figure 4.34 Comparison of the Axial Apparent Solid Fraction Distribution between the Downer and the Riser at U_g=3.1m/s, G_s=149kg/m^{2}s

It has been found that a core-annulus radial flow structure occurs in both the downer and the riser. In order to determine which kind of reactor behaves more plug flow like, a comparison of radial solid fraction profiles between the downer and the riser is shown in Figure 4.35 at about the same distances from the bed entrances and the same operating conditions. It can be seen that the radial solid fraction distribution

is much more uniform in the downer than in the riser. Therefore, gas-solid contact efficiency should be greatly improved in the downer as compared to the riser.

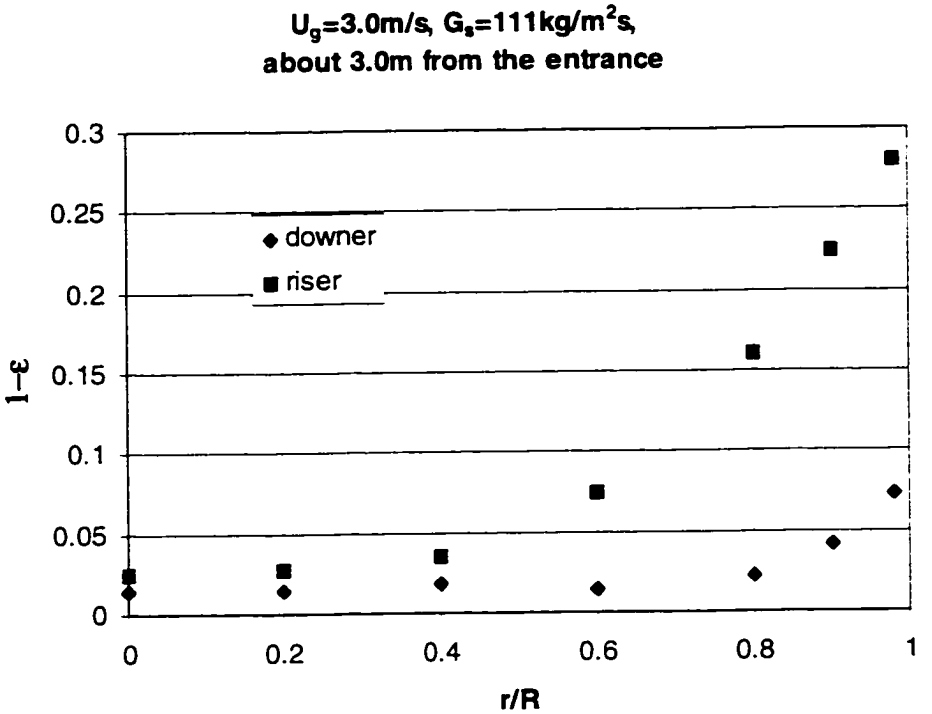

Figure 4.35 Comparison of the Radial Solid Fraction Profiles between the Downer and the Riser about 3.0m from the entrances under similar operating conditions (U_g=3.0m/s, G_s=111kg/m^{2}s)

Figure 4.36 shows the comparison of the local solid flux in the downer and the riser. Considerable difference can be observed from this chart. Solid flux profiles measured in the downer indicate that the solid downflow flux is small in the central

core and relatively constant and rises sharply to a large value near the wall. This is an important difference between downer and riser flow where the high density wall region is characterized by low flux values or even reversed solid flow. Solid upflow flux in the central core region of the riser has a very large value, which is in direct contrast to the small downflow flux in the core region of the downer.

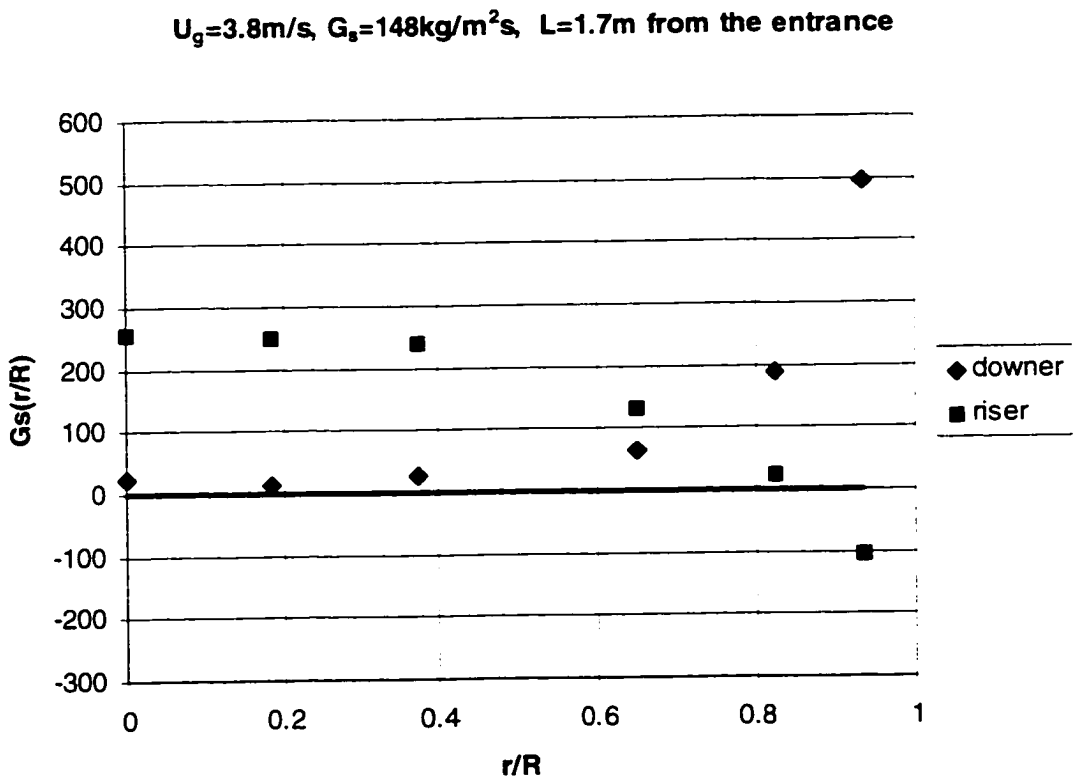

Figure 4.36 Comparison of the Solid Flux Profiles between the Downer and the Riser

Estimated values of solid and gas velocities in the downer and riser provide the comparisons in Figure 4.37 and Figure 4.38. They show that the riser displays a fast upflowing dilute core and slow downflowing dense particle annulus. The gas near the wall of the riser is usually upflowing which results in large slip velocity. On the contrary, the dense wall region in the downer has much higher downflowing gas and particle velocities than does the dilute core. Thus, the particle segregation and gravitational force field provide a dense, fast-moving annulus and a slow, dilute core in direct contrast to riser flow where the dense annulus is accompanied by low particle velocity. Furthermore, higher solids concentration in the annular region of the downer leads to higher slip velocity and higher particle velocity. This is contrary to risers, where a higher slip velocity results in a reduced particle velocity.

Such flow patterns in the downer may provide a great advantage over the conventional riser in improving the product yield and selectivity. For a catalytic cracking process, the catalyst concentration is higher in the downer wall region than the core region, but the residence time in the wall region is shorter than that in the core region due to the higher particle velocity in the wall region. This coupling of solid fraction with velocity should lead to more uniform cracking across the whole cross-sectional area.

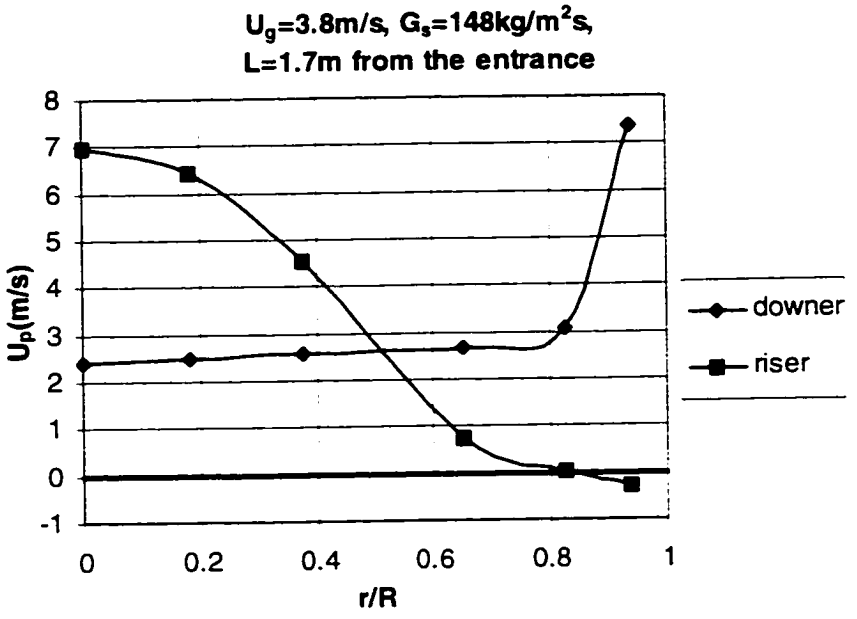

Figure 4.37 Comparison of the Solid Velocity Profiles between the Downer and the Riser

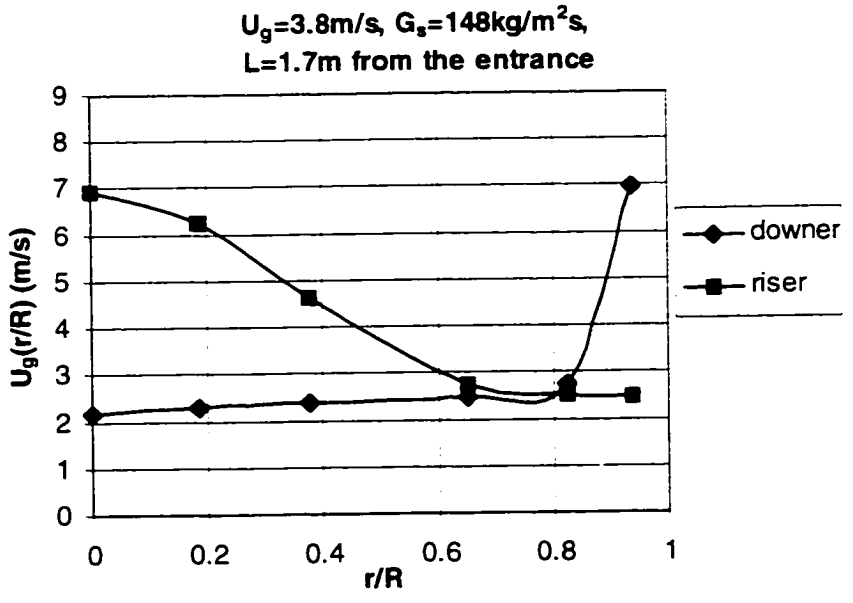

Figure 4.38 Comparison of the Gas Velocity Profiles between the Downer and the Riser

It has been determined that gas backmixing in the riser is the result of spatially distributed heterogeneity (Weinstein et al, 1989). Helium tracing tests (Li and Weinstein, 1989) show that the tracer concentration detected upstream near the wall is much higher than that in the dilute core region when the injector was located near the wall. On the other hand, injection in the core region produced a very low level of backmixed tracer concentration, and the circumferential mixing in the annular region was considerable. They concluded that the assumption of gas plug flow in the riser was inappropriate for the whole bed.

The same gas tracing equipment was used to measure the gas backmixing in the downer as was used in the riser (Li and Weinstein, 1989). A comparison is shown in Figure 4.39. The injection point in the riser was near the wall (r/R=0.89), but at the center in the downer. Figure 4.39 clearly shows that true gas backmixing occurring from a reverse flow region near the wall is very limited or nonexistent in the downer comparing to riser flow. It is even undetectable when the detector is located 30cm away from the injector source in the downer. The large reduction of true gas backmixing in the downer offers the advantage of improving the selectivity and productivity in many short contact reaction processes. On the other hand, the local mixing with a scale of about a diameter gives good lateral mixing characterized by the Peclet number which is comparable between the riser and the downer. As shown in Figure 4.40, dispersion coefficients obtained in a riser (Adams, 1988) are plotted

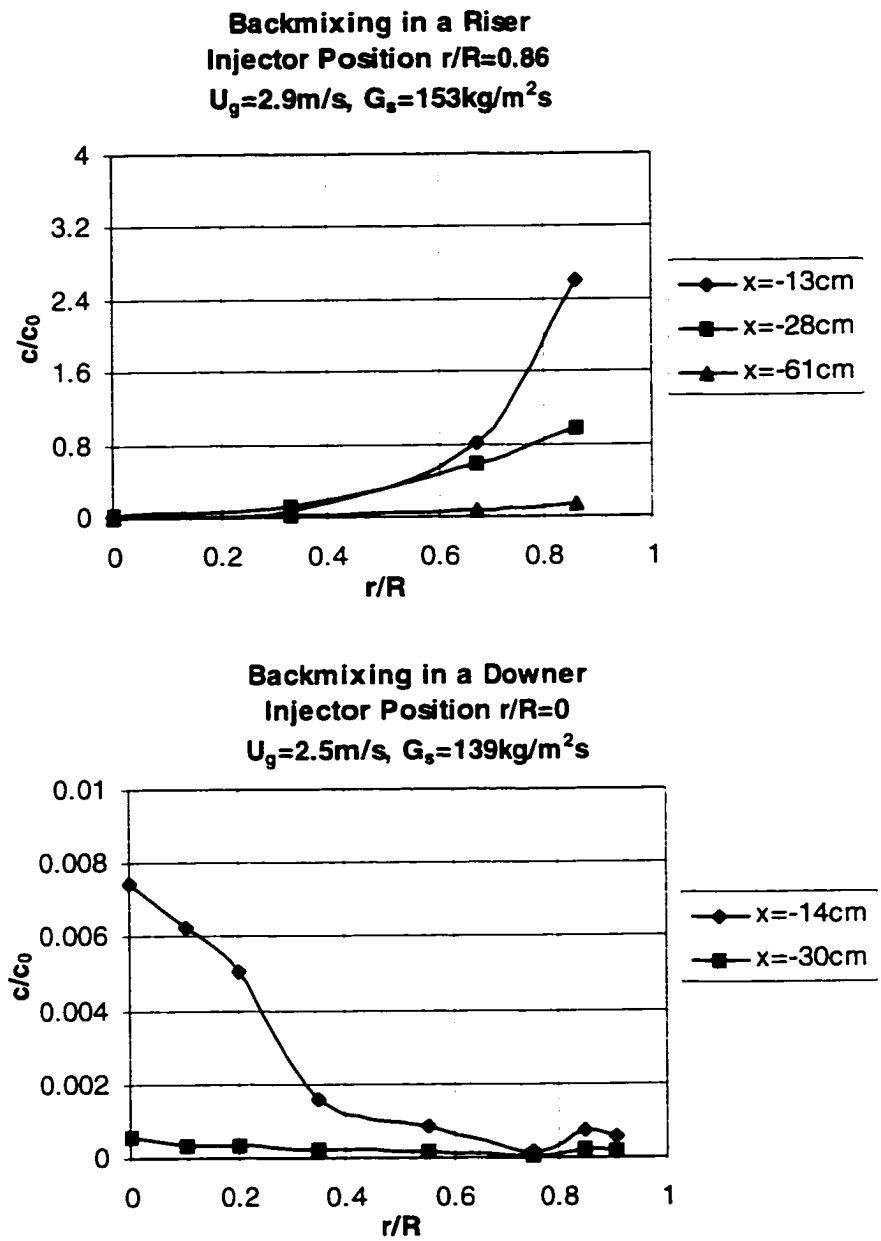

Figure 4.39 Comparison of Gas Backmixing between a Downer and a Riser

with the data obtained in the downer of this investigation. It can be seen that the radial gas dispersion coefficients in the downer have the same order of magnitude as

in the riser. This ensures the good gas-solids contact which is required in catalytic and thermal processes.

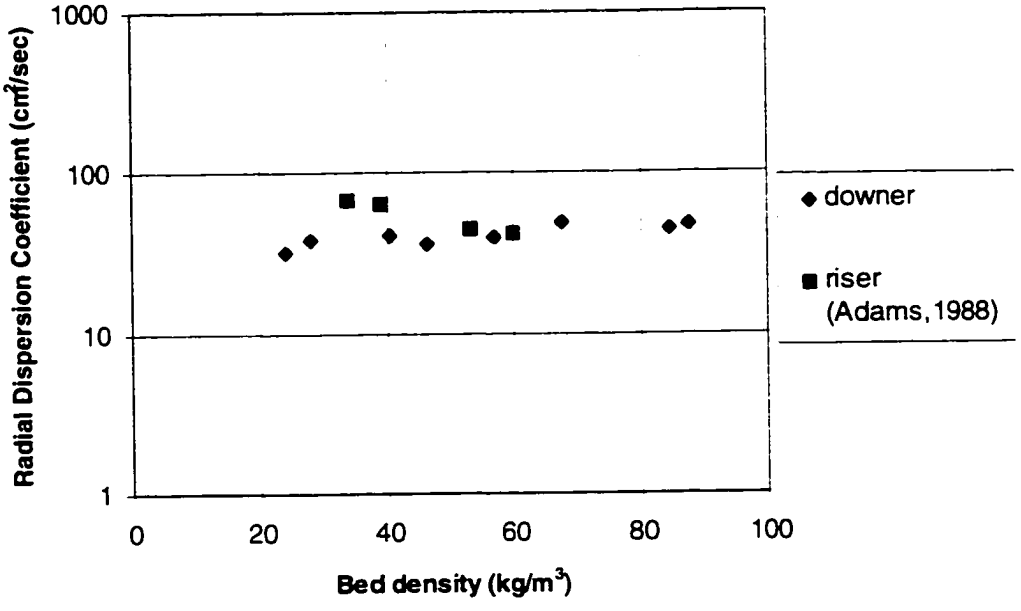

Figure 4.40 Comparison of Gas Lateral Mixing between a Downer and a Riser

4.10 Advantages of the Downer over the Conventional Riser

In general, the co-current downflowing gas-solid fluidized beds provide many advantages over conventional risers in which beds are upflowing. The main advantages are:

(1). Gas backmixing is reduced, so overreaction and underreaction can be minimized. Performance of the reactor should be significantly improved.

(2). Overall flow patterns of the downer provide a relatively more uniform axial and radial solid distribution which can lead to improvement of the gas-sold contacting efficiency.

(3). Shorter residence time in the downer wall region due to the high speed flow is coupled with faster reaction rates due to the accompanying dense catalyst annulus, while the dilute core has slower reaction rate with longer residence time due to the lower catalyst concentration and flow velocity. This results in much more uniform reaction extent over the cross-sectional area of the downer, and therefore, should improve the product selectivity.

(4) The developing flow region in which particles accelerate is much shorter in the downer than in the riser. This meets the kinetic requirements of relative short residence time reactions.

(5). Since particles need not be supported by the gas flow in the downer, the solid-gas loading ratio can be much higher than it can be in the riser which cannot operate below a certain gas velocity.

V. CONCLUSIONS

A downer-riser circulating high velocity fluidization apparatus has been developed to study the fundamentals of gas-solid particle mixture downflow. Flow quantities including the real time pressure fluctuation, solid fraction, solid flux and gas mixing properties have been determined experimentally. The conclusions can be drawn from the experimental results and analysis follow:

(1). Measurements of pressure distribution along the downflow fluidized bed show first particle acceleration and then deceleration. The acceleration and deceleration of solids due to the influences of the entrance and exit sections result in a relatively uniform axial solids distribution. The flow developing region in which the particles accelerate is shorter in the downer than in the riser. This can meet the kinetic requirements of relative short contact time reactions.

(2). X-ray visualization and solid fraction measurements indicate the existence of a core-annulus flow with a dilute core surrounded by a denser wall region.

(3). The local solids flux profiles obtained with an aspirating probe device and the solid velocity profile obtained from the flux and solid fraction these two

measurements confirm that the majority of solids aggregate in the wall region and flows faster than in the dilute core region in contrast to riser flow.

(4). Such a flow pattern in the downer provide a great advantage over the conventional riser in improving the products yield and selectivity. The reason is that shorter residence time but higher reaction speed due to the high solid fraction in the downer wall region and longer residence time with lower speed dilute solid flow in the central region result in much more uniform reaction extent across the cross-sectional area of the downer.

(5). Tracer measurements show that gas backmixing is very limited in the downflow high velocity fluidized bed, while the lateral mixing is comparable with that in the riser. Performance criteria in short contact or residence time processes should be significantly improved. Furthermore, radial gas dispersion in the downer is affected by the solid fraction of the bed. Higher solid fraction results in more uniform lateral gas dispersion. A mathematical model is applied to characterize the behavior of the gas dispersion in the two-phase downflow.

(6). The downer reactor furnishes significant advantages over the conventional riser reactor particularly for short residence time reactions due to its specific flow pattern, reduced backmixing, shorter flow development region and

capability of handling higher solids/gas loading ratios.

VI. OUTLOOK

A systematic investigation has been carried out on downer hydrodynamics in the first generation City College downer fluidization unit. Future studies would aim to develop more commercially applicable flow entrance, exit and gas-solids separator designs. Formation of a more homogeneous downflow gas/solid suspension at high velocities would be the goal of improved design to reduce the entrance and exit effects. Studies of heat and mass transfer characteristics are also necessary. Development of realistic hydrodynamic and reactor models would be necessary for process simulation and reactor design.

APPENDIX A:

Table A. EXPERIMENTAL RUNS

U_g(m/s)	G_s(kg/m^{2}s)	Measurements Performed, yes(✔), no(✗)				
		Axial Pressure	X-ray	Flux	Helium Tracing	Radial Pressure
1.88	106	✔	✔	✔	✗	✗
1.88	142	✔	✔	✔	✗	✗
1.88	191	✔	✔	✔	✗	✗
2.1	116	✔	✔	✔	✗	✗
2.1	123	✔	✔	✔	✗	✗
2.1	176	✔	✔	✔	✗	✗
2.9	51	✔	✔	✔	✗	✗
2.9	112	✔	✔	✔	✗	✗
2.9	227	✔	✔	✔	✗	✗
3.1	67	✔	✔	✔	✗	✗
3.1	102	✔	✔	✔	✗	✗
3.1	149	✔	✔	✔	✗	✗
3.7	50	✔	✔	✔	✗	✗
3.7	123	✔	✔	✔	✗	✔
3.7	236	✔	✔	✔	✗	✗
4.2	104	✔	✔	✔	✗	✗
4.2	140	✔	✔	✔	✗	✗
4.2	195	✔	✔	✔	✗	✗
4.71	96	✔	✔	✔	✗	✗

U_g(m/s)	G_s(kg/m^{2}s)	Measurements Performed, yes(✔), no(✗)				
		Axial Pressure	X-ray	Flux	Helium Tracing	Radial Pressure
4.71	147	✔	✔	✔	✗	✗
4.71	218	✔	✔	✔	✗	✗
3.4	123	✔	✔	✗	✗	✗
2.41	152	✗	✔	✗	✗	✗
2.15	99	✗	✔	✗	✗	✗
3.7	227	✗	✔	✗	✗	✗
4.76	137	✗	✔	✗	✗	✗
2.9	123	✔	✗	✗	✗	✗
3.15	67	✔	✗	✗	✗	✗
3.15	122	✔	✗	✗	✗	✗
2.38	140	✔	✗	✗	✗	✗
3.67	141	✗	✗	✔	✗	✗
3.67	156	✗	✗	✔	✗	✗
2.16	95	✗	✗	✔	✗	✗
3.81	150	✗	✗	✔	✗	✗
2.13	140	✗	✗	✔	✗	✗
3.22	0	✗	✗	✗	✔	✗
3.22	117	✗	✗	✗	✔	✗
3.22	128	✗	✗	✗	✔	✗
2.52	116	✗	✗	✗	✔	✗
2.52	142	✗	✗	✗	✔	✗
2.52	169	✗	✗	✗	✔	✗

U_g(m/s)	G_s(kg/m^{2}s)	Measurements Performed, yes(✔), no(✗)				
		Axial Pressure	X-ray	Flux	Helium Tracing	Radial Pressure
4.65	131	✗	✗	✗	✔	✗
5.0	121	✗	✗	✗	✔	✗
3.0	121	✗	✗	✗	✔	✗
1.0	121	✗	✗	✗	✔	✗
2.52	0	✗	✗	✗	✔	✗
2.52	139	✗	✗	✗	✔	✗
1.59	138	✗	✗	✗	✗	✔
2.36	125	✗	✗	✗	✗	✔
2.4	144	✗	✗	✗	✗	✔
2.82	134	✗	✗	✗	✗	✔
3.4	0	✗	✗	✗	✗	✔
3.65	0	✗	✗	✗	✗	✔
3.65	124	✗	✗	✗	✗	✔
3.7	128	✗	✗	✗	✗	✔
3.66	123	✗	✗	✗	✗	✔
3.96	0	✗	✗	✗	✗	✔
3.92	147	✗	✗	✗	✗	✔
4.3	142	✗	✗	✗	✗	✔
5.4	0	✗	✗	✗	✗	✔(riser)
6.4	116	✗	✗	✗	✗	✔(riser)
7.4	110	✗	✗	✗	✗	✔(riser)

APPENDIX B. AXIAL PRESSURE PROFILE

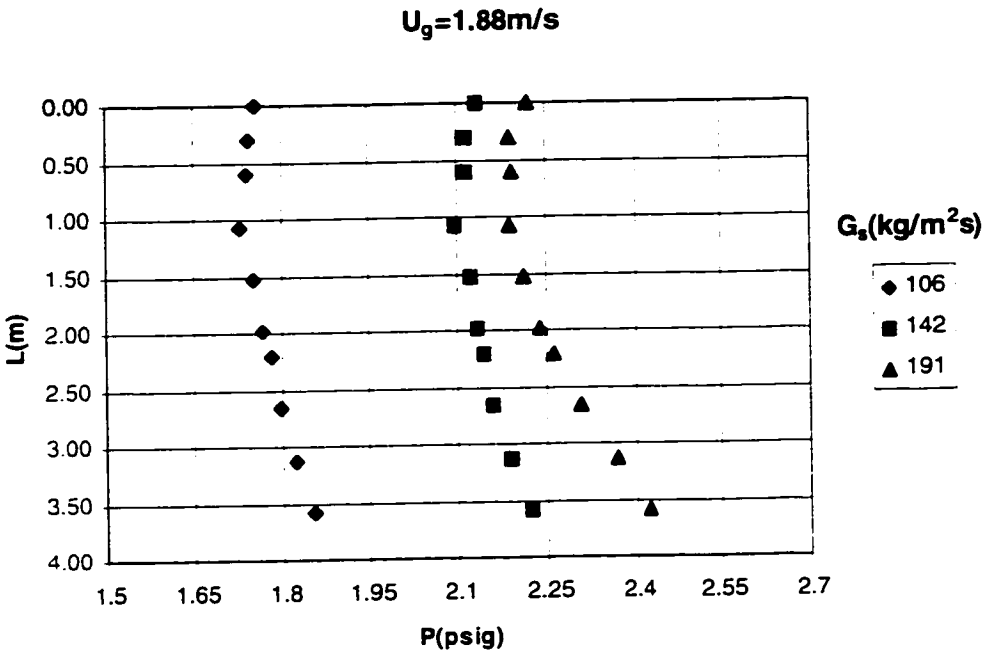

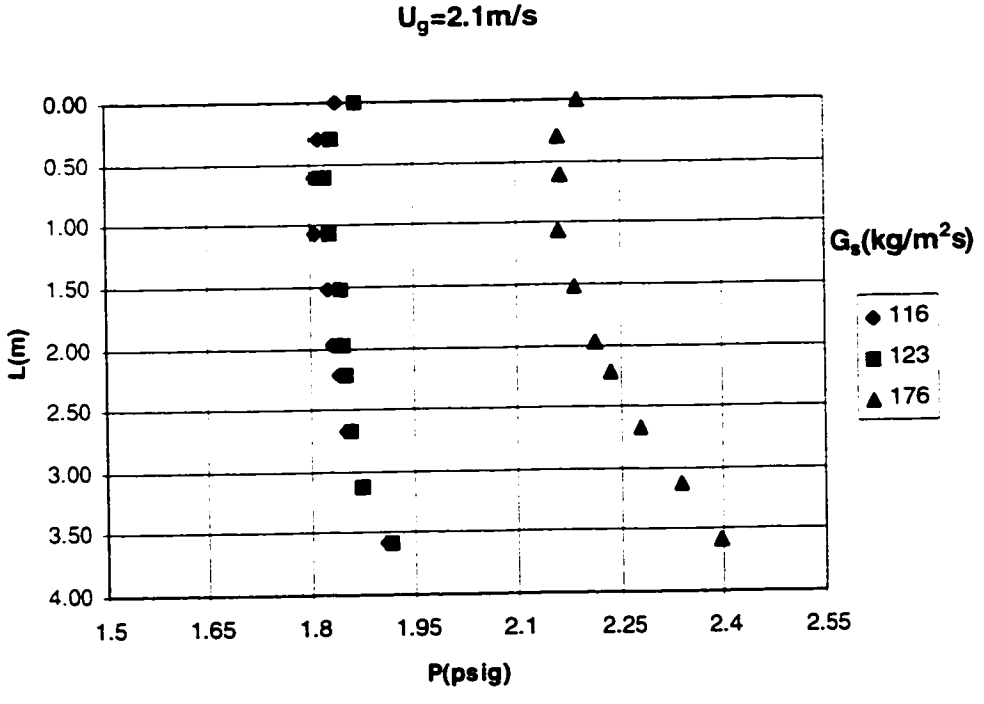

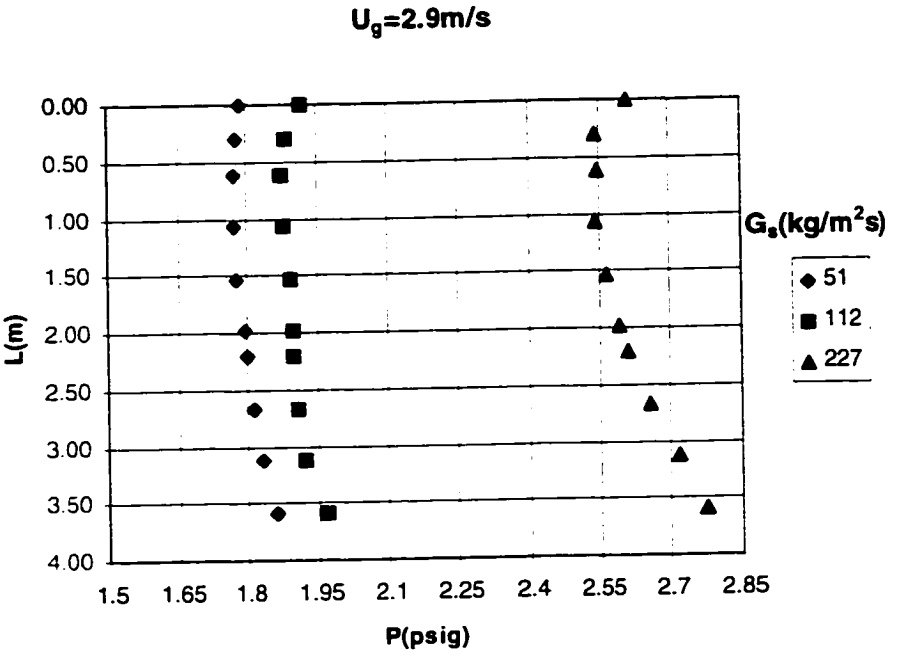

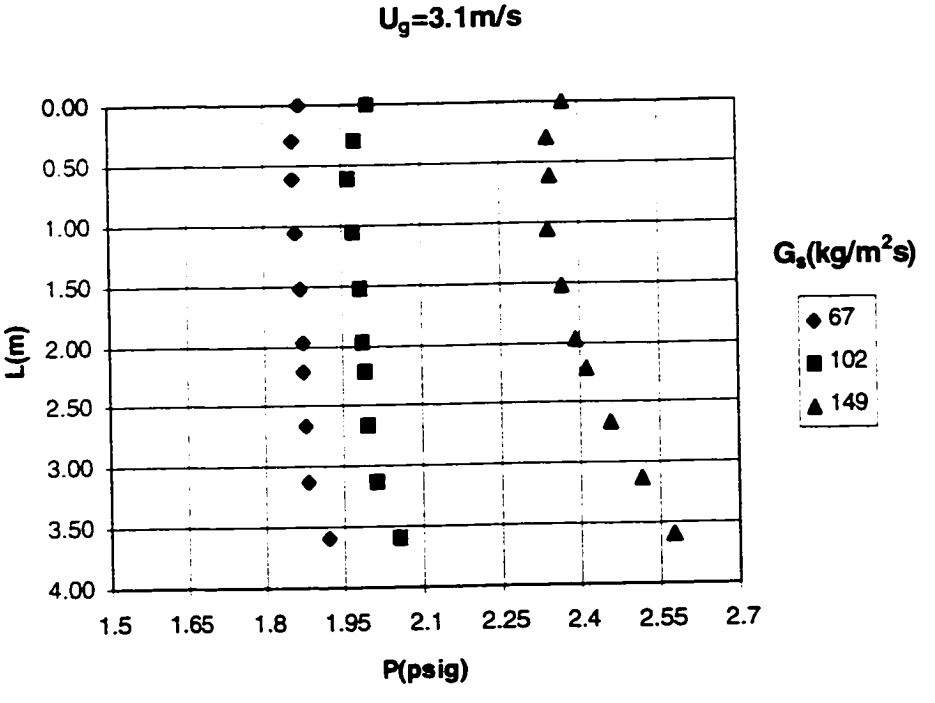

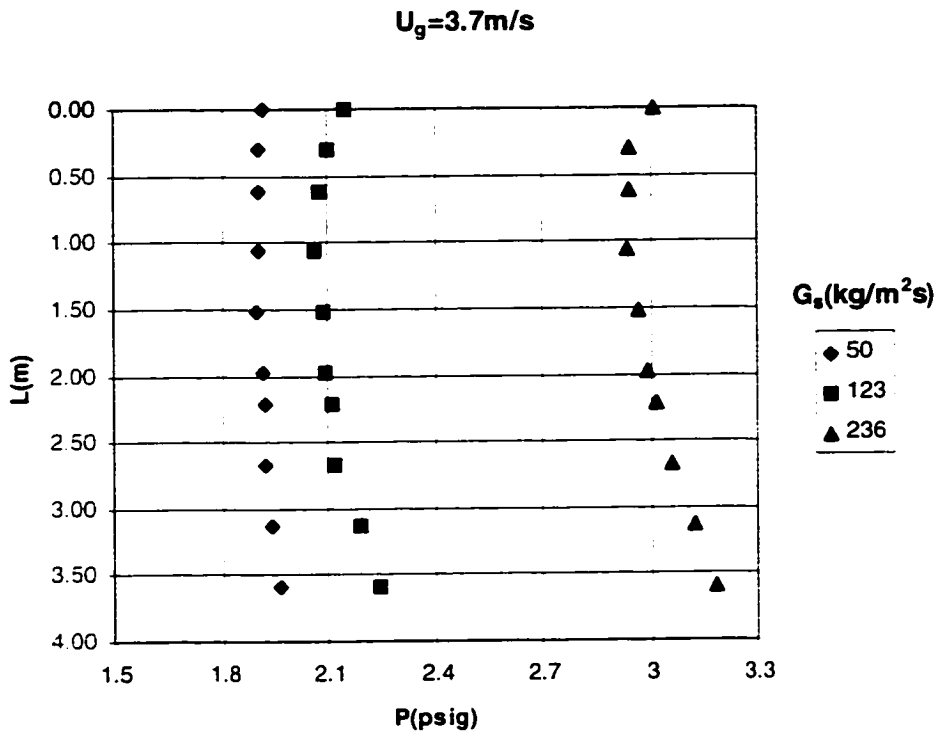

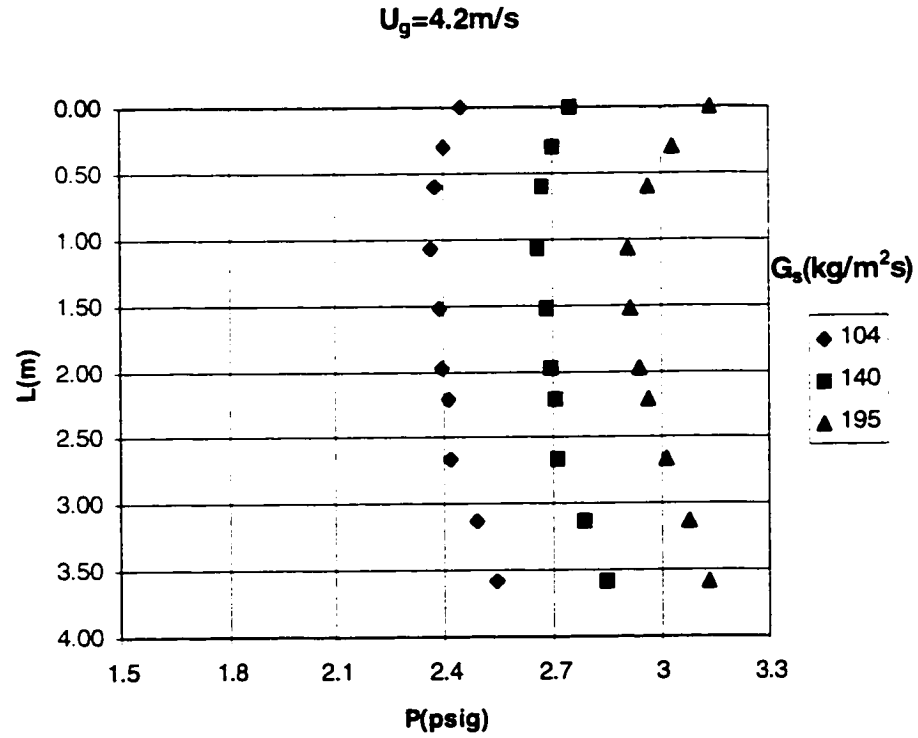

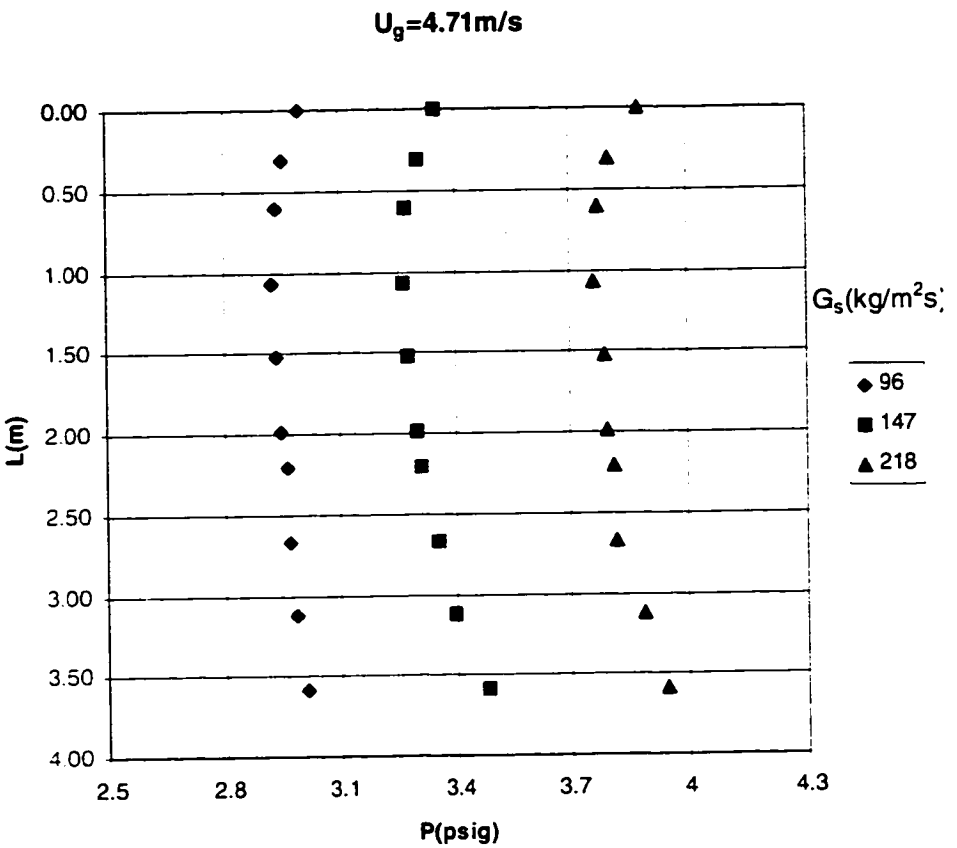

APPENDIX C. RADIAL SOLID FRACTION PROFILE

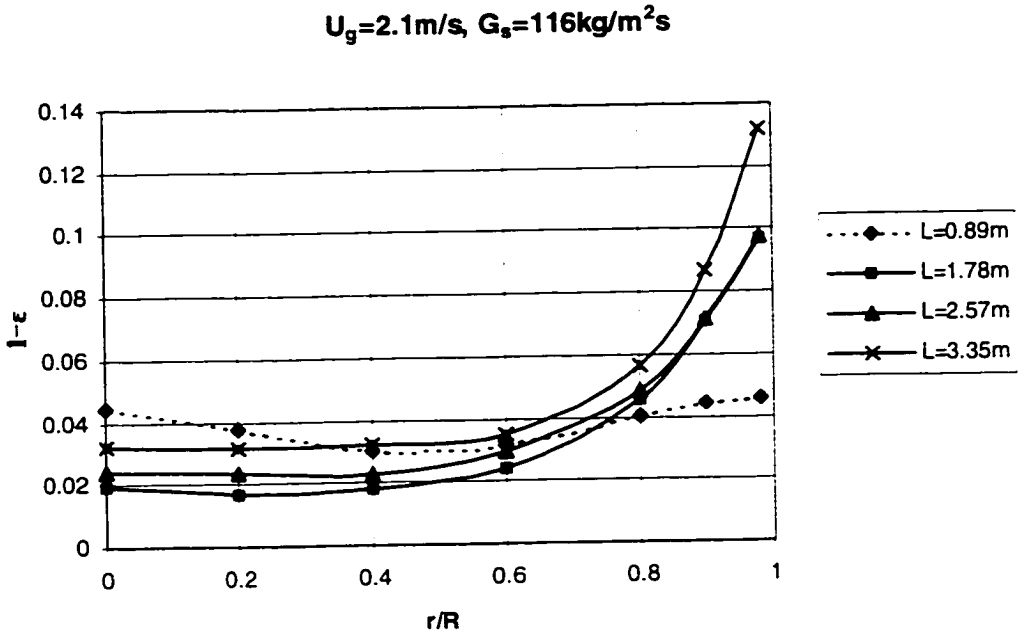

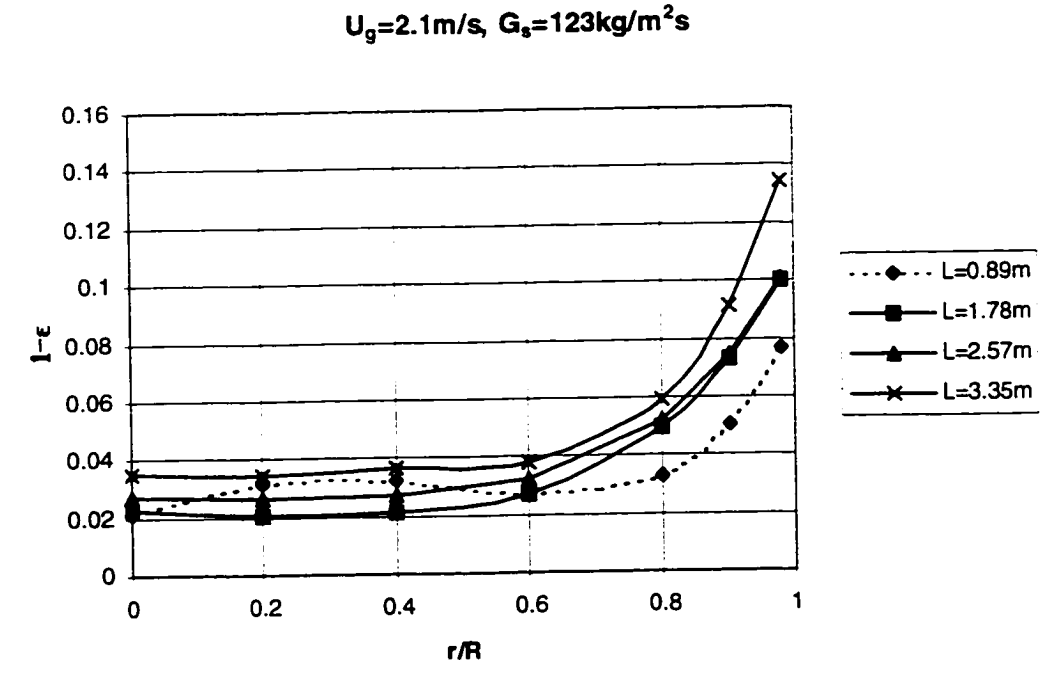

U_g=2.1m/s, G_s=176kg/m^{2}s

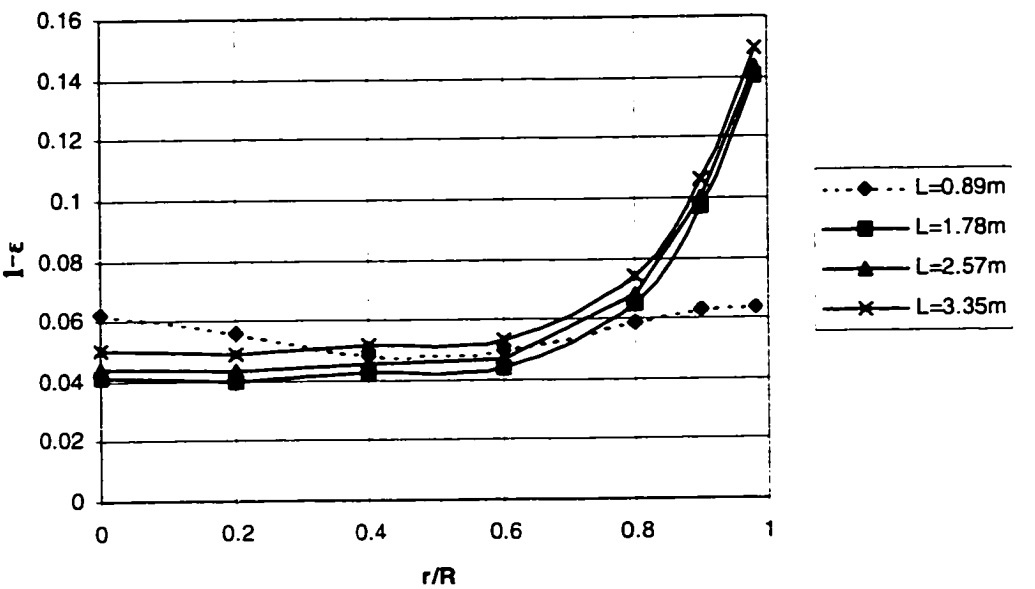

U_g=2.9m/s, G_s=51kg/m^{2}s

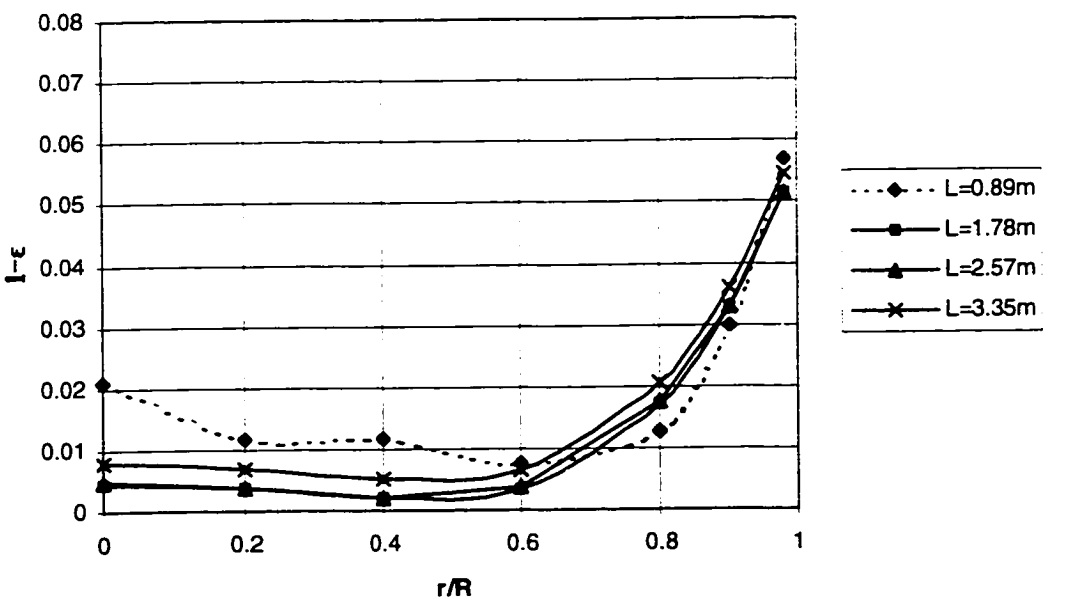

U_g=2.9m/s, G_s=112kg/m^{2}s

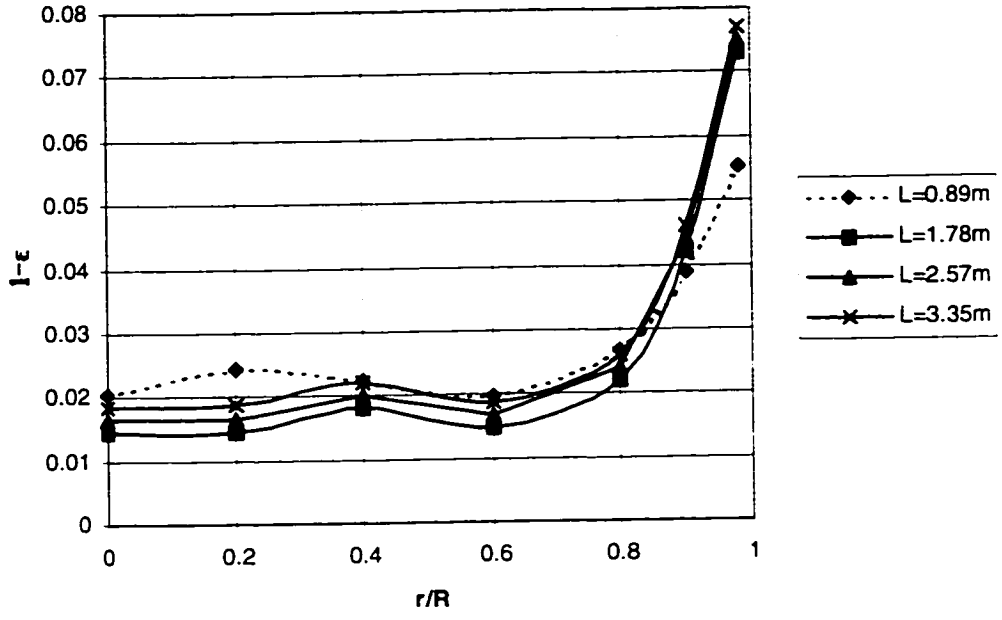

U_g=2.9m/s, G_s=227kg/m^{2}s

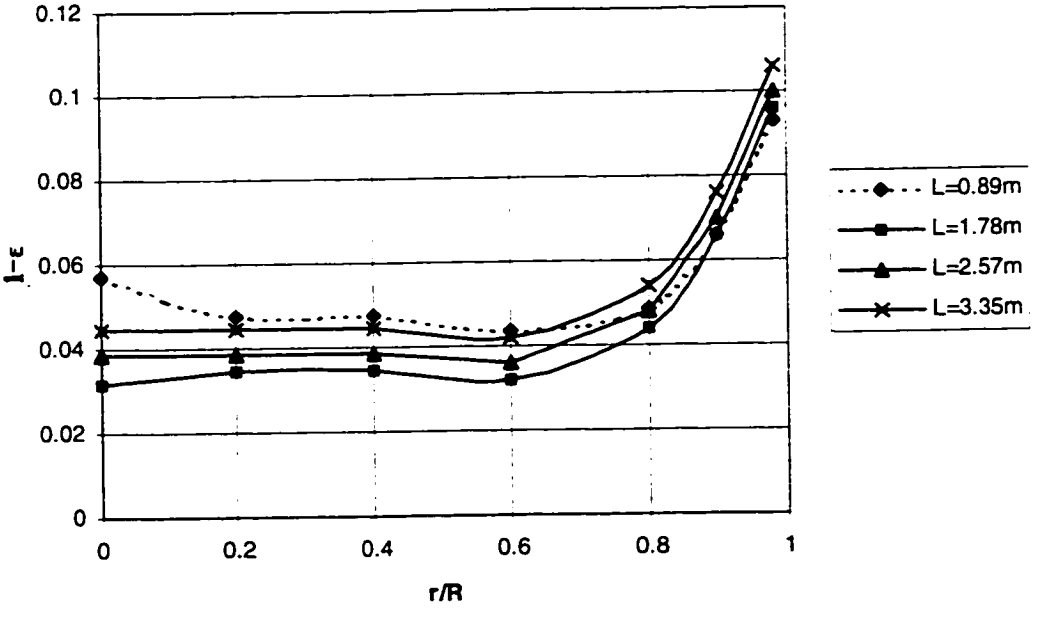

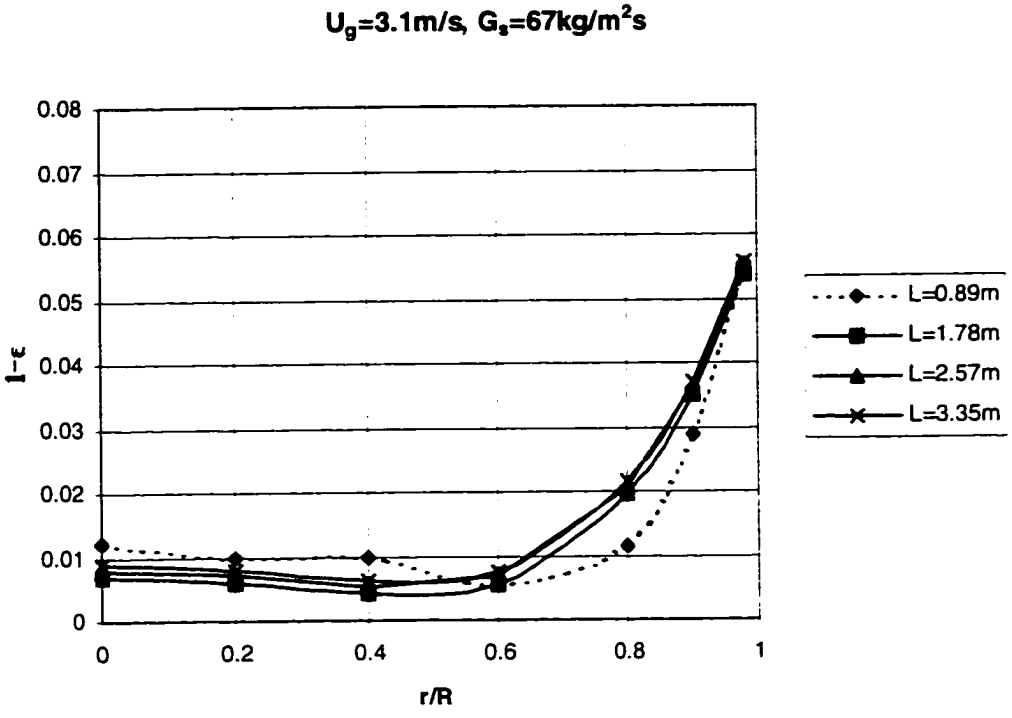

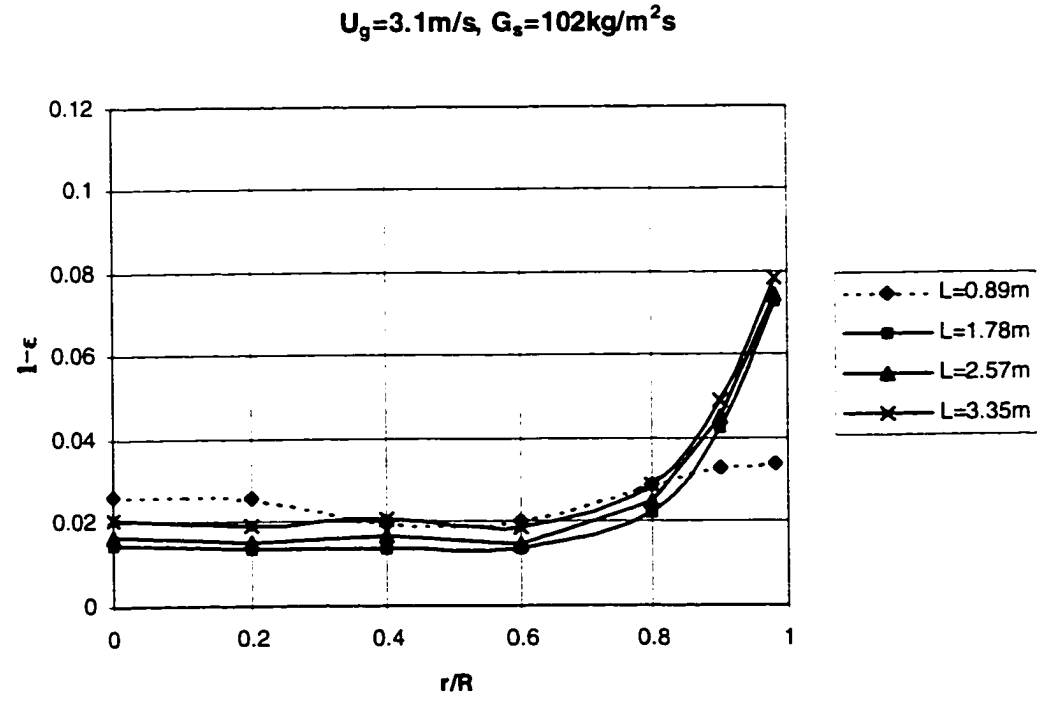

U_g=3.1m/s, G_s=149kg/m^{2}s

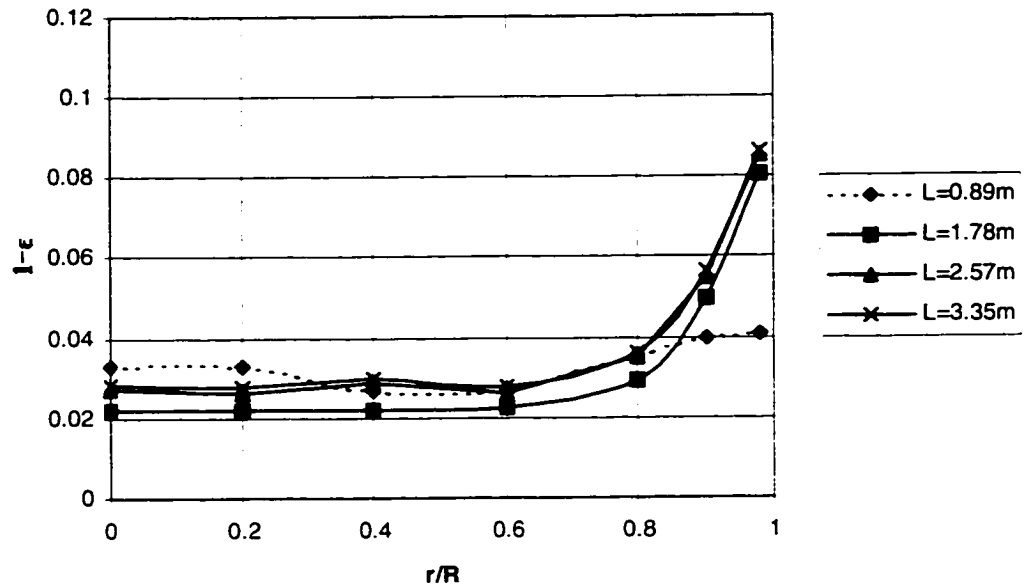

U_g=3.7m/s, G_s=50kg/m^{2}s

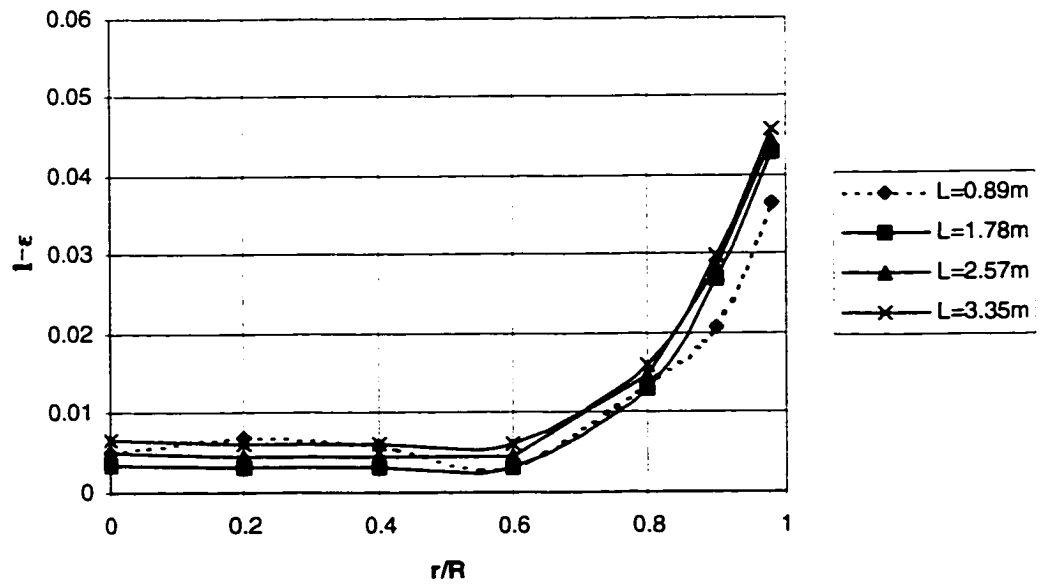

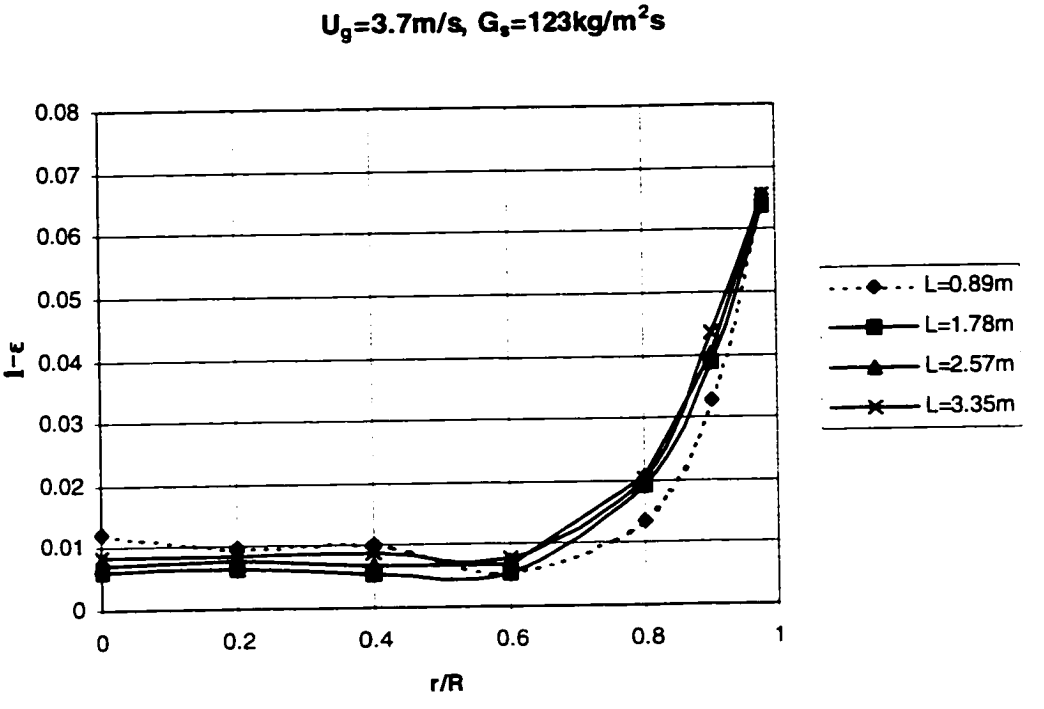

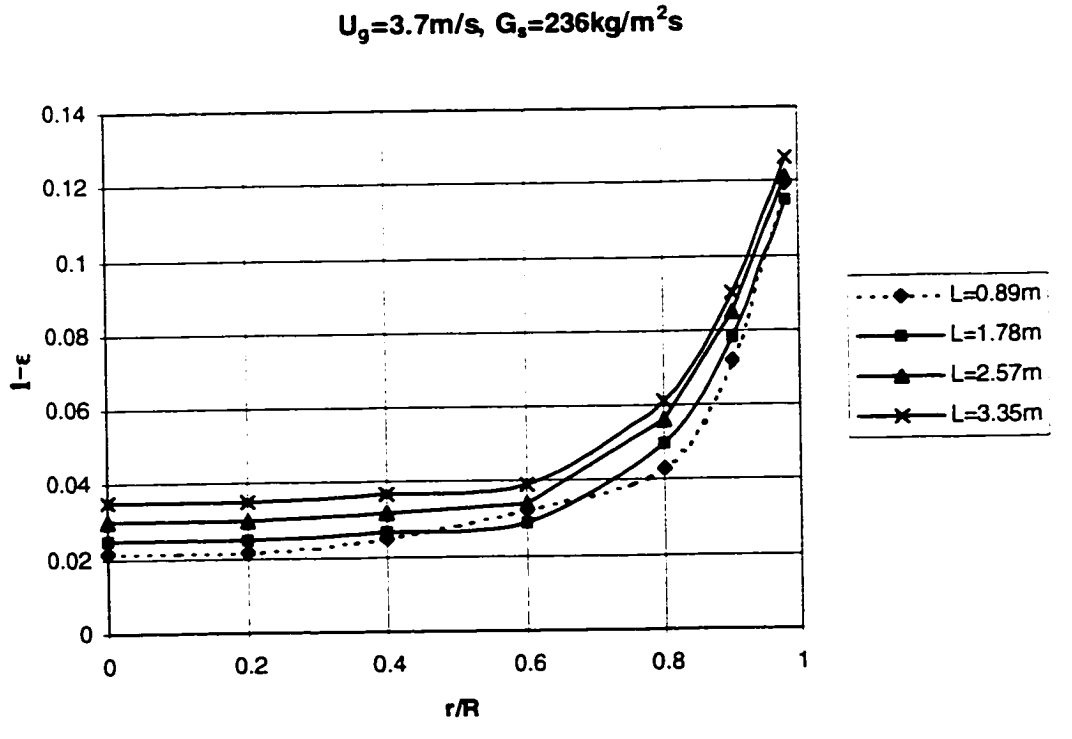

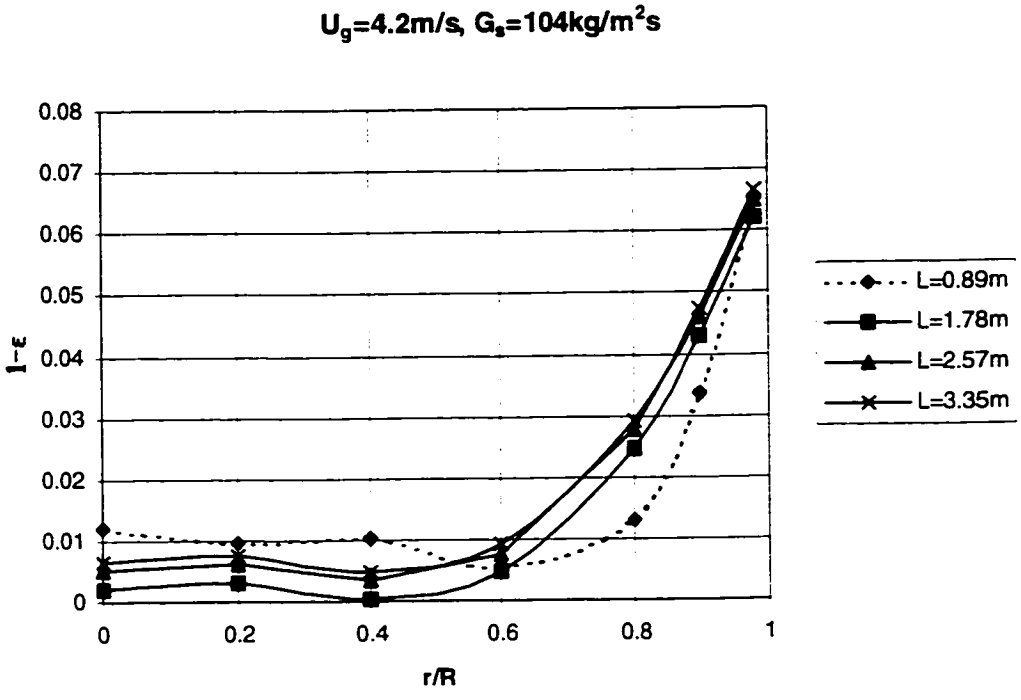

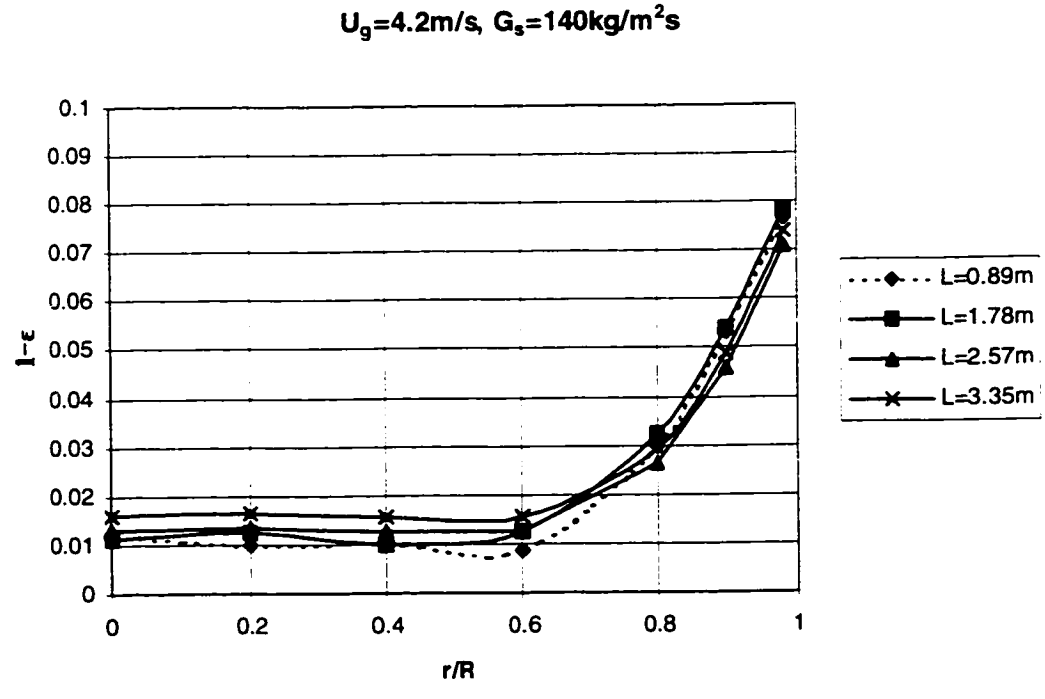

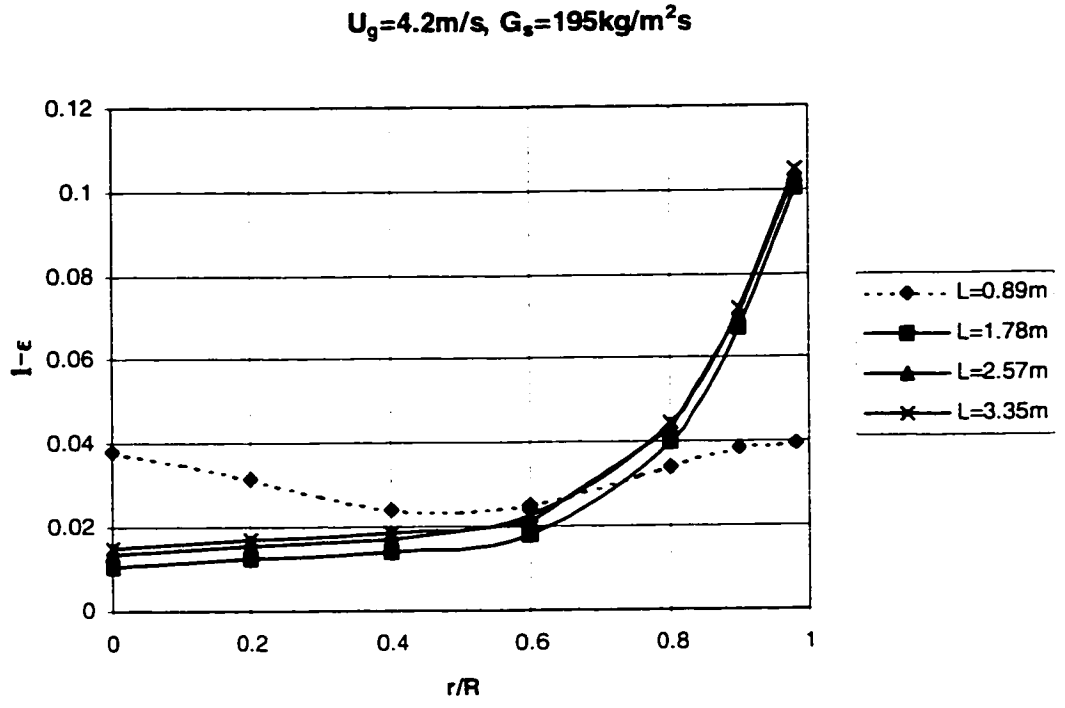

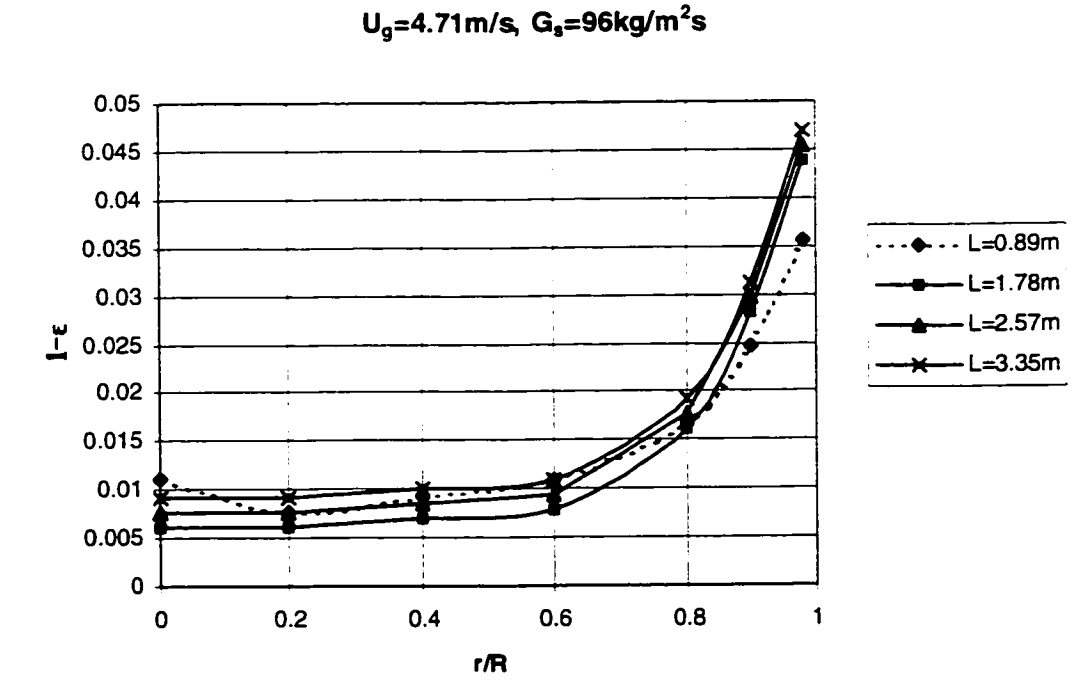

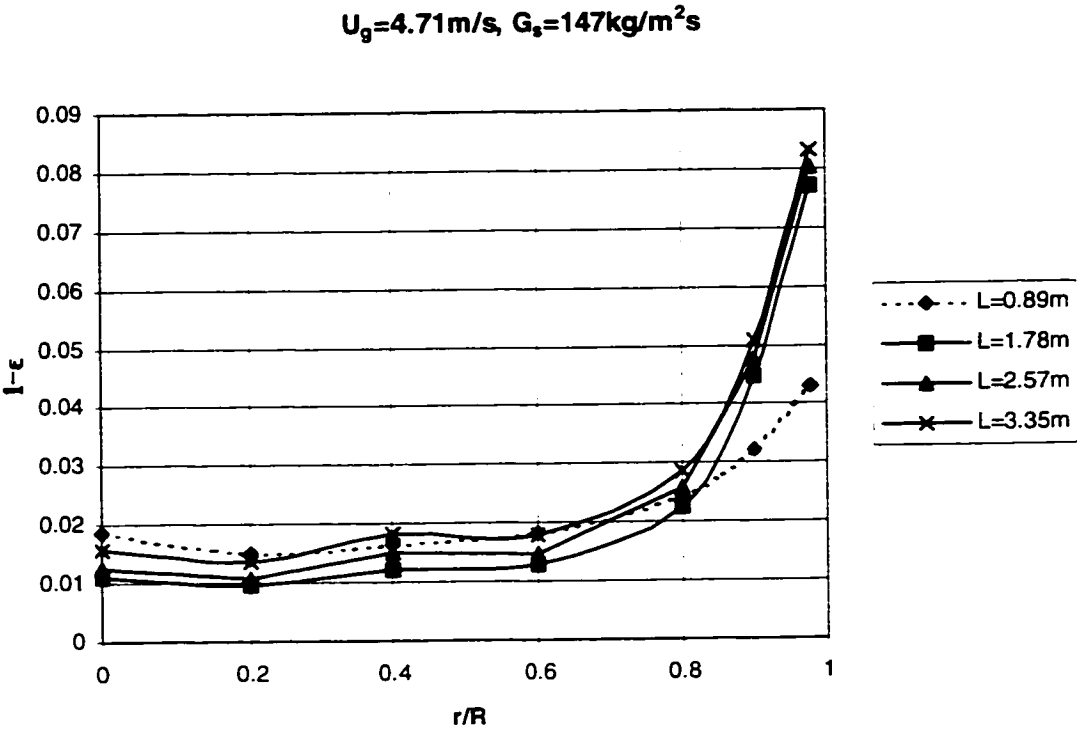

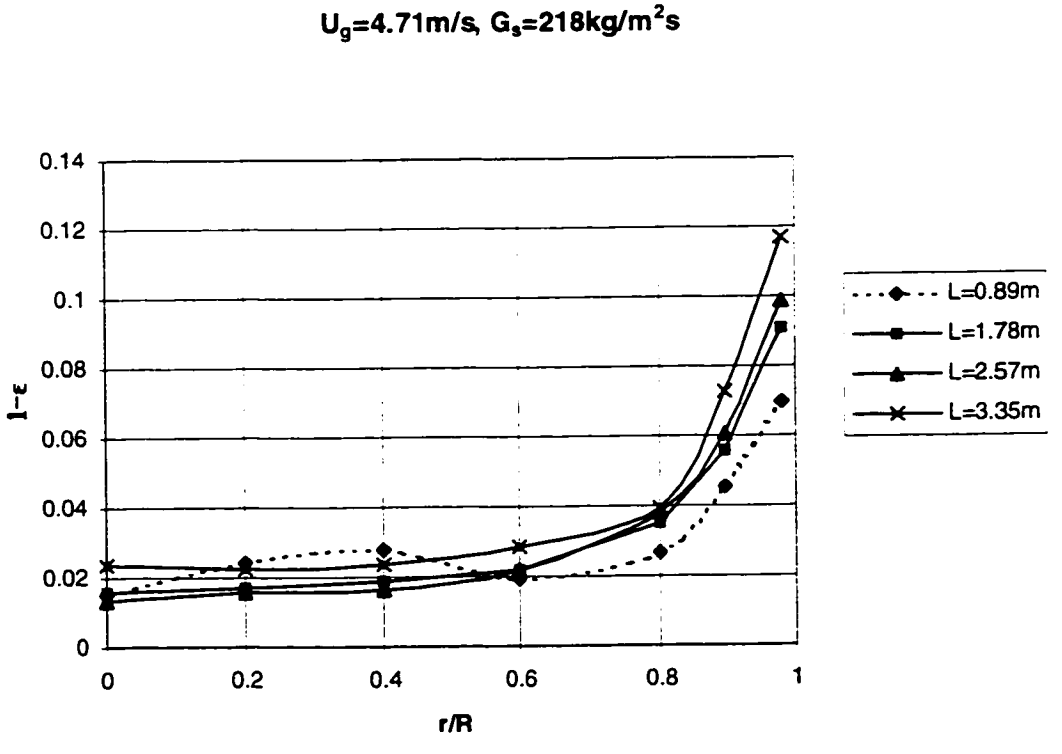

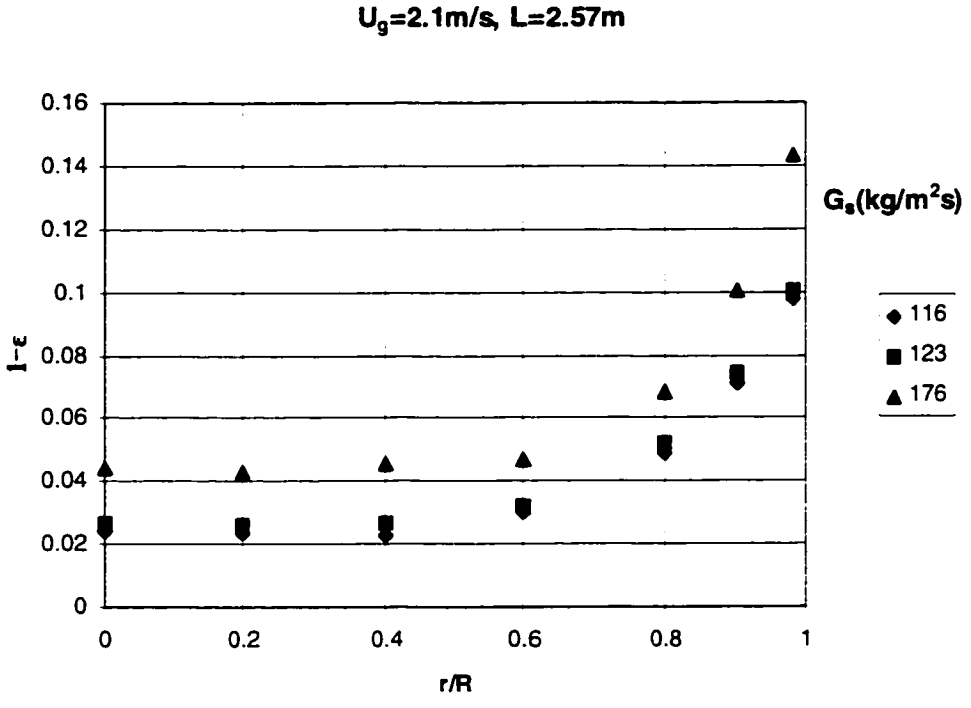

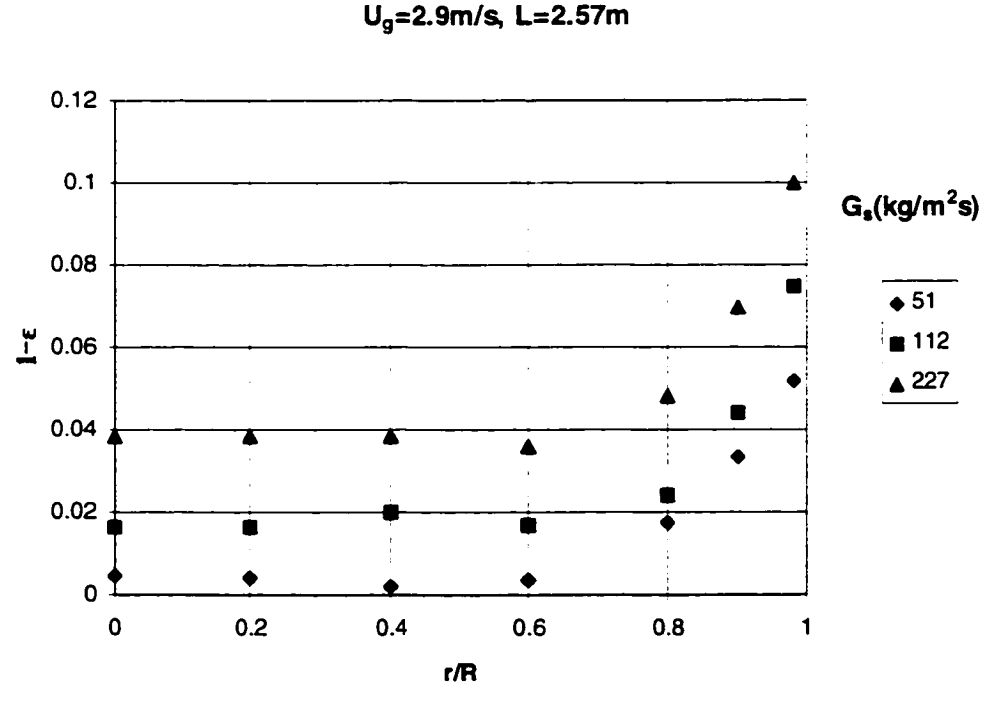

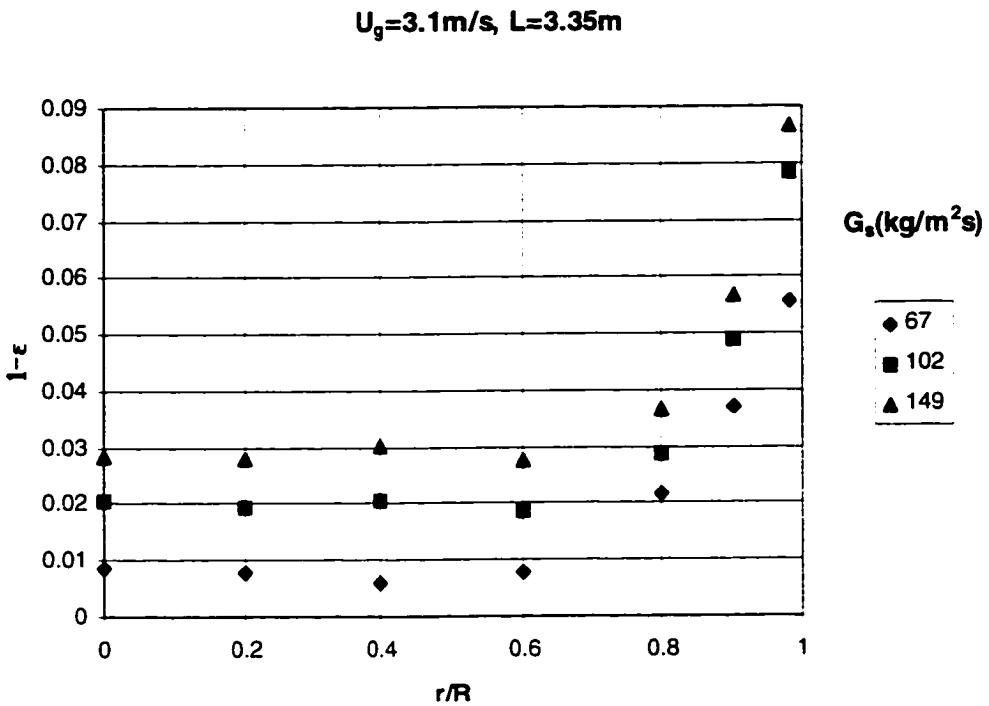

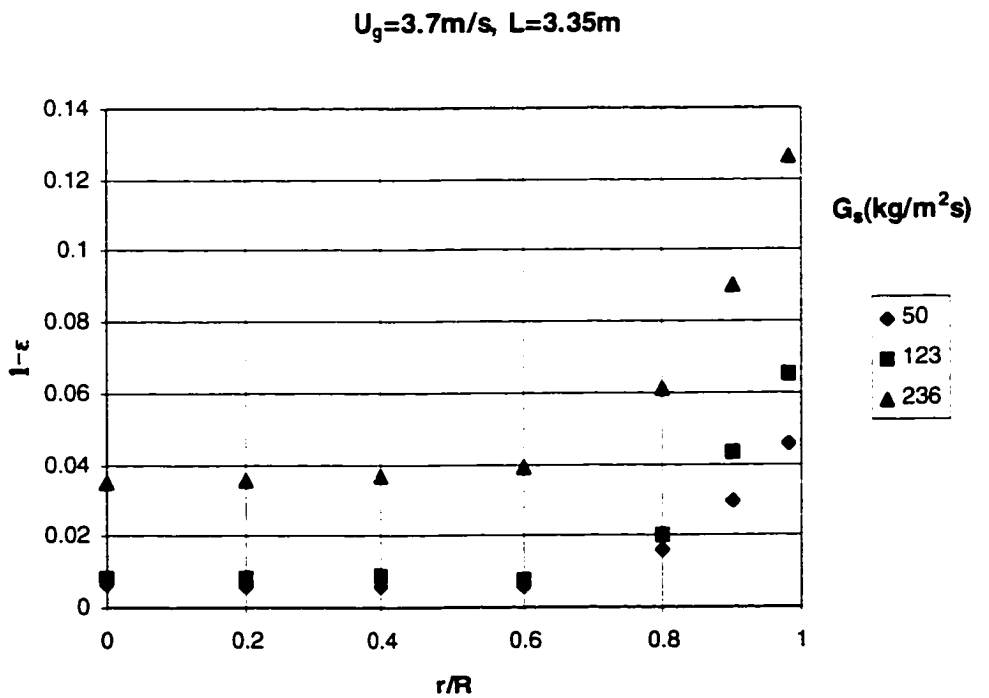

U_g=4.2m/s, L=1.78m

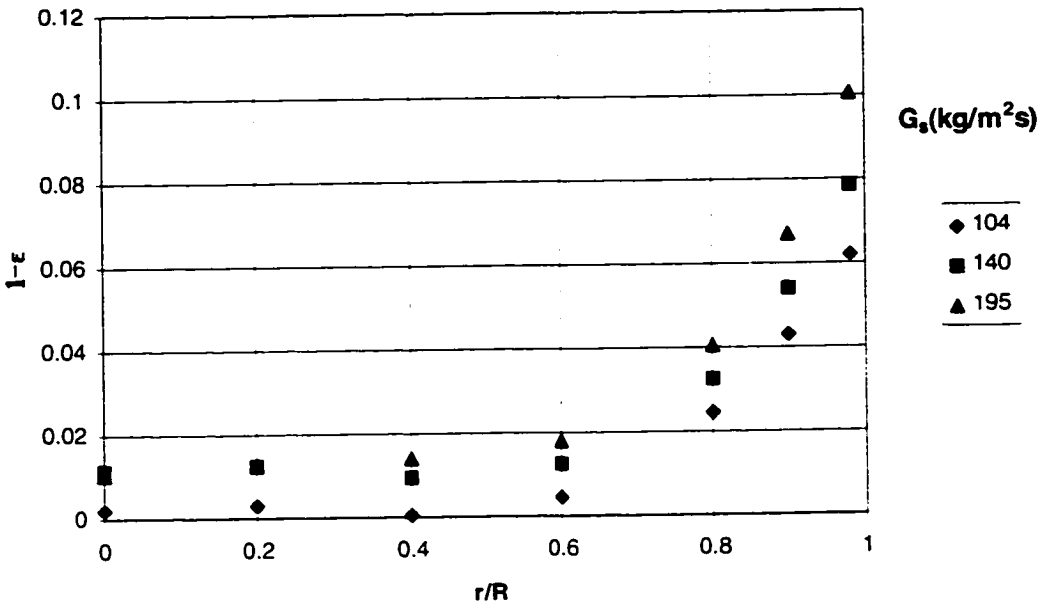

U_g=4.71m/s, L=1.78m

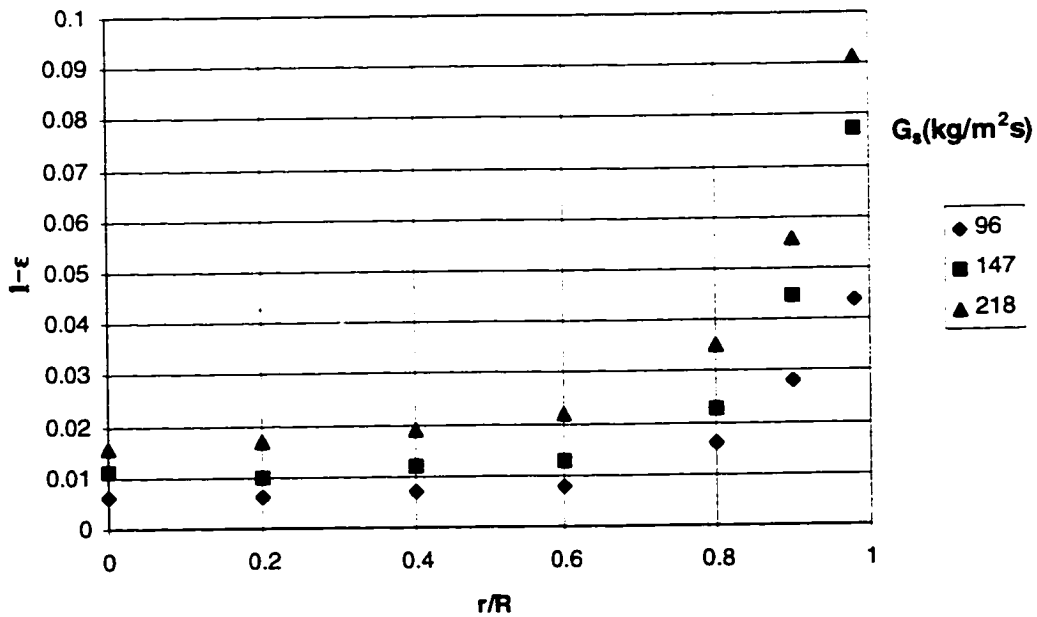

APPENDIX D. AXIAL SOLID FRACTION PROFILE

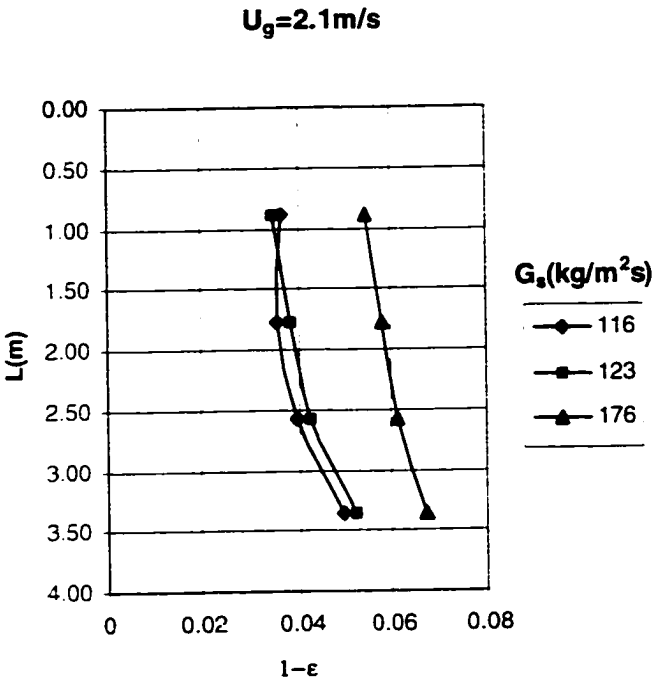

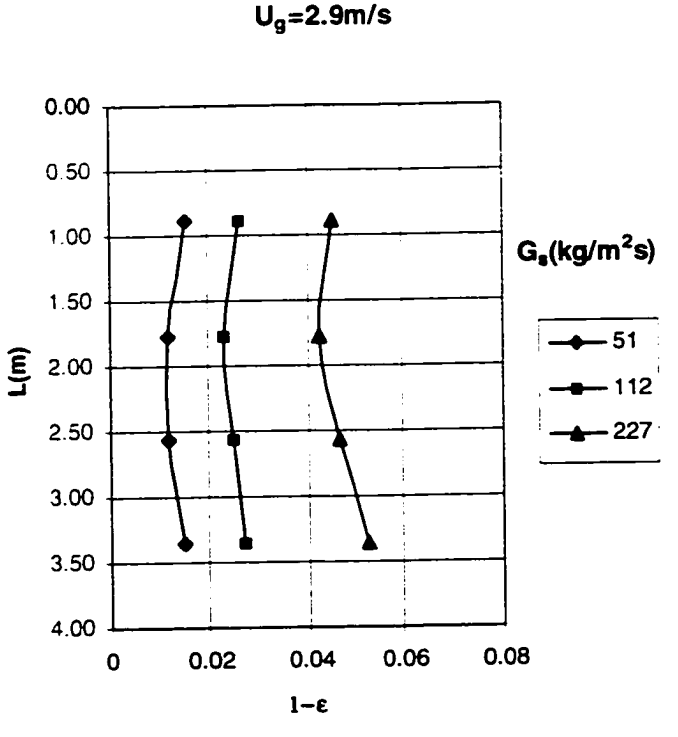

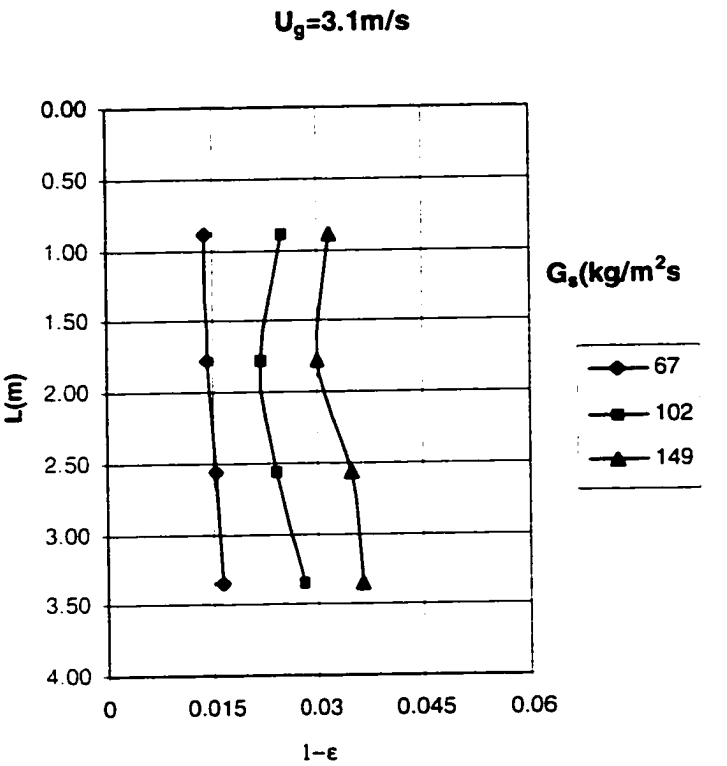

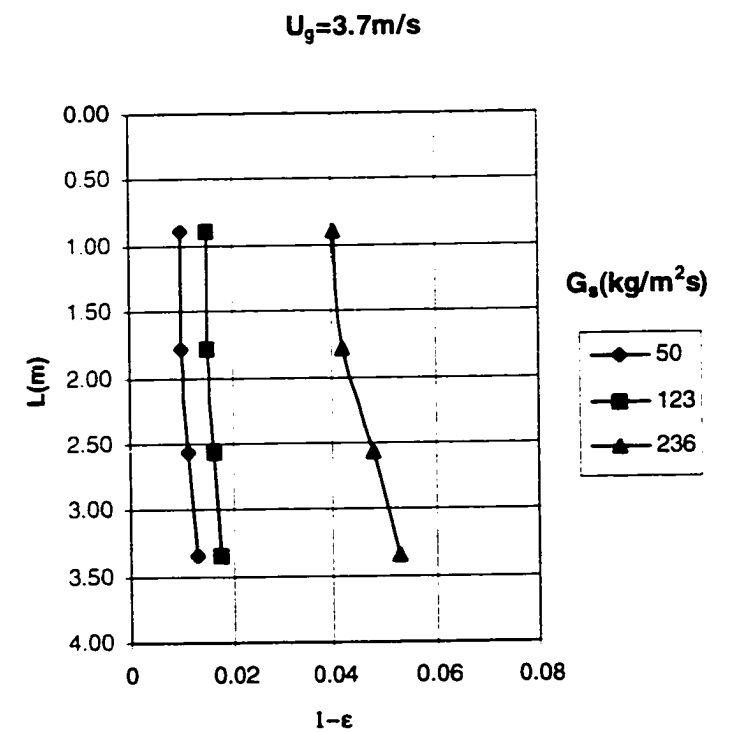

U_g=4.2m/s

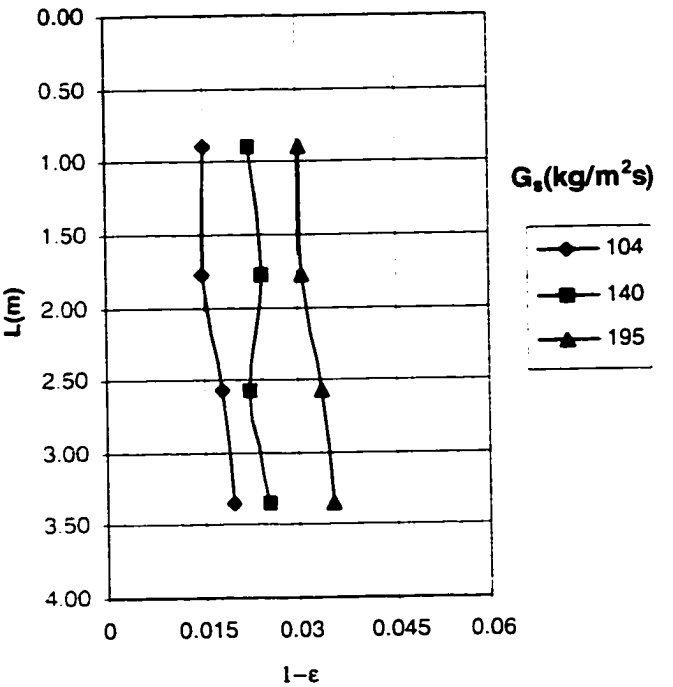

U_g=4.71m/s

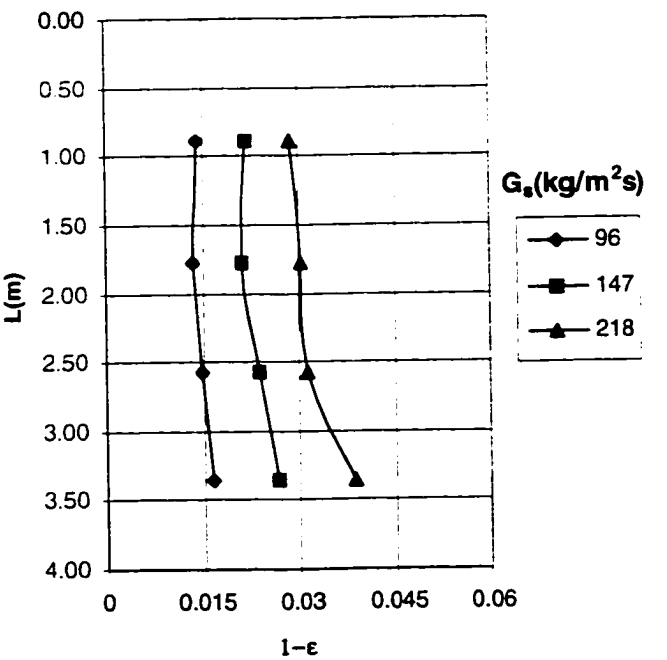

U_g=2.1m/s, G_s=123kg/m^{2}s

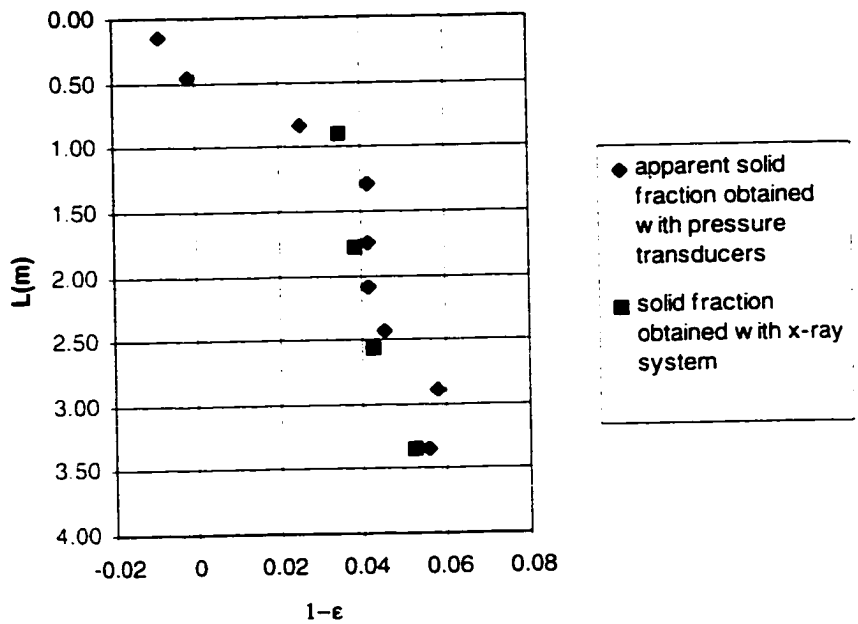

U_g=2.9m/s, G_s=112kg/m^{2}s

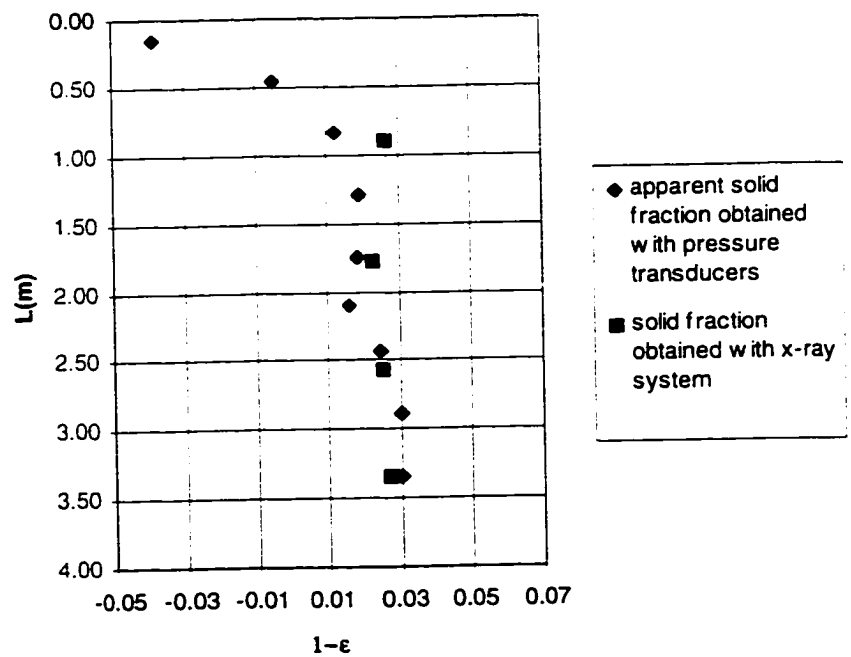

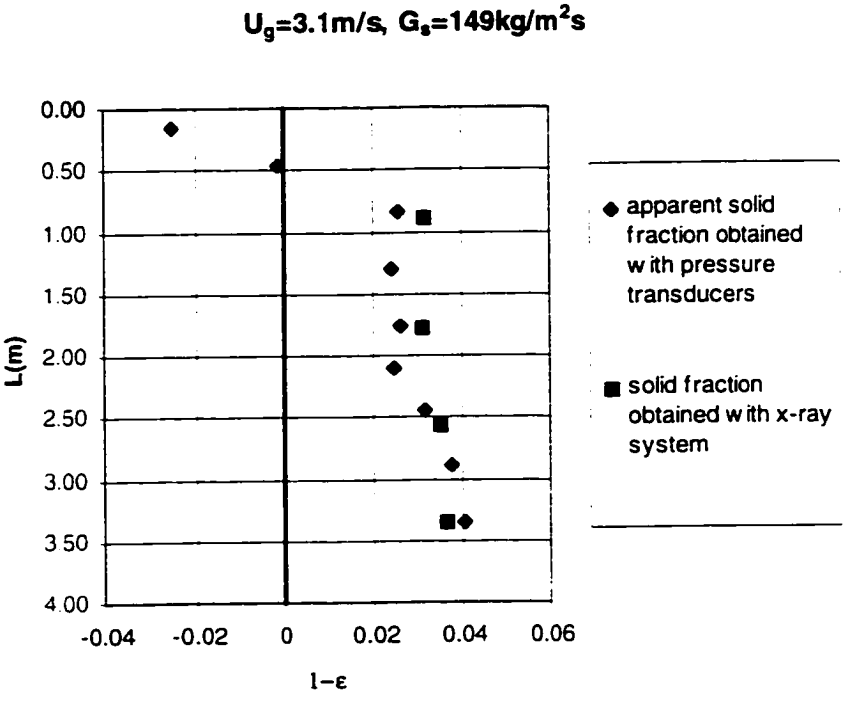

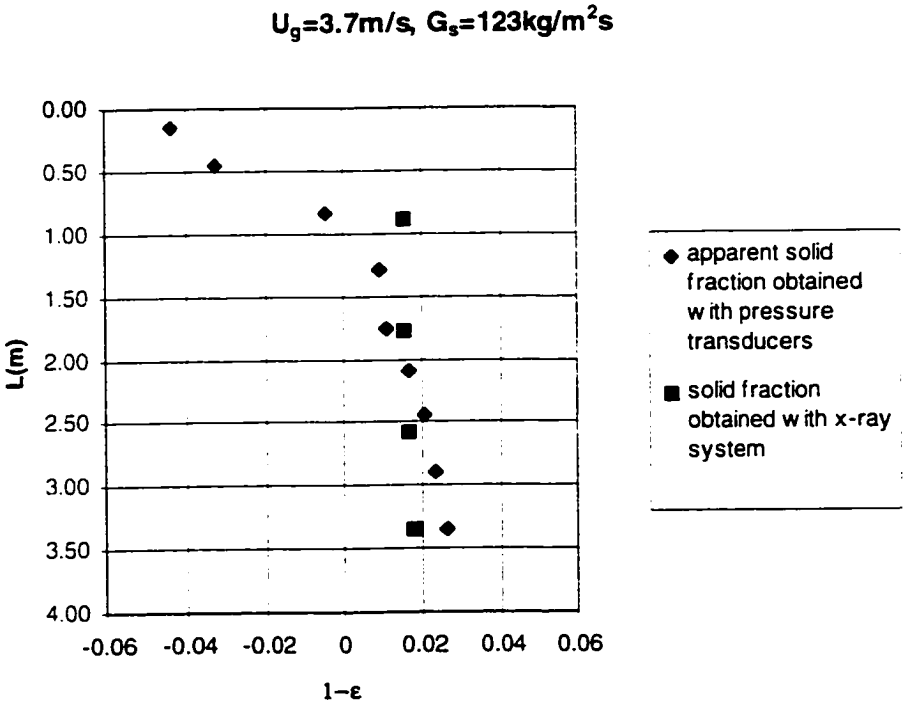

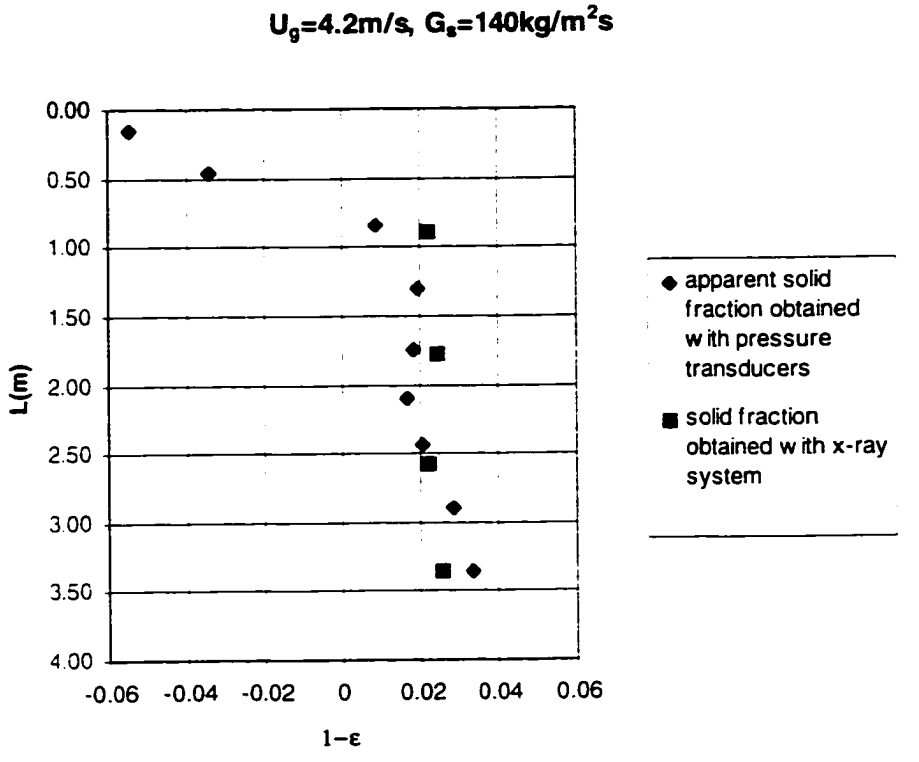

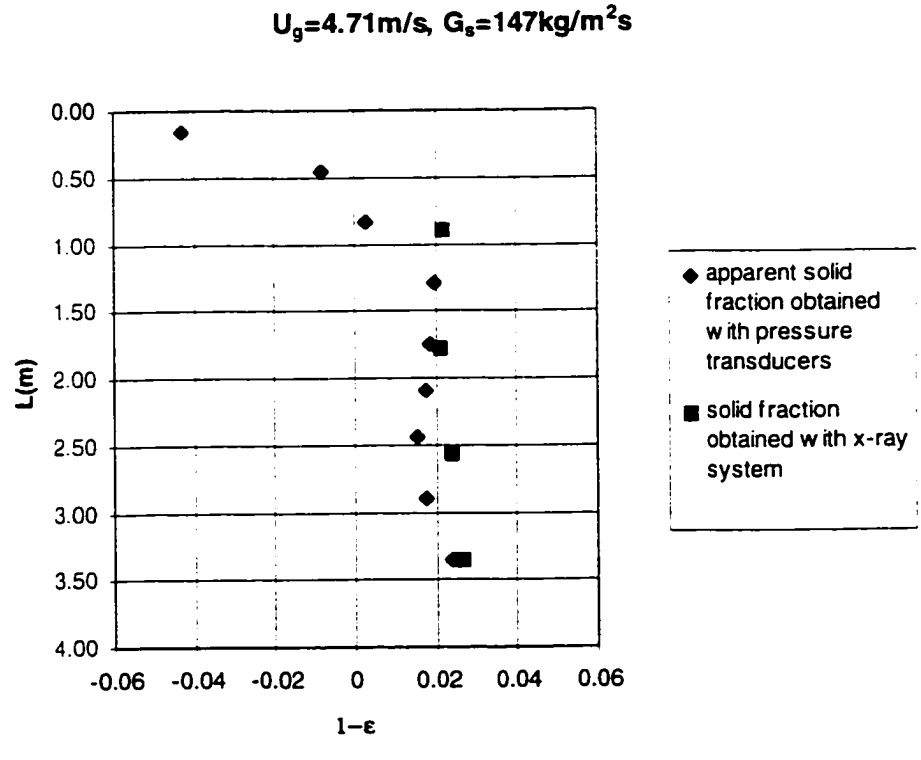

APPENDIX E. LOCAL SOLID FLUX PROFILE

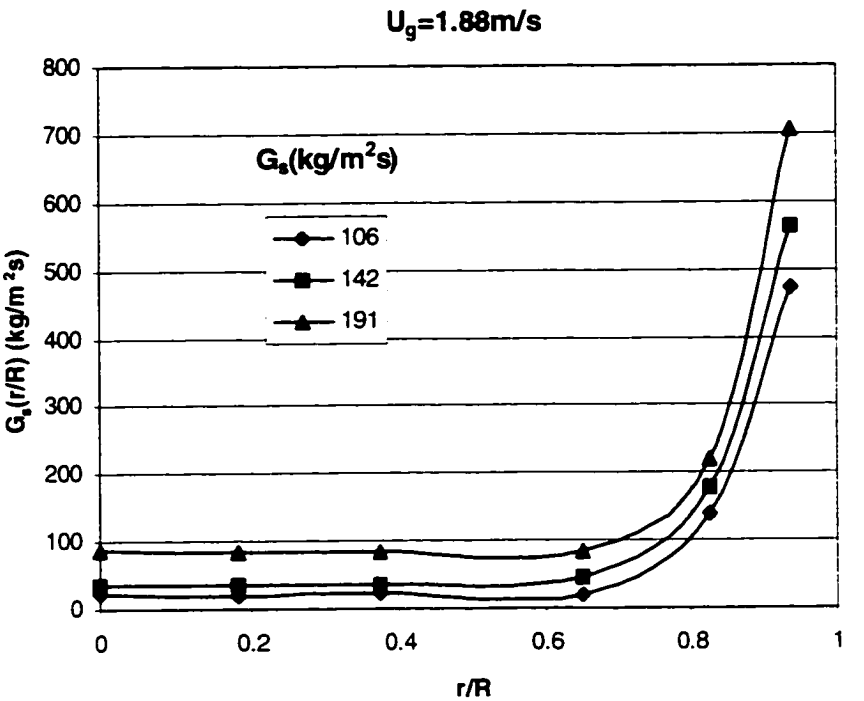

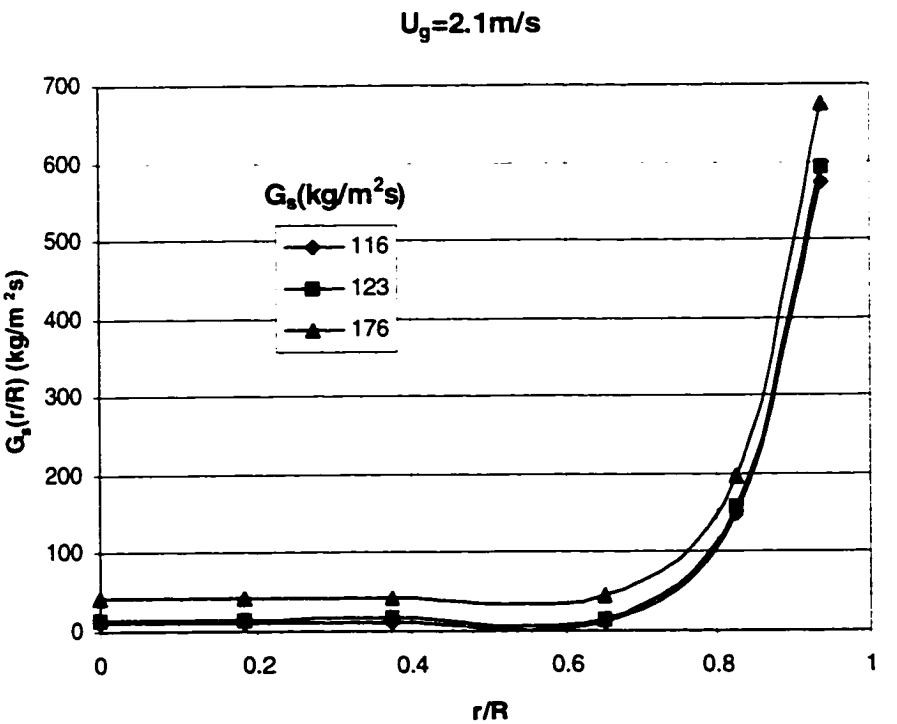

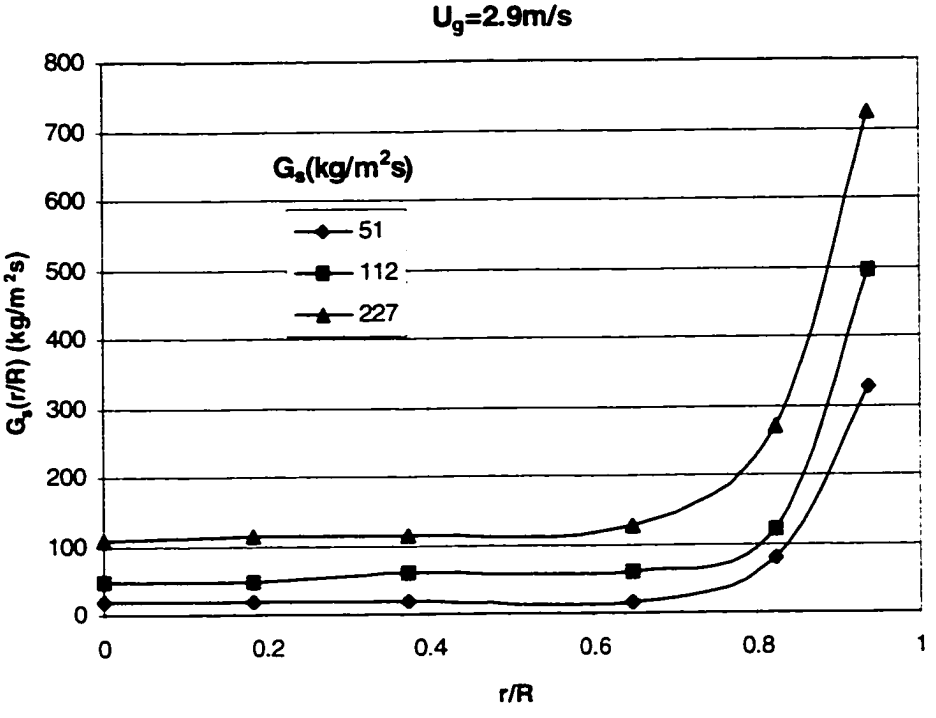

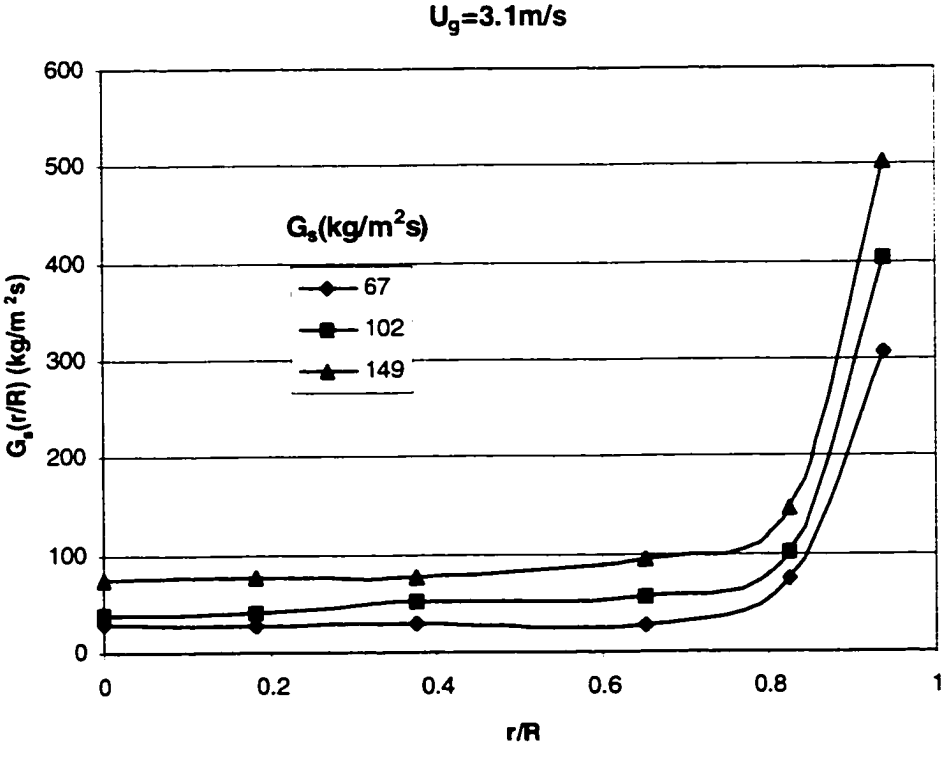

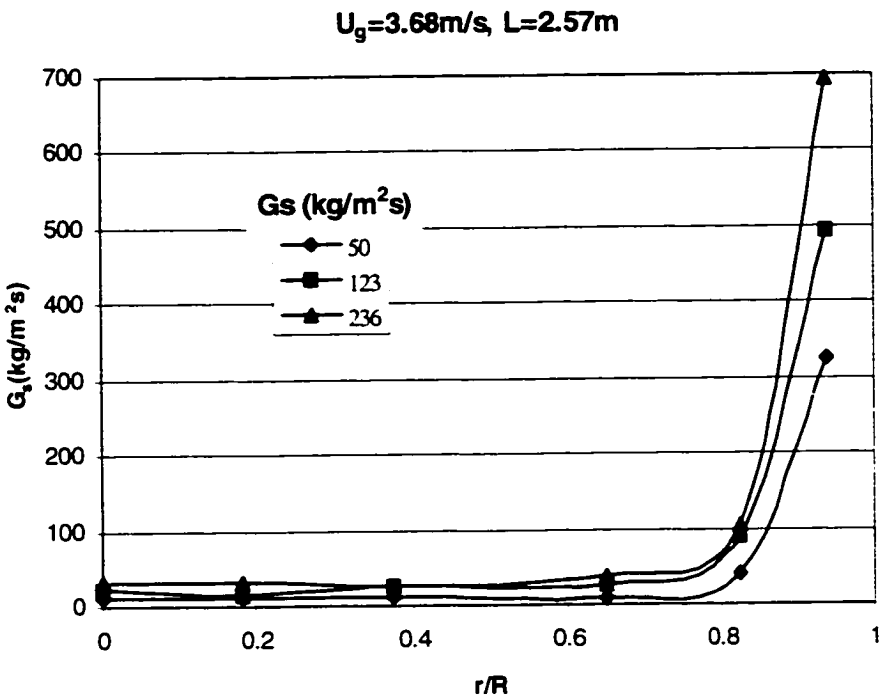

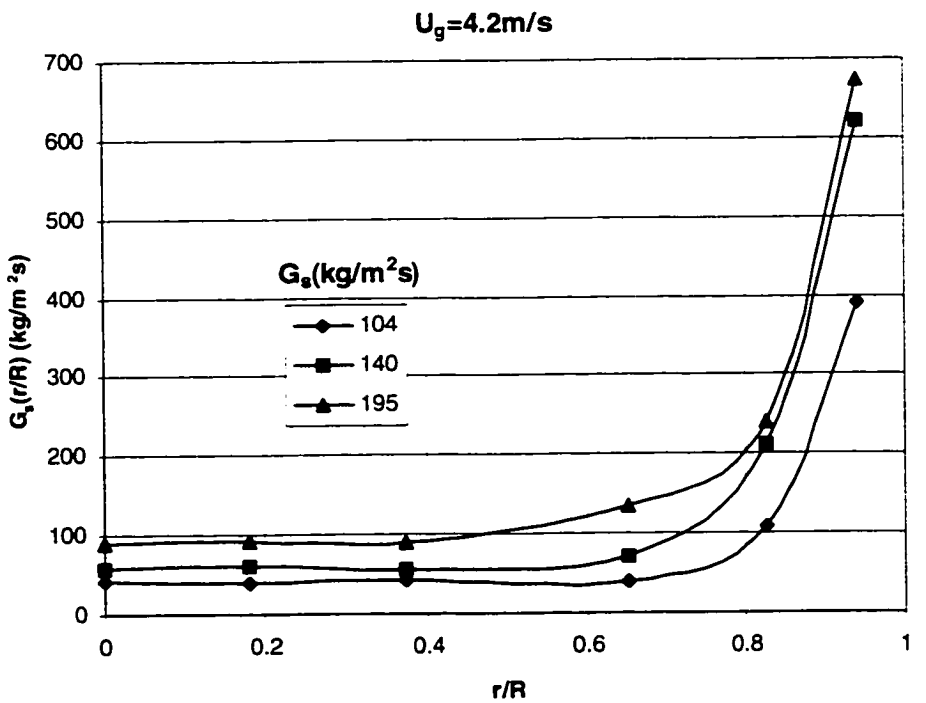

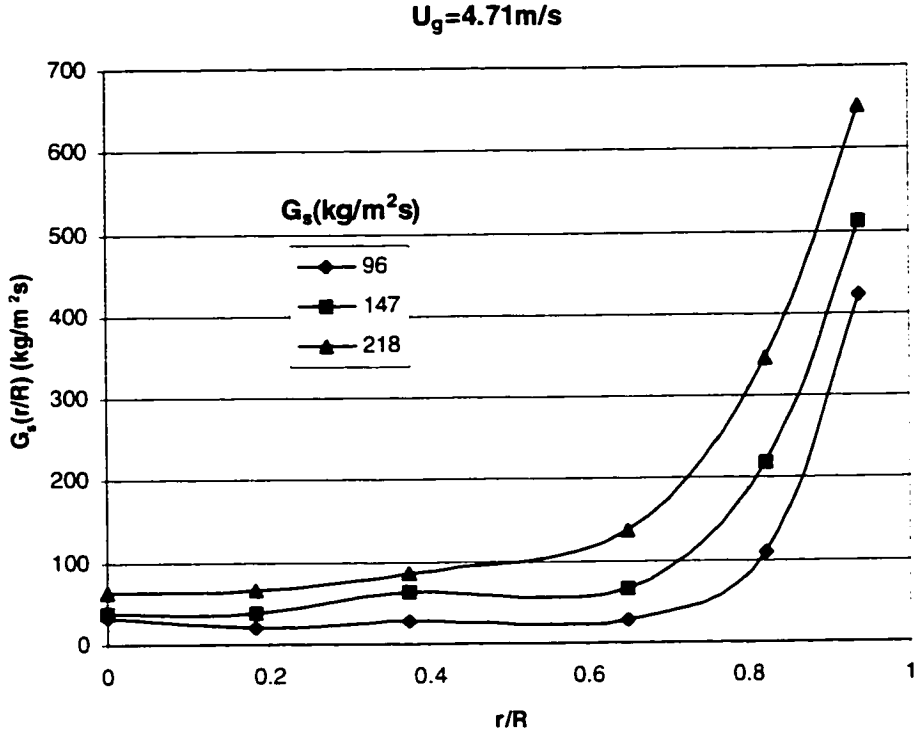

APPENDIX F. ESTIMATED GAS-SOLID VELOCITY PROFILE

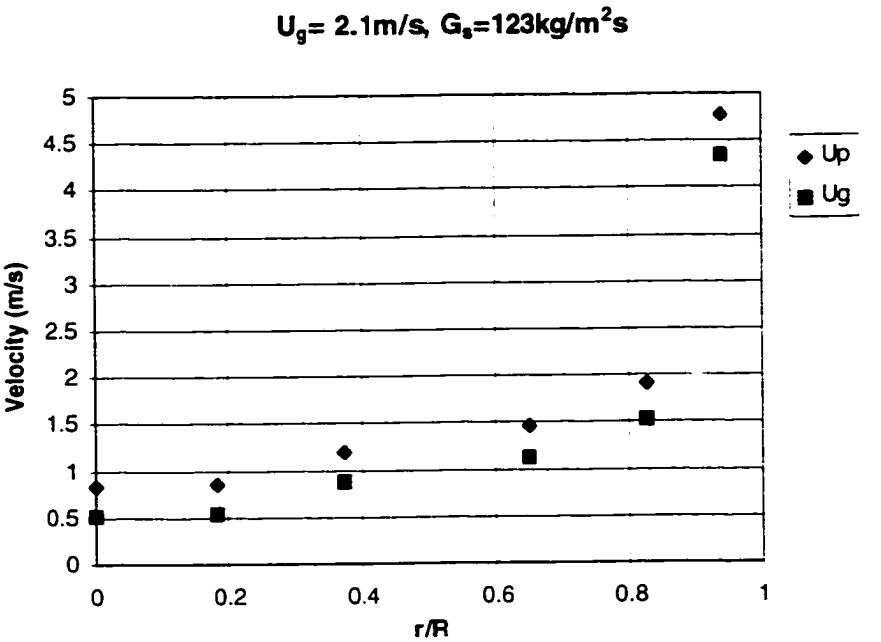

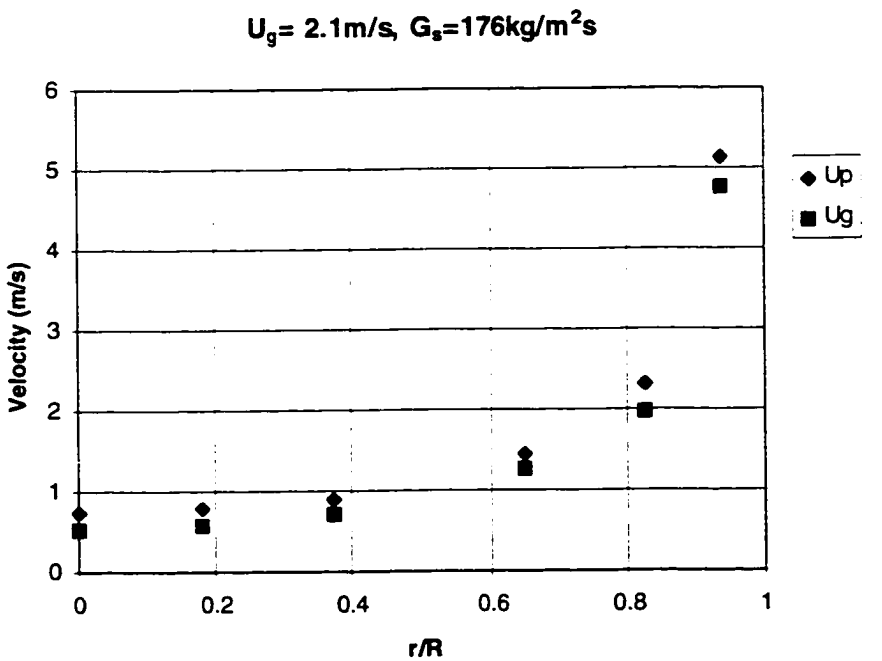

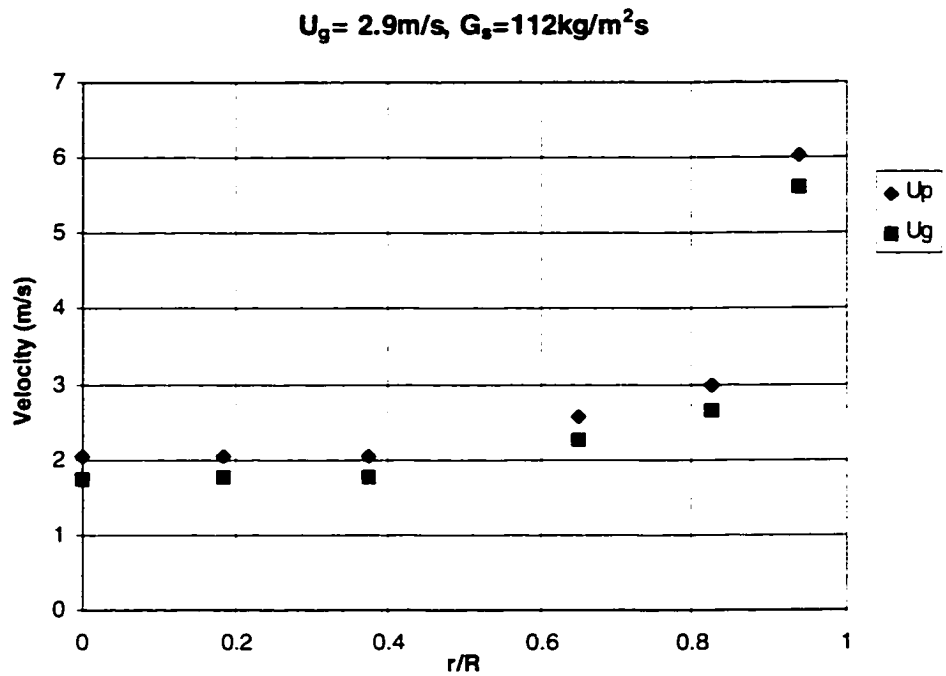

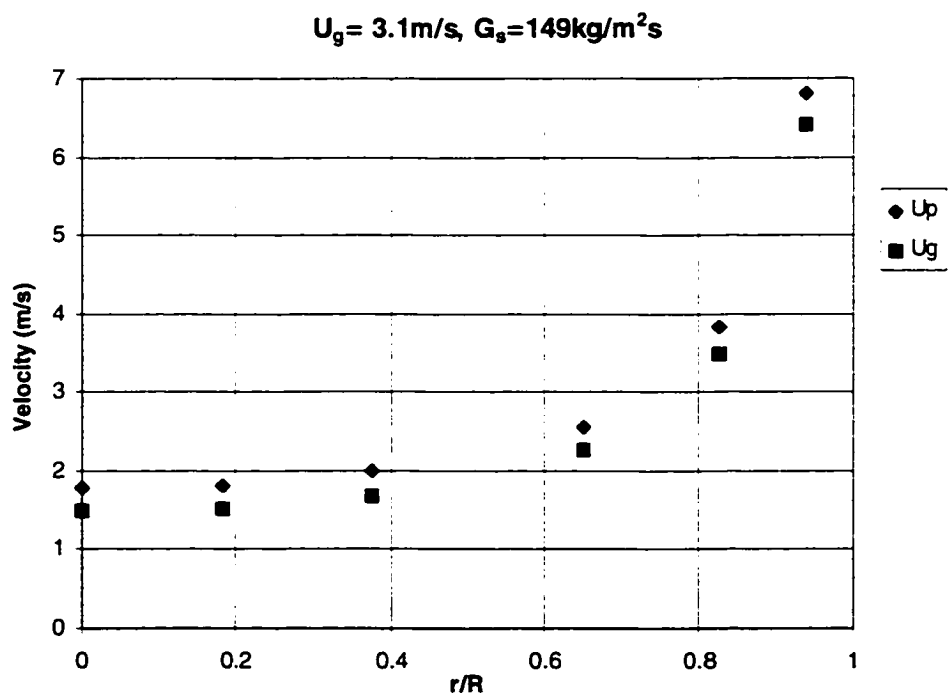

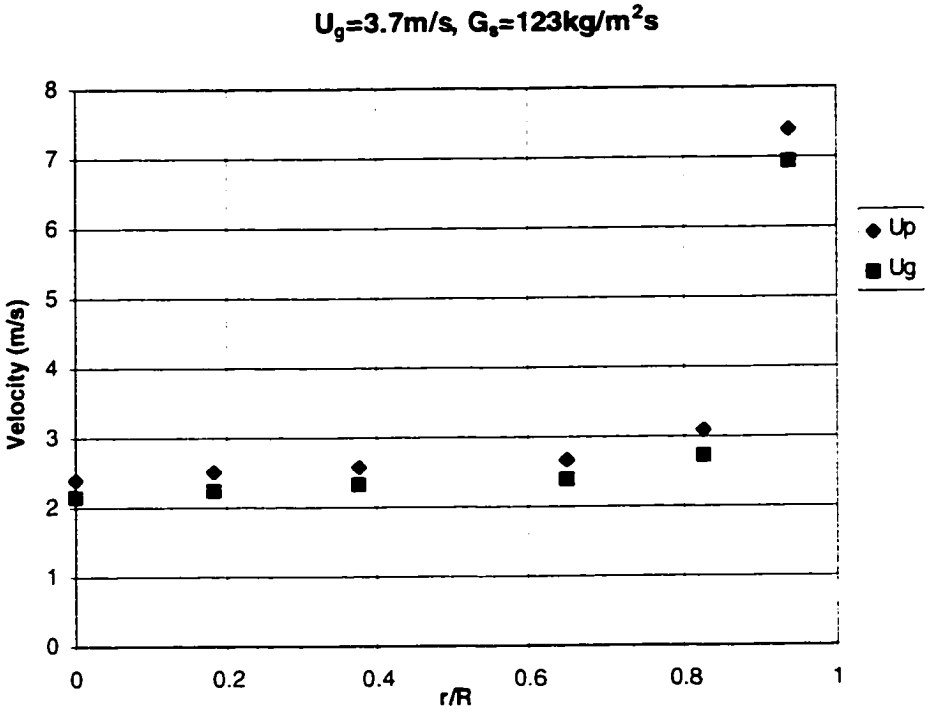

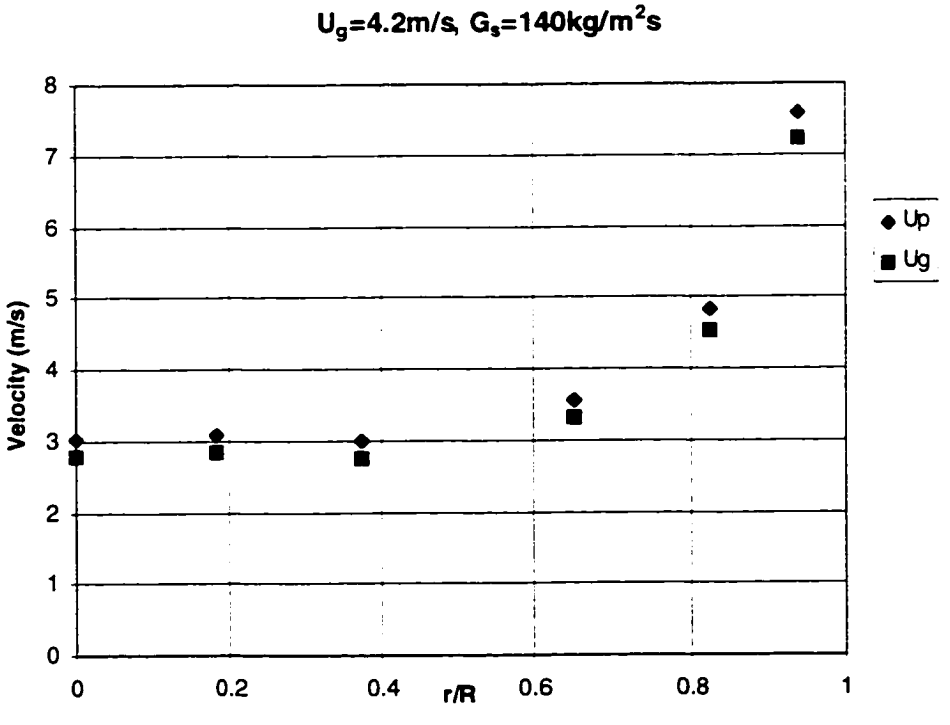

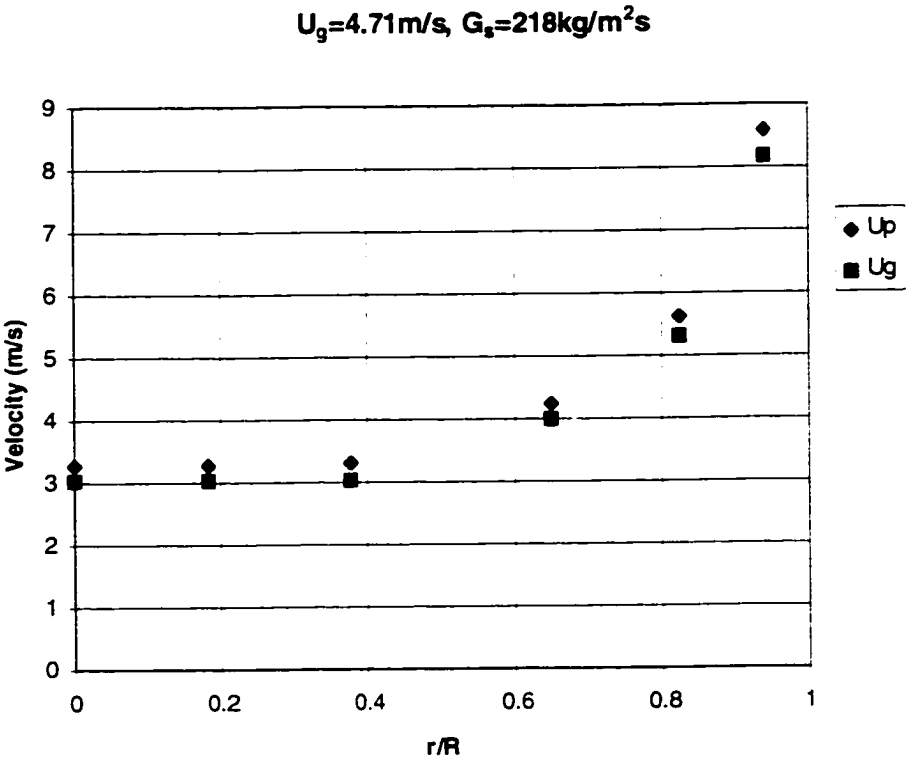

REFERENCES

Adams C. K., "Gas Mixing in a Fast Fluidized Bed", in Circulating Fluidized Bed Technology II, P. Base and J. F. Large, Ed., Pergamon Press, Toronto (1988), pp. 299-306.

Aubert E., D. Barreteau, T. Gauthier and R. Pontier, "Pressure Profiles and Slip Velocities in a Co-Current Downflow Fluidized Bed Reactor", in Circulating Fluidized Bed Technology IV, A. A. Avidan, Ed., AIChE, New York (1994), pp. 403-405.

Bai, D. R., Y. Jin, Z. Q. Yu and N. J. Gan, "Radial Profiles of Local Solid Concentration and Velocity in a Concurrent Downflow Fast Fluidized Bed", in Circulating Fluidized Bed Technology III, P. Basu, M. Horio and M. Hasatani, Eds, Pergamon Press, Toronto (1991), pp. 157-162.

Berg, D. A., C. L. Briens, M. A. Meunier, B. A. Freel and M. A. Bergougnou, "Rapid Mixing Studies between Transported Solids in an Ultra-Rapid Fluidized (URF) Reactor", Proc. 10th Annual Powder Solids Conf., May 7-9, Rosemont, IL (1986), pp. 553-558.

Berg, D. A., C. L. Briens and M. A. Bergougnou, "Reactor Development for the Ultrapyrolysis Reactor", Can. J. Chem. Eng. 67, 96-101 (1989).

Cao, C. S., Y. Jin, Z. Q. Yu and Z. W. Wang, "The gas-Solids Velocity Profiles and Slip Phenomenon in a Concurrent Downflow Circulating Fluidized Bed", in Circulating Fluidized Bed Technology IV, A. A. Avidan, Ed., AIChE, New York (1994). pp. 406-413.

Feindt, Hans-Jacob, "Radial and Axial Density Fluctuations in a High Velocity Fluidized Bed", Ph.D. thesis, The City University of New York, 1990.

Gartside, R. J., "QC- A New Reaction System", in Fluidization VI, J.R. Grace, L. W. Shemilt and M. A. Bergougnou, Eds., Engineering Foundation, New York (1989), pp. 25-32.

Gartside, R. J. and A. F. Ellis, "Thermal Regenerative Cracker: A Development Update", Chem. Eng. Prog. 79(3), (1983), pp. 82-85.

Gartside, R. J. and H. N. Woebecke, "Solid Feeding Device and System", U.S. Patent 4338187 (1982)

Graham, R. G., B.A. Freel and M. A. Bergougnou, "Scale-up and Commercialization of Rapid Biomass Pyrolysis for Feul and Chemical Production", in Energy for Biomass and Wastes XIV", D. L. Klass, Ed., Inst. Gas Technol., Chicago IL (1991), pp. 1091-1104.

Gross, B., "Heat Balance in FCC Process and Apparatus with Downflow Reactor riser", U.S. Patent 4411773 (1983).

Gross, B. And M. P. Ramage, "FCC Reactor with a Downflow Reactor Riser", U.S. Patent 4385985 (1983).

Herbert, P. M., T. A. Gauthier, C. L. Briens and M. A. Bergougnou, "Application of Fiber Optic Reflection Probes to the Measurement of Local Particle Velocity and Concentration in Gas-solid Flow", Powder Technology, 80, 243-252 (1994).

Kim, J. M. And J. D. Seader, "Pressure Drop for Cocurrent Downflow of Gas-Solids Suspensions", AIChE J. 29, 353-360 (1983).

Kim, J. M. And J. D. Seader, "Heat Transfer to Gas-solids Suspensions Flowing Cocurrently Downwards in a Circular Tube", AIChE J. 29, 306-311 (1983).

Kostazos. A., "An Investigation of the Entrance Region of a Riser Fluidized Bed", Ph.D. thesis, The City University of New York, 1997.

Li, J. and H. Weinstein, "An Experimental Comparison of Gas Backmixing in Fluidized Beds across the Regime Spectrum", Chemical Engineering Science, 44, No.8, pp.1697-1705, 1989.

Li, Y. and M. Kwauk, "The Dynamics of Fast Fluidization", in Fluidization, Grace J. R., and J. M. Matsen, Plenunm Press, New York - London, 1980, pp. 537-544.

Matsen, J. M., "Flow of Fluidized Solids and Bubbles in Standpipes and Risers", Powder Technology, 7 (1973), pp. 93-96.

Matsen, J. M., "The Rise and fall of Recurrent Particles: Hydrodynamics of Circulation", in Circulating Fluidized Bed Technology II, P. Base and J. F. Large, Ed., Pergamon Press, Toronto (1988), pp. 3-11.

Monceaux, L., M. Azzi, Y. Molodtsof and J. F. Large, "Overall and Local Characterization of Flow Regimes in a Circulating Fluidized Bed", in Circulating Fluidized Bed Technology, ed. by P. Basu, Canada ,1985. pp. 185-191.

Murphy, J. R., "Evolutionary Design Changes Mark FCC Process", oil Gas J., may

18, 49-58 (1992).

Niccum, P. K. And D. P. Bunn, "Catalytic Cracking System", U.S. Patent 4514285 (1985).

Oberg, C. L. And A. Y. Falk, "Coal Liquefaction by Flash Hydropyrosis", Coal Process Technology, 6, 159-165 (1980).

Rhodes, M. J., V. S. Laussmann and D. Geldart, "Measurements of Radial & Axial Solids Flux Variations in the Riser of a Circulating Fluidized Bed", in Circulating Fluidized Bed Technology II, P. Base and J. F. Large, Ed., Pergamon Press, Toronto (1988), pp. 155-164.

Rodden, G., "The New Alchemy: Turning Waste into Oil and Chemicals", Chemical News 45(8), 35-37 (1993).

Roques, Y., T. Gauthier, R. Pontier, C. L. Briens, and M. A. Bergougnou, "Residence Time Distributions of Solids in a gas-Solids downflow Transport Reactor", in Circulating Fluidized Bed Technology IV, A. A. Avidan, Ed., AIChE, New York (1994), pp. 555-559.

Schnitzlein Michael G. and H. Weinstein, "Flow Characterization in High Velocity Fluidized Beds Using Pressure Fluctuations", Chem. Eng. Sci., 43 (1988), pp.2605-2614.

Schnitzlein Michael G. and H. Weinstein, "Design Parameters determining Solid Hold-up in Fast Fluidized Bed System", in Circulating Fluidized Bed Technology II, P. Base and J. F. Large, Ed., Pergamon Press, Toronto (1988), pp. 205-212.

Shimizu, A., R. Echigo, S. Hasegawa and M. Hishida, "Experimental Study of the Pressure Drop and the Entry length of the Gas-Solid Suspension Flow in a Circular Tube", Int. J. Multiphase flow 4, 53-64 (1978).

Wang, Z. W., D. R. Bai and Y. Jin, " Hydrodynamics of Concurrent Downflow Circulating Fluidized Bed (CDCFB)", Powder Technology, 70, 271-275 (1992).

Wei, F., J. Liu,Y. Jin and Z.Q. Yu, "Hydrodynamics and Mixing Behaviors in the Entrance Region of a Downer", in Circulating Fluidized Bed Technology V, M. Kwauk and J. Li, Ed., Science Press, Beijing (1997), pp. 122-127.

Weinstein, H. et al. "The Radial Pressure Gradient in a Fluidized Riser", presented at the 1995 Annual Meeting of the AIChE.

Weinstein, H., J. Li, E. Bandlamudi, H. J. Feindt and R. A. Graff, "Gas Backmixing of Fluidized Beds in Different Regimes and Different Regions", Fluidization VI, J.R. Grace, L. W. Shemilt and M. A. Bergougnou, Eds., Engineering Foundation, New York (1989), pp. 57-64.

Yang, Y. L., Y. Jin, Z. Q. Yu and Z. W. Wang, "Particle Flow Pattern in a Dilute Concurrent Upflow and Downflow Circulating Fluidized Bed", in Fluidization 91: Science and Technology", M. Kwauk and M. Hasatani, Eds., Science Press, Beijing (1991), pp. 66-75.

Zenklusen, F., R. T.Meili, M. Tesch and L. Reh, "Formation of Homogeneous Downflow Gas/Solid-Suspensions at High Velocities", in Circulating Fluidized Bed Technology V, M. Kwauk and J. Li, Ed., Science Press, Beijing (1997), pp. 84-89.

Zhu, J. X., Z.Q. Yu, Y. Jin, J. R. Grace and A. Issangya, "Concurrent Downflow Circulating Fluidized Bed (Downer) Reactors - A State of the Art Review", the Canadian Journal of Chemical Engineering, 73, Oct., 1995, pp.662-677.

IMAGE EVALUATION TEST TARGET (QA-3)

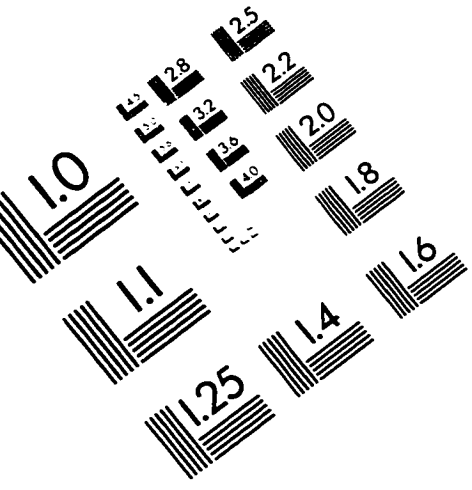

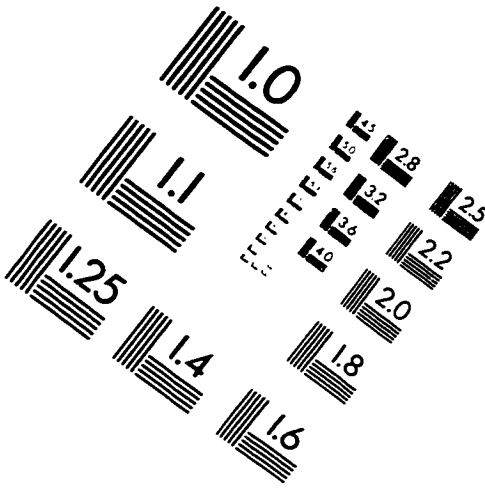

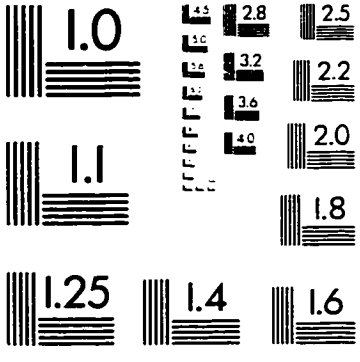

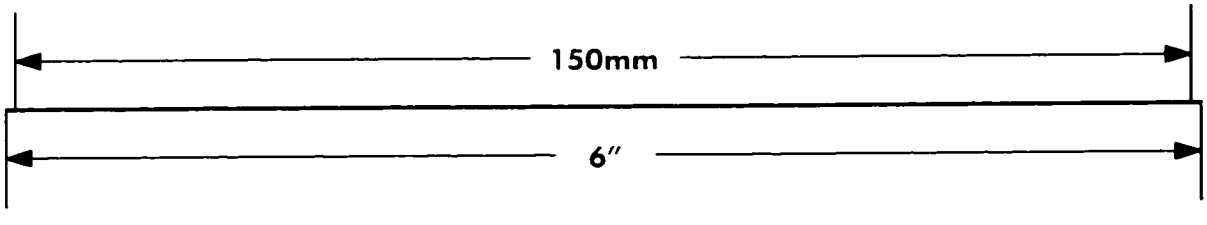

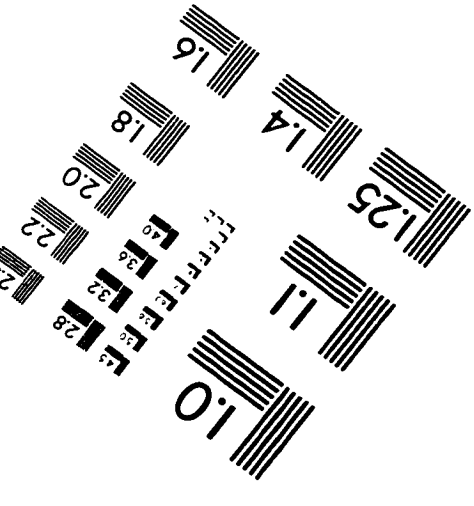

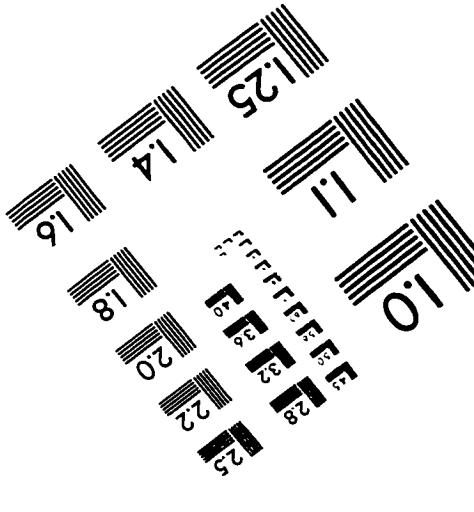

APPLIED IMAGE, Inc
1653 East Main Street
Rochester, NY 14609 USA
Phone: 716/482-0300
Fax: 716/288-5989